Study, development and evaluation of the subgroup methods based on the physical probability tables in APOLLO3® for thermal reactor calculations

Emeline Rosier

université PARIS-SACLAY

Study, development and evaluation of the subgroup methods based on the physical probability tables in APOLLO3® for thermal reactor calculations

Étude, développement et évaluation des méthodes des sous-groupes basées sur les tables de probabilités physiques dans APOLLO3® pour le calcul des réacteurs thermiques

Thèse de doctorat de l'université Paris-Saclay

École doctorale n°576, Particules, Hadrons, Energie, Noyau : Instrumentation, Image, Cosmos et Simulation (PHENIICS)
Spécialité de doctorat: Energie Nucléaire
Graduate School : Physique, Référent : Faculté des sciences d'Orsay

Thèse préparée au Service d'Études des Réacteurs et de Mathématiques Appliquées (Université Paris-Saclay, CEA),
sous la direction de Luiz LEAL, Directeur de recherche,
de l'encadrement de Li LEI-MAO, Ingénieure de recherche,
et du co-encadrement de Richard SANCHEZ, Directeur de recherche.

Thèse soutenue à Paris-Saclay, le 12 décembre 2022, par

Emeline ROSIER

Composition du jury

Frank Gunsing Directeur de recherche, CEA Saclay	Président
Alain Hébert Professeur, École Polytechnique de Montréal	Rapporteur & Examinateur
Han Gyu Joo Professor, Seoul National University	Rapporteur & Examinateur
Yunlin Xu Assistant professor, Purdue University	Examinateur
Danny Lathouwers Associate Professor, Delft University of Technology	Examinateur
Luiz Leal Directeur de recherche, IRSN	Directeur de thèse

THESE DE DOCTORAT
NNT : 2022UPASP139

Acknowledgments

What an adventure.

In these first few pages, I wish to express my deepest thanks to everyone that has had the (mis ?)fortune to navigate with me through the intricacies of self-shielding.

I am grateful to the CEA, and more particularly to the SERMA, for providing me with a favorable professional environment. I am honored to be part of such a fruitful scientific community.

My gratitude goes to Alain Hébert and Han Gyu Joo for their precious expertise in reviewing my PhD dissertation, and to all the members of the jury for their evaluation of my work.

A very special thanks to Luiz Leal for having so benevolently directed this thesis. Thank you for your availability and unconditional support. I feel privileged for being your last PhD student.

My deepest gratitude to Li Lei Mao, for introducing me to the fascinating, albeit very complex, domain of self-shielding for neutronics codes. I have grown so much in my understanding of reactor physics and modelling. Thanks for your unfaltering support in all the stages of this thesis, both from a professional and a personal point of view.

Thanks should also go to Richard Sanchez for having followed the advancement of this project and offered all along insightful comments and suggestions. I am deeply appreciative of the time and energy you put into reviewing my dissertation.

Lastly, I would like to acknowledge a few coworkers who have significantly contributed to this thesis. Igor Zmijarevic, of course, for all the productive discussions and your help in preparing my defense. Stéphane Mengelle, Claude Mounier, and all the GALILEE team for helping me generate the multigroup libraries of nuclear data I needed to carry out my calculations. Odile Petit and Thierry Visonneau for their availability and guidance on the use of the TRIPOLI-4® code, and Cedric Jouanne for the generation of the modified nuclear data employed in the TRIPOLI-4® reference calculations.

Je me permets de conclure ces remerciements par quelques mots en français, adressés à tous ceux qui ont partagé mes joies et mes galères de ces trois dernières années. Je ne citerai aucun nom, ils se reconnaitront. Merci.

université PARIS-SACLAY

ÉCOLE DOCTORALE
Particules, hadrons, énergie et noyau : instrumentation, imagerie, cosmos et simulation (PHENIICS)

Titre: Étude, développement et évaluation des méthodes des sous-groupes basées sur les tables de probabilités physiques dans APOLLO3® pour le calcul des réacteurs thermiques.
Mots clés: Autoprotection, méthode des sous-groupes, tables de probabilités physiques, APOLLO3®, code déterministe, code réseau

Résumé: Les méthodes des sous-groupes sont une catégorie de méthodes d'autoprotection reposant sur l'utilisation de tables de probabilités pour calculer les grandeurs intégrées en énergie sur un maillage multigroupe. Dans la partie réseau du code APOLLO3®, les tables de probabilités employées sont dites « mathématiques » car elles reposent sur la méthode de quadrature de Gauss. Elles sont calculées à la volée par le code de traitement de données nucléaires GALILÉE. La méthode des sous-groupes d'APOLLO3® fournit d'excellents niveaux de précisions sur des calculs typiques de réacteurs thermiques, au prix d'un temps de calcul élevé. Ce coût temporel est principalement dû à l'utilisation d'une discrétisation énergétique fine de plusieurs centaines de groupes, et au calcul à la volée des tables de probabilités de mélange.

Une autre catégories de tables de probabilités, dîtes « physiques », consiste à conserver des grandeurs caractéristiques du réacteur, telles que des taux de réactions ou des sections efficaces de référence. Elles sont couramment utilisées dans des méthodes d'autoprotection sur des maillages énergétiques de quelques dizaines de groupes. Le travail de cette thèse consiste à évaluer les performances des méthodes des sous-groupes basées sur les tables de probabilités physiques dans le code APOLLO3® pour le calcul des réacteurs thermiques.

Il a été choisi de calculer des sections efficaces de référence en milieu homogène infini en traitant le mélange d'isotopes résonants comme isotope unique, menant ainsi à la génération de tables de probabilités physiques de mélange. Ces tables de probabilités ont été couplées à la méthode des sous-groupes d'APOLLO3®, basée sur la résolution de l'équation de structure fine grâce au modèle « Toutes Résonances », et testées sur plusieurs maillages énergétiques, mettant ainsi en évidence l'incompatibilité de cette méthode des sous-groupes avec une discrétisation grossière en énergie. Une méthode des sous-groupes résolvant l'équation de ralentissement élastique avec le modèle « Résonance Intermédiaire » a été implémentée dans APOLLO3®. Les premiers tests numériques montrent des résultats encourageants, avec des erreurs maximales de l'ordre de la centaine de pcm (10^{-5}) sur le facteur de multiplication.

Title: Study, development and evaluation of the subgroup methods based on the physical probability tables in APOLLO3® for thermal reactor calculations.

Keywords: Self-shielding, subgroup method, physical probability tables, APOLLO3®, deterministic code, lattice code

Abstract: The subgroup methods are a category of self-shielding methods based on the use of probability tables to compute group-averaged quantities. The probability tables traditionally employed in APOLLO3® lattice calculations are computed on-the-fly for a mixture of resonant isotopes by the GALILEE nuclear data processing system according to the Gauss quadrature methodology, therefore preserving the first moments of the point-wise cross sections. They are called mathematical probability tables. The APOLLO3® subgroup method provides an excellent accuracy on typical PWR calculations, at the cost of a large CPU time. This expensive computational time is partly due to the online generation of mixture mathematical probability tables, limiting in practice the composition of the mixture to less than 10 resonant isotopes, and to the necessity of using a fine energy discretization of a few hundreds of groups.

Another type of probability tables, called physical probability tables, preserve typical physical quantities of the reactor calculation, such as reference reactions rates or effective cross sections. The existing literature shows they can be employed in self-shielding calculations on coarse energy meshes of a few dozens of groups. This PhD thesis aims at evaluating the subgroup methods based on the physical probability tables for thermal reactor calculations in the APOLLO3® code.

It was chosen to calculate the reference cross sections in an infinite homogeneous medium by treating the resonant mixture as a single isotope, leading to the generation of homogeneous mixture physical probability tables. They were coupled with the APOLLO3® subgroup method, based on the resolution of the fine-structure equation using the "General Resonance" model. Numerical tests on a coarse 69 group energy structure have shown that this method was not compatible with the use of such a coarse discretization. A subgroup method based on the resolution of the elastic slowing down equation using the "Intermediate Resonance" model has been implemented in APOLLO3®. Numerical tests on a series of increasingly complex geometries, from infinite homogeneous media to 17x17 fuel-pin assemblies, have yielded encouraging results, with a maximal error of a hundred pcm (10^{-5}) on the global multiplication factor.

Table of Contents

List of Figures

List of Tables

List of Acronyms

CP Collision Probability.

DR Direct Resolution.

EDC Equivalent Dancoff-factor Cell.

FSM Fine-Structure Method.

GR General Resonance.

IDM Improved Direct Method.

IHM Infinite Homogeneous Medium.

IR Intermediate Resonance.

MPO Multiparameter Output.

MPT Mathematical Probability Table.

NR Narrow Resonance.

OP Orthogonal Polynomials.

PPT Physical Probability Table.

PWR Pressurized Water Reactor.

RIF Resonance Interference Factor.

SG Subgroup.

SMA Same Material Approximation.

SPH Superhomogenization.

ST Statistical.

WR Wide Resonance.

1 - Introduction

1.1 . General Context

The neutron distribution in a nuclear reactor is described by the neutron transport equation, oftentimes called the Boltzmann equation for its similarity with the kinetic theory of gases. A complexity of this equation comes from the fast variations in energy of its coefficients, called the macroscopic cross sections, which characterize the probability for a neutron to undergo collisions in the medium through which it propagates. Between 1 eV and 100 keV, the cross sections of heavy nuclides can fluctuate rapidly of several orders of magnitudes. These fast variations are called resonances. Because the probability of interaction increases drastically, the neutron flux is depressed in the vicinity of these resonances.

Two main approaches exist to solve the Boltzmann equation. On the first hand, the Monte Carlo methods derive the average behavior of the nuclear reactor from a large collection of random sampling of neutron trajectories. Monte Carlo methods do not introduce any approximation, except for the simulation of the unresolved energy domain; their solution can therefore be considered as high fidelity. Their accuracy is only restricted by the uncertainty on the nuclear data evaluations. The main limitation stems from the need to simulate a large number of particles to decrease the statistical uncertainty, inducing a considerable computational time. On the other hand, the deterministic methods rely on the discretization of the phase space: energy, position and direction. This discretization introduces approximations and biases; the choice of the refinement has to be a compromise between accuracy and computational resources, in terms of computational time and memory.

In particular, the energy treatment is operated through the use of the multigroup approximation, consisting of dividing the energy domain into groups where the neutrons are considered to be mono-kinetic. The macroscopic cross sections in the Boltzmann equation are replaced by their group-averaged values. The determination of the multigroup cross sections in the resonant domain is called the self-shielding calculation. The accuracy of the solution of the Boltzmann equation is highly dependent on the quality of the self-shielding procedure.

There exist a large variety of self-shielding methods, as each deterministic code has developed its own solution to compute multigroup cross sections [1]. The methods can be separated in three main families: equivalence-based methods [2] [3] [4] [5], ultra-fine group methods [6] [7] and subgroup methods [8] [9] [10] [11] [12]. For the application on large geometries, the subgroup methods seem to be the best options. They rely on the use of probability tables to compute group-averaged quantities. Two kinds of probability tables can be distinguished, namely mathematical and physical probability tables. The feature of mathematical probability tables [13] [14] [3] is that they preserve the values of the first moments of the point-wise cross sections, similarly to a Gauss quadrature. On the other hand, physical probability tables [4] [12] [15] preserve the typical quantities of a thermal reactor calculation, such as effective cross sections, resonance integrals, reaction rates, etc.

This thesis work has been completed at the Service d'Étude des Réacteurs et de Mathématiques Appliquées (SERMA), where the APOLLO3® [16] multi-purpose modular deterministic code for reactor physics analyses is under development with the collaboration and financial support of Framatome

and EDF. APOLLO3® is able to perform both lattice and core calculations of a traditional two-step computational scheme, where the transport equation, or an approximation of it, is solved using pin-homogenized or assembly-homogenized energy-condensed multigroup cross sections, obtained in a preliminary finely detailed transport calculation.

The calculation of the effective multigroup cross sections has to account for the actual distribution of the neutron flux. The subgroup method of APOLLO3® is based on the fine-structure equation [2], on the use of the General Resonance (GR) model [3] to approximate the resonant scattering operator, on the mixture mathematical probability tables generated on-the-fly by the GALILEE nuclear data processing system [17] and on the Superhomogenization correction [18]. A fine energy discretization of a few hundreds of energy groups is required in order to avoid a heterogeneous-homogeneous equivalence technique, known to distort the spatial distribution the reaction rates. The numerical tests carried out to verify the APOLLO3® subgroup methods evidenced its excellent accuracy on typical thermal reactor calculations, but also highlighted its large computational time. The implementation of the Equivalent Dancoff-factor Cell method [19] has led to a considerable acceleration of the self-shielding calculations, but the use of a fine energy mesh is still a strong constraint on the computational time.

In existing deterministic codes, such as DRAGON [1], HELIOS [8], WIMS [9] [4], DeCART [10], nTRACER [20], MPACT [11], or NECP-X [12] [21], the subgroup methods are successfully employed with the physical probability tables and with a coarse energy discretization of a few dozens of groups. None of the aforementioned codes rely on the use of the GR model in their subgroup method; this is a specificity of APOLLO3®. The literature shows that the Intermediate Resonance (IR) model is much more common for an application on coarse energy meshes.

The objective of this thesis is to investigate the possibility to reduce the number of energy groups in APOLLO3® by the means of subgroup methods based on the physical probability tables. The advantage of a coarse energy discretization is evident, as the computational time is linearly dependent on the number of groups.

The first part of the thesis consists of the implementation and validation in the APOLLO3® code of a module to compute on-the-fly the physical probability tables for a resonant mixture, for a coarse energy mesh of less than 100 energy groups.

The second part is dedicated to the study and evaluation of the subgroup methods coupled with the physical probability tables on the coarse energy mesh, for thermal reactor calculations. The use of the GR model for coarse-group calculations should be investigated. Also, the use of the IR model, which had never before been considered in French deterministic codes, should be examined. A comparison of the fine-group GR-based subgroup method with the coarse-group IR-based method should highlight the strengths and weaknesses of both methods.

1.2 . Outline of the Manuscript

The manuscript is segmented as follows.

Chapter 2 recaps some fundamental notions of neutronics essential for the comprehension of the manuscript. The neutron-material interactions are explained, with an accent on the definition of the cross sections. The neutron transport equation is presented and the main deterministic solutions are

summarized.

Chapter 3 details the self-shielding methods for thermal reactor calculations already existing in the APOLLO3® code, as well as the calculation of the mathematical probability tables for a resonant mixture.

Chapter 4 introduces the several numerical benchmarks employed later in the manuscript, for the verification and validation of the implemented methods.

Chapter 5 explains the validation methodology of the APOLLO3® ultra-fine group slowing-down solver in an infinite homogeneous medium. This solver provides the effective cross sections of the resonant mixture of reference, based on which the physical probability tables are computed.

Chapter 6 describes the module implemented in APOLLO3® for the on-the-fly calculation of the physical probability tables of a resonant mixture. Validation tests are carried out for some representative mixtures in thermal reactor calculation.

Chapter 7 shows the evaluation tests performed on the APOLLO3® fine-structure subgroup method, when it is coupled to the physical probability tables instead of the mathematical probability tables. The tests are carried out for several energy meshes to study the impact of the number of groups on the accuracy of the self-shielding calculation.

Chapter 8 describes the implementation of a subgroup method based on the "Intermediate Resonance" model in APOLLO3®. The preliminary calculation of the Goldstein-Cohen factors using Monte Carlo simulations is explained. Numerical tests are carried out with the 69-group energy mesh in order to evaluate both the accuracy and computational efficiency of this newly implemented subgroup method.

Chapter 9 provides the conclusions and perspectives of this thesis work.

1.3 . List of Published Materials

- E. Rosier, L. Mao, I. Zmijarevic, L. Leal and R. Sanchez, *Comparison of two Subgroup Methods based on the Physical Probability Tables*, Proceedings of PHYSOR 2022, Pittsburgh, Pennsylvania, USA, May 2022, pp. 2561–2569.
- E. Rosier, L. Mao and L. Leal, *Dynamic Construction of Physical Probability Tables for Resonant Mixture*, Proceedings of M&C 2021, Virtual Meeting, October 2021, pp. 1992-2021

2 - Fundamentals of Neutronics

This chapter provides some key elements of neutronics for the understanding of the rest of this document. It starts with a quick explanation of the neutron-matter interactions theory, with a focus on the notion of cross sections. The second section describes the neutron transport equation, also known as the Boltzmann equation, and explains each of its terms. The last subsection provides a non-exhaustive state of the art of the solution of the Boltzmann equation in a traditional two-step deterministic calculation scheme.

2.1 . Quick Introduction to Neutron Interactions with Matter

A nuclear reaction can occur when an incident particle collides with a target nucleus. In the field of reactor physics, the predominant incident particle of interest is the neutron. This section defines first the concept of cross section, as the probability for a neutron-induced reaction to happen, before providing a non-exhaustive list of the different nuclear reactions of interest for the study of nuclear reactors.

2.1.1 . Notion of cross section

The cross section is a concept quantifying the probability for a neutron to undergo a specific nuclear reaction ρ on a particular nucleus x. It is expressed in the unit "barn" (10^{-24} cm^2). It shares the same unit as a surface, as the cross section is often described as the "shadow" of the neutron projected onto the sphere of the nucleus. The value of the cross section is dependent, of course, on the type of nuclear reaction and on the target nucleus, but also on the energy of the incident neutron, and the temperature of the target.

The microscopic cross section is written in this document as $\sigma_{\rho,x}$, and corresponds to the probability for a neutron impinging on a unit area (cm^2) of the target to interact with a single nucleus of type x through a reaction ρ. It is also common to multiply the microscopic cross section by the density of x in the material, N_x (in cm^{-3}), in order to obtain the so-called macroscopic cross section

$$\Sigma_{\rho,x} = N_x \sigma_{\rho,x}, \tag{2.1}$$

which corresponds to the probability for the neutron to interact per centimeter of distance traveled. In a material composed of different types of target nuclides, the macroscopic cross sections can be summed over all the present nuclides.

2.1.2 . Classification of the nuclear reactions

A neutron colliding against a nucleus can undergo different types of nuclear reactions. In the field of reactor physics, the main reactions of interest are:

- Neutron capture when an incident neutron is absorbed by the target nucleus to form a heavier nucleus, in an excited state. The excess energy is released when the formed nucleus decays into the ground state with the emission of gamma ray.

- Neutron-induced fission, where the incident neutron is absorbed by the target nucleus, causing it to split into two or more fission products. The nature of these fission fragments is somewhat probabilistic; the fission yield is dependent on the type of target nucleus and on the energy of the incident neutron. The fission also produces neutrons, called prompt neutrons, which are responsible for maintaining the chain reaction in the core of the reactor. More neutrons can be emitted later on, when the radioactive fission products decay, and are called delayed neutrons. The energy released during the fission (about 200 MeV) is the main heat source of the nuclear reactor.

- Elastic scattering, where the incoming neutron is scattered off by the target nucleus. The total energy of the whole system "neutron + nucleus" remains unchanged by this type of nuclear reaction, but the neutron is in fact slowed down by this interaction, as a proportion of its energy is transferred as recoil energy to the nucleus. The lighter the isotope, the more effective the slowing-down of neutrons, making hydrogen the privileged choice as a moderator for thermal reactors.

- Inelastic scattering, where some of the energy of the neutron is absorbed by the target nucleus to reach an excited state. The kinetic of the global system "nucleus + neutron" is therefore not preserved in this interaction.

The first two reactions, capture and fission, form the neutron absorption. The total cross section σ is often described as being the sum of the absorption cross section σ_a and the scattering cross section σ_s.

Some of these neutron-induced nuclear reactions involve the formation of an intermediate state called the compound nucleus, formed by the target nucleus absorbing the incident neutron. If the energy of the incident neutron is close to an excitation level of that compound nucleus, then the probability of the nuclear reaction is drastically increased. These specific energies can be observed experimentally on the cross sections measurements: the cross sections exhibit very fast variations, sometimes of multiple orders of magnitude, called resonances. This is especially true for heavy isotopes, as evidenced on the Figure 2.1.

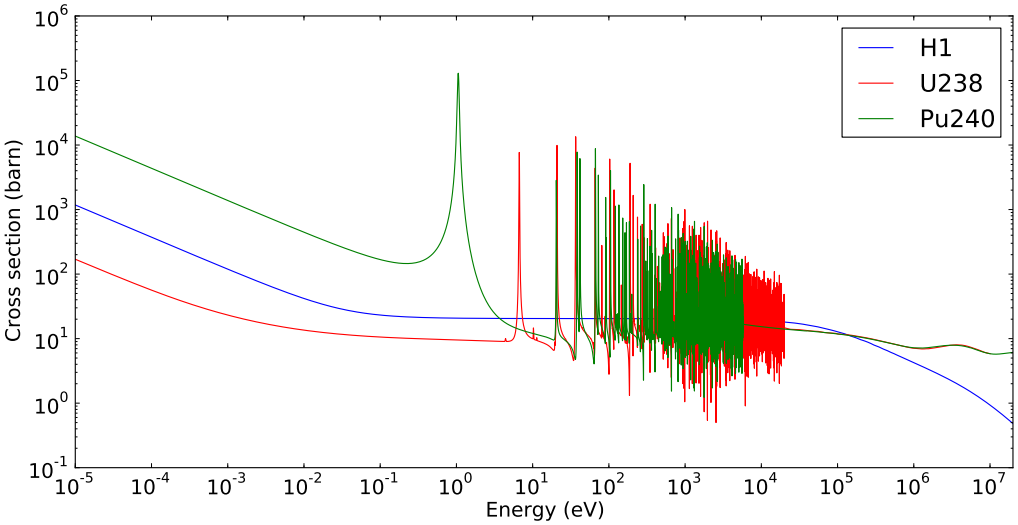

Figure 2.1: Total cross section at 0K (nuclear data evaluation JEFF 3.1 [22])

2.2 . Neutron Transport Equation

The neutron distribution within a nuclear reactor is entirely described by the following set of variables: the time t, the energy E, a three dimensional vector of position in space $\vec{r}$ and a two dimensional vector of direction $\vec{\Omega}$. The angular flux Ψ is defined by the relation

$$\Psi(\vec{r}, \vec{\Omega}, E, t) = v(E) \times n(\vec{r}, \vec{\Omega}, E, t), \tag{2.2}$$

where $n(\vec{r}, \vec{\Omega}, E, t)$ is the density of neutrons (in cm^{-3}), and $v(E)$ is the velocity of the neutrons having a kinetic energy E. It is natural to study populations of neutrons having the same velocity, or energy, since they will share the same probability of interaction with the atoms of the medium which they are traveling through. By integrating expression (2.2) over a solid angle of 4π, the scalar flux is derived:

$$\Phi(\vec{r}, E, t) = \int_{4\pi} d\vec{\Omega}\ \Psi(\vec{r}, \vec{\Omega}, E, t). \tag{2.3}$$

The interest of the scalar flux is its direct relation with the reaction rates (in s^{-1}.cm^{-3}):

$$\tau_{\rho,x} = \Phi(\vec{r}, E, t) \times \Sigma_{\rho,x}, \tag{2.4}$$

with $\Sigma_{\rho,x}$ being the previously introduced macroscopic cross section for a nuclear reaction ρ and a nucleus x. The reaction rate $\tau_{\rho,x}$ describes the number of neutrons undergoing the reaction ρ on a nucleus x per unit time and unit volume.

The neutron flux is the solution of the neutron transport equation, also known as the Boltzmann equation for its similarity with the gas theory. This equation and some of its equivalent forms are presented in the next subsections.

2.2.1 . Steady state integro-differential equation

The integro-differential form of the neutron transport equation is a balance equation expressing the conservation of neutrons inside an elementary volume of the phase space. The following assumptions are adopted:

- The neutron-neutron interactions are neglected. Such interactions are indeed very rare because the density of the neutron gas is much less than that of the surrounding materials, making this kind of event unlikely to happen.
- Neutrons are assumed to be point particles.
- Neutrons move in straight line, called free path, defined as the distance between two collision sites. This free path is much larger than the neutron size.
- The nuclides composing the surrounding materials are supposed to be in a thermal equilibrium with their neighbors.
- The medium in the reactor is assumed to be isotropic, meaning it is invariant by rotations.

The derivation of the neutron transport equation under these assumptions is not detailed in this document, but can easily be found in the literature, such as Reference [23]. Considering a spatial domain $\mathcal{D}$ with a border $\partial\mathcal{D}$, the steady state form (independent of the time) equation reads:

$$\begin{aligned}\left[\vec{\Omega}\cdot\vec{\nabla}+\Sigma(\vec{r},E)\right]\Psi(\vec{r},\vec{\Omega},E) = &\int_0^{+\infty}dE'\int_{4\pi}d^2\Omega'\,\Sigma_s(\vec{r},\vec{\Omega'}\cdot\vec{\Omega},E'\rightarrow E)\Psi(\vec{r},\vec{\Omega}\,',E') \\ &+S(\vec{r},E,\vec{\Omega}) \text{ if } (\vec{r},\vec{\Omega})\in\mathcal{D},\end{aligned} \tag{2.5}$$

and

$$\Psi(\vec{r},\vec{\Omega},E)=\Psi_-(\vec{r},\vec{\Omega},E) \text{ if } (\vec{r},\vec{\Omega})\in\partial\mathcal{D}, \tag{2.6}$$

with $\Psi_-(\vec{r},\vec{\Omega},E)$ being the incoming angular flux [24]. Each term of the transport equation (2.5) represents either a gain or a loss of neutrons in the elementary phase space volume:

- The term $\vec{\Omega}\cdot\vec{\nabla}\Psi(\vec{r},\vec{\Omega},E)$ represents the loss due to the neutrons leaking out of the elementary volume of the phase space.
- $\Sigma(\vec{r},E)\Psi(\vec{r},\vec{\Omega},E)$ is the removal term designating the neutrons undergoing any collision in the material. Absorption reactions will entirely remove the neutrons, while scattering reactions will change their direction or energy, effectively removing them from the considered elementary volume of the phase space.
- $\Sigma_s(\vec{r},\vec{\Omega'}\cdot\vec{\Omega},E'\rightarrow E)$ is called the differential scattering cross section. It represents the probability for a neutron with an energy E' and a direction $\vec{\Omega}'$ to be scattered to a new direction $\vec{\Omega}$ with a remaining kinetic energy E after a collision. The first term in the right hand side of the equation therefore represents the arrival of neutrons by scattering.

- $S(\vec{r}, E, \vec{\Omega})$ is the source term, encompassing the fission sources and the external sources:

$$S(\vec{r}, E, \vec{\Omega}) = \sum_x \frac{\chi_x(\vec{r}, E)}{4\pi} \int_0^{+\infty} dE' \int_{4\pi} d^2\Omega' \nu_x(E') \Sigma_{f,x}(\vec{r}, E') \Psi(\vec{r}, \vec{\Omega}', E') + S_{ext}(\vec{r}, \vec{\Omega}, E). \tag{2.7}$$

  χ_x, $\Sigma_{f,x}$ and ν_x are the fission spectrum, the macroscopic fission cross section and the averaged number of neutrons emitted per fission of isotope x. Oftentimes, for numerical purposes, $\nu_x \Sigma_{f,x}$ is stored as one quantity, called the macroscopic production cross section. It is supposed that the neutrons resulting from the fission are emitted isotropically, resulting in a uniform emission probability in the angular space of 4π.

The sum of the two terms on the right hand side of the transport equation is the neutron emission density:

$$q(\vec{r}, \vec{\Omega}, E) = \int_0^{+\infty} dE' \int_{4\pi} d^2\Omega' \; \Sigma_s(\vec{r}, \vec{\Omega}' \cdot \vec{\Omega}, E' \to E) \Psi(\vec{r}, \vec{\Omega}, E) + S(\vec{r}, E, \vec{\Omega}). \tag{2.8}$$

By defining the loss operator $L = (\vec{\Omega} \cdot \vec{\nabla} + \Sigma)$, the scattering operator H and the production operator F, the neutron transport equation can be written in a more compact form:

$$\begin{cases} L\Psi = H\Psi + F\Psi + S_{ext} \;\; \text{if } (\vec{r}, \vec{\Omega}) \in \mathcal{D} \\ \Psi = \Psi_- \;\; \text{if } (\vec{r}, \vec{\Omega}) \in \partial\mathcal{D} \end{cases} \tag{2.9}$$

In the case where there is no fission source ($F = 0$), for example in shielding calculations, Equation (2.9) is a fixed-source equation of the type $(L - H)\Psi = S$.

In criticality calculations, when the fission source is the only source of neutrons in the system ($S_{ext} = 0$), Equation (2.9) reduces to the homogeneous equation $(L - H - F)\Psi = 0$. In order to retrieve another solution than the trivial solution $\Psi = 0$, it is formulated in the form of an eigenvalue equation $(L - H)^{-1} F\Psi = k_{eff}\Psi$, where k_{eff} is the multiplication factor, and is the only real and positive eigenvalue. It is defined as the ratio between the neutrons produced by fission in the system and the loss of neutrons (absorption, leakage), indicating thus the growth of the neutron population inside the system. It is not affected by the scattering sources since neutrons are neither absorbed nor produced by scattering reactions. The multiplication factor is employed to divide the production operator in order to retrieve the steady-state equation:

$$\begin{cases} (L - H)\Psi = \dfrac{1}{k_{eff}} F\Psi \;\; \text{if } (\vec{r}, \vec{\Omega}) \in \mathcal{D} \\ \Psi = \Psi_- \;\; \text{if } (\vec{r}, \vec{\Omega}) \in \partial\mathcal{D}. \end{cases} \tag{2.10}$$

2.2.2 . Steady state integral equation

The neutron transport equation can be derived in an equivalent form, with only integral terms, by considering the angular flux at a fixed point $\vec{r}$ along a characteristic line of direction $\vec{\Omega}$ [23] [24], as shown in Figure 2.2. Neutrons with a direction $\vec{\Omega}$ at a position $\vec{r}' = \vec{r} - s\vec{\Omega}$ reach, if not absorbed or deflected, the position $\vec{r}$.

The probability that a neutron reaching position $\vec{r}$ and following direction $\vec{\Omega}$ has traveled the distance s without undergoing any collision is denoted $e^{-\tau(\vec{r}, \vec{\Omega}, E, s)}$, where

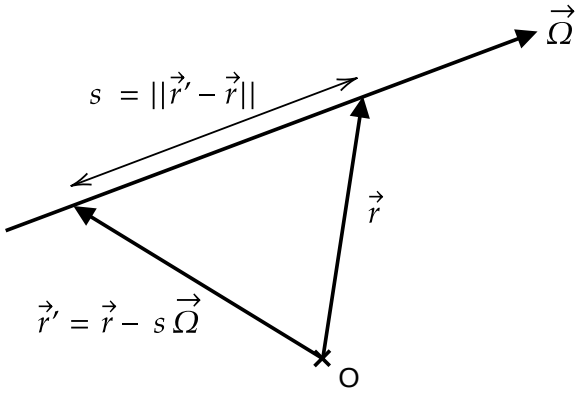

Figure 2.2: Illustration of the notations employed in the expression of the integral neutron transport equation

$$\tau(\vec{r}, \vec{\Omega}, E, s) = \int_0^s \Sigma(\vec{r} - s\vec{\Omega}, E)\, ds \tag{2.11}$$

is called the optical length. Using this notation, and employing the energy variable rather than the velocity, the integral form of the neutron transport equation is:

$$\Psi(\vec{r}, \vec{\Omega}, E) = \int_0^{s_b} q(\vec{r} - s\vec{\Omega},\, \vec{\Omega},\, E)\, e^{-\tau(\vec{r}, \vec{\Omega}, E, s)}\, ds + \Psi_-(\vec{r}_b, \vec{\Omega}, E)\, e^{-\tau(\vec{r}, \vec{\Omega}, E, s_b)}, \tag{2.12}$$

where $\vec{r}_b = \vec{r} - s_b\vec{\Omega}$ is the intersecting point with the boundary of the domain of the back trajectory $(\vec{r},\, -\vec{\Omega})$.

2.3 . Deterministic Solution of the Transport Equation

The numerical solution with deterministic methods of the neutron transport equation requires to discretize all the variables of the phase space. The first part of this section recaps the principle of this discretization process. The second subsection focuses on the so-called two-step calculation scheme, and especially the way it is implemented in the APOLLO3® code.

2.3.1 . Discretization of the phase space

Today's computers are only able to operate on discrete variables. This is the reason why each variable of the phase space of the neutron transport equation has to be discretized first before solving the equation. This discretization introduces errors in the calculated neutron flux; the finer the discretization is, the smaller the error is.

Let us note that the time variable is not discretized properly speaking. It is treated through the solution of steady states equations at different time steps, rather than time-dependent ones. In this subsection, we will focus on the discretization of the energy, space and direction variables.

Multigroup formalism

In all deterministic codes, the multigroup approximation is adopted to discretize the energy variable E, or in an equivalent manner the lethargy variable u. A condensation procedure is applied to divide the energy domain into a finite set of energy groups, indexed with the letter g, in which the neutrons are supposed to behave as mono-kinetic particles. The integration of the Boltzmann equation over the range of each energy group leads to a system of one-speed neutron transport equations, known as multigroup equations:

$$\vec{\Omega} \cdot \vec{\nabla} \Psi^g(\vec{r}, \vec{\Omega}) + \Sigma^g(\vec{r}, \vec{\Omega}) \Psi^g(\vec{r}, \vec{\Omega}) = q^g(\vec{r}, \vec{\Omega}), \tag{2.13}$$

where we define the following multigroup quantities

$$\Psi^g(\vec{r}, \vec{\Omega}) = \int_{E_g}^{E_{g-1}} \Psi(\vec{r}, \vec{\Omega}, E)\, dE, \tag{2.14}$$

$$q^g(\vec{r}, \vec{\Omega}) = \int_{E_g}^{E_{g-1}} q(\vec{r}, \vec{\Omega}, E)\, dE, \tag{2.15}$$

$$\Sigma^g(\vec{r}, \vec{\Omega}) = \frac{\displaystyle\int_{E_g}^{E_{g-1}} \Sigma(\vec{r}, E) \Psi(\vec{r}, \vec{\Omega}, E)\, dE}{\displaystyle\int_{E_g}^{E_{g-1}} \Psi(\vec{r}, \vec{\Omega}, E)\, dE}. \tag{2.16}$$

Definitions (2.14) and (2.15) represent respectively the multigroup angular neutron flux and neutron source. It should be highlighted that through this integration in energy, the multigroup cross section defined in (2.16) has gained an unwanted dependence in the angular variable. This is commonly treated by using the scalar flux instead of the angular flux in Equation (2.16):

$$\Sigma^g(\vec{r}) = \frac{\displaystyle\int_{E_g}^{E_{g-1}} \Sigma(\vec{r}, E) \Phi(\vec{r}, E)\, dE}{\displaystyle\int_{E_g}^{E_{g-1}} \Phi(\vec{r}, E)\, dE}, \tag{2.17}$$

and by keeping in mind that this approximation will introduce errors in the calculation if it is not properly corrected later on. It is important to insist that all these multigroup quantities are here defined by the mean of the flux, which is the solution of the Boltzmann equation, and is thus yet unknown. The use of a weight function $f(E)$ to replace the real flux in the definition of the multigroup cross sections would introduce a large error, since the flux is both energy-dependent and space-dependent, and therefore specific to the core geometry. But in practice, it is the solution adopted to obtain a first approximation of the coefficients of the mono-kinetic transport equations:

$$\Sigma^g(\vec{r}) = \frac{\displaystyle\int_{E_g}^{E_{g-1}} \Sigma(\vec{r}, E) f(E)\, dE}{\displaystyle\int_{E_g}^{E_{g-1}} f(E)\, dE}. \tag{2.18}$$

The weight function $f(E)$ has to be carefully selected to represent as well as possible the neutron flux in a thermal reactor. At high energies (> 1.3 MeV), a fission spectrum is adopted. In the slowing-down domain, a function inversely proportional to the energy of the neutron is employed. Below 0.1 eV, the thermalization of neutrons with their surrounding nuclei is represented using a Maxwell spectrum. While this weight function is pretty close to the shape of the flux in a thermal nuclear reactor, it fails to represent the depressions of the flux in the vicinity of resonances of cross sections. The role of the self-shielding calculation is to correct the use of this inaccurate weight function in the generation of multigroup cross sections in the resonance domain.

Expansion of the transfer cross sections on the Legendre polynomials

The transfer cross section $\Sigma_s(\vec{r}, \vec{\Omega}' \cdot \vec{\Omega}, E' \rightarrow E)$ appears in the arrival term of the neutron transport equation. It denotes the probability per unit path traveled for a neutron at a position $\vec{r}$ to be scattered from a direction $\vec{\Omega}'$ to a new direction $\vec{\Omega}$, and from an energy E' to an energy E. The cosine of the scattering angle associated with this collision is noted $\mu = \vec{\Omega}' \cdot \vec{\Omega}$. It is common practice to expand the transfer cross section onto a truncated set of Legendre polynomials P_l:

$$\Sigma_s(\vec{r}, \vec{\Omega}' \cdot \vec{\Omega}, E' \rightarrow E) = \sum_{l=0}^{L} \frac{2l+1}{4\pi} \Sigma_{s,l}(\vec{r}, E' \rightarrow E) P_l(\mu), \tag{2.19}$$

with

$$\Sigma_{s,l}(\vec{r}, E' \rightarrow E) = 2\pi \int_{-1}^{1} \Sigma_s(\vec{r}, \mu, E' \rightarrow E) P_l(\mu)\, d\mu. \tag{2.20}$$

The addition theorem ensures that it is possible to develop the Legendre polynomials on the basis of the spherical harmonics Y_m^l:

$$P_l(\mu) = \sum_{m=-l}^{l} Y_m^l(\vec{\Omega}) Y_m^l(\vec{\Omega}'). \tag{2.21}$$

The left terms of the multigroup neutron transport equation (2.13) are left unchanged by this expansion, but the term on the right hand side can be re-written as:

$$q^g(\vec{r}, \vec{\Omega}) = \sum_{l=0}^{L} \frac{2l+1}{2} \sum_{m=-l}^{l} Y_m^l(\mu) \sum_{g'} \Sigma_{s,l}^{g' \rightarrow g}(\vec{r}) \Phi_m^{l,g'}(\vec{r}) + S^g(\vec{r}), \tag{2.22}$$

where we define the following angular moment of the neutron flux:

$$\Phi_m^{l,g}(\vec{r}) = \frac{1}{4\pi} \int_{4\pi} Y_m^l(\vec{\Omega}) \Psi^g(\vec{r}, \vec{\Omega})\, d\vec{\Omega}. \tag{2.23}$$

In a criticality calculation, where the term $S^g(\vec{r})$ is only composed of the fission sources, the multigroup transport equation becomes:

$$\vec{\Omega}\cdot\vec{\nabla}\Psi^g(\vec{r},\vec{\Omega})+\Sigma^g(\vec{r},\vec{\Omega})\Psi^g(\vec{r},\vec{\Omega})=\sum_{g'}\sum_{l=0}^{L}\frac{2l+1}{2}\Sigma_{s,l}^{g'\to g}(\vec{r})\sum_{m=-l}^{l}Y_m^l(\mu)\Phi_m^{l,g'}(\vec{r}) + \frac{1}{k_{eff}}\sum_x\frac{\chi_x^g(\vec{r})}{4\pi}\sum_{g'}\nu\Sigma_{f,x}^{g'}(\vec{r})\Phi^{g'}(\vec{r}). \tag{2.24}$$

Angular discretization

The expansion of the transfer cross section above-mentioned is only a preliminary step of the angular discretization of the variable $\vec{\Omega}$ of the neutron transport equation. There exist two main methods that will be described here.

Spherical Harmonics Method

The first discretization method of the angular variable is called the Spherical Harmonics Method, denoted the $\mathsf{P_N}$ method. It is the natural continuity of the transfer cross section expansion, as it consists in projecting the multigroup flux over a truncated set of spherical harmonics:

$$\Psi^g(\vec{r},\vec{\Omega})=\sum_{l=0}^{L}\sum_{m=-l}^{l}\Psi_m^{l,g}(\vec{r})Y_m^l(\vec{\Omega}). \tag{2.25}$$

This expression is injected into the mono-kinetic Boltzmann equation, leading to a linear system of differential equations strongly coupled in space. This method can be very expensive in computational time for highly anisotropic problems, where the order of the truncation L is elevated.

Discrete Ordinate Method

The second method for the discretization of the angular variable is the so-called Discrete Ordinate Method, noted $\mathsf{S_N}$. It consists in selecting a discrete set of values for the angular variables $\{\vec{\Omega}_n\}_{n=1,\dots,N}$, from which the quadrature formulas of the form

$$\int_{4\pi}f(\vec{\Omega})\,d\vec{\Omega}=\sum_{n=1}^{N}\omega_n f(\vec{\Omega}_n), \tag{2.26}$$

are derived, with f being any function dependent on the angular variable, and ω_n being the weight associated to the base point $\vec{\Omega}_n$. The multigroup neutron transport equation is solved for each of the N directions $\vec{\Omega}_n$:

$$\left[\vec{\Omega}_n\cdot\vec{\nabla}+\Sigma^g(\vec{r},\vec{\Omega}_n)\right]\Psi^g(\vec{r},\vec{\Omega}_n)=\sum_{l=0}^{L}\frac{2l+1}{2}\sum_{m=-l}^{l}Y_m^l(\vec{\Omega}_n)\sum_{g'}\Sigma_{s,l}^{g'\to g}(\vec{r})\Phi_m^{l,g'}(\vec{r})+S^g(\vec{r},\vec{\Omega}_n), \tag{2.27}$$

where the integral for the angular moment of the flux is discretized using the quadrature formula (2.26)

$$\begin{aligned}\Psi_m^{l,g}(\vec{r}) &= \int_{4\pi} Y_m^l(\vec{\Omega})\Psi^g(\vec{r},\vec{\Omega})\,d\vec{\Omega} \\ &= \sum_{n=1}^{N} \omega_n Y_m^l(\vec{\Omega}_n)\Psi^g(\vec{r},\vec{\Omega}_n).\end{aligned} \tag{2.28}$$

In the case of a local source, the S_N method suffers from what is known as the ray-effect phenomenon, which is a distortion of the spatial distribution of the neutron flux. This effect can be diminished by increasing the number of angular directions.

Spatial discretization: collision probability method

The last variable of the phase space needing to undergo the discretization process is the space variable $\vec{r}$. It is common to divide the geometry into smaller regions forming a spatial mesh, on which the neutron transport equation is solved. This has been the application subject of various methods [24], such as the Finite Difference Method or the Finite Element Method. The Method of Characteristics (MOC) [25] is very appreciated for large and complex geometries for its flexibility and precision, and because it does not require a meshing of the geometry into subdomains. The Collision Probability (CP) Method is still mostly employed in self-shielding calculations. The use of the CP method is mainly limited to small geometries because of its consequent computational time when applied to large geometries.

Collision Probability Method

The CP method is described in the case of isotropic scattering and sources [24] [26] [27]. The one-group integral equation for the scalar flux, derived from Equation (2.12), is

$$\begin{aligned}\Phi(\vec{r}) = 4\pi &\int_{\partial\mathcal{D}} |\vec{\Omega}_s \cdot \vec{n}|\, k(\vec{r},\vec{r}')\, \Psi_-(\vec{r}',\vec{\Omega}_s)\, dS \\ &+ \int_{\mathcal{D}} k(\vec{r},\vec{r}-s\vec{\Omega})\, q(\vec{r}-s\vec{\Omega})\, ds,\end{aligned} \tag{2.29}$$

where $\vec{n}$ is a unit vector normal to the surface of $\partial\mathcal{D}$, and $k(\vec{r},\vec{r}') = k(\vec{r}',\vec{r}) = \dfrac{e^{-\tau(\vec{r},s)}}{4\pi s^2}$, with $s = ||\vec{r}-\vec{r}'||$. The expression of the angular flux Ψ_- entering in the domain $\mathcal{D}$ through the surface S depends on the boundary condition. It can be formulated in a general approach as

$$\begin{aligned}\Psi_-(\vec{r},\vec{\Omega}) &= \Psi_0(\vec{r},\vec{\Omega}) \\ &+ \int_{\partial\mathcal{D}} dS' \int_{2\pi} d\Omega'\, \beta((\vec{r}',\vec{\Omega}') \to (\vec{r},\vec{\Omega}))\, \Psi_+(\vec{r}',\vec{\Omega}'),\end{aligned} \tag{2.30}$$

where Ψ_0 is the uncollided flux, the albedo β represents the reflection or the transmission coefficient at surface S' and Ψ_+ is the notation adopted for the angular flux exiting the domain $\mathcal{D}$:

$$\Psi_+(\vec{r},\vec{\Omega}) = e^{-\tau(\vec{r},s_b)}\Psi_-(\vec{r}_b,\vec{\Omega}) + \int_0^{s_b} s^2\, k(\vec{r},\vec{r}-s\vec{\Omega}) q(\vec{r}-s\vec{\Omega})\, ds. \tag{2.31}$$

The discretization of the spatial variable $\vec{r}$ is operating through the division of the domain $\mathcal{D}$ into a set of I homogeneous regions $\mathcal{D}_i$, of border $\partial\mathcal{D}_i$. On each of these regions, the cross sections

are considered spatially-independent, and the flat flux approximation leads to the use of a volume-averaged flux Φ_i in each region i. The volume integral on the whole domain of Equation (2.29) therefore becomes a sum over all the regions i of volume V_i, and the boundary condition becomes a sum over the surfaces S_b of area A_b. It is common to regroup similar regions into one, even if they are not adjacent, therefore reducing the effective size of the following system of equations, written in a compact form [27]:

$$\begin{cases} V\vec{\Phi} = P_{VV}\vec{Q} + P_{VS}\vec{J}_- \\ \vec{J}_+ = P_{SV}\vec{Q} + P_{SS}\vec{J}_- \\ \vec{J}_- = \vec{J}_0 + A\vec{J}_+ \end{cases} \tag{2.32}$$

V designates the diagonal matrix containing the volumes of each region, $\vec{\Phi}$ and $\vec{J}_\pm$ are the vectors of the scalar flux and the entering (-) and exiting (+) angular currents. Q is the matrix of the neutron emission density and A is the geometrical matrix, connecting the different domains, whose expression depends on the boundary conditions between the regions. P, P_{SV} and P_{VS} are matrices diagonal per bloc:

- P_{VV} is the collision matrix. Its coefficients are the collision probabilities P_{ij}:

$$P_{ij} = \int_{V_i}\int_{V_j} k(\vec{r},\vec{r}')\,dr'\,dr. \tag{2.33}$$

  The probability for a neutron, born uniformly and in an isotropic manner in a region j, to undergo its first collision in a region i, is calculated as $\dfrac{\Sigma_i P_{ij}}{V_j}$, with Σ_i the macroscopic total cross section of the region i.

- P_{SV} is the escape matrix, whose coefficients are:

$$P_{S_\alpha i} = \pi S_\alpha \int_i dr \int_\alpha |\vec{\Omega}'\cdot\vec{n}|\,k(\vec{r},\vec{r}')\,\Psi_{+,\alpha}(\vec{r}',\vec{\Omega})\,dS', \tag{2.34}$$

  with S_α being a surface on the border $\partial\mathcal{D}$.

- P_{VS} is the transpose of P_{SV}.

- P_{SS} is the transmission matrix, with coefficients

$$P_{S_\alpha S_\beta} = 4\pi^2 S_\alpha \int_\alpha dS \int_\beta |\vec{\Omega}\cdot\vec{n}|\,k(\vec{r},\vec{r}')\,\Psi_{+,\alpha}(\vec{r}',\vec{\Omega})\,\Psi_{-,\beta}(\vec{r}',\vec{\Omega})\,dS'. \tag{2.35}$$

The calculation of the coefficients of these matrices is a complicated problem. It is detailed in Reference [24] for some geometries on which the transport equation can be simplified, thanks to specific symmetries.

2.3.2 . Two-step deterministic calculations

Deterministic methods for the numerical simulations of reactors are thought as a compromise between accuracy and speed. Even with today computers' capability, it is still arduous to solve the Boltzmann equation finely discretized, in energy, angle and space, over the whole core geometry, as the number of unknown can easily reach thousands of billions [28]. The need arises for what is called a computational scheme, in order to balance effectiveness and fast calculation time.

APOLLO3® [29] [16] is a multipurpose deterministic nuclear code, developed in the frame of the neutronics simulation project of the DES ("Direction des Énergies") of the CEA, with the partnership and financial support of EDF and Framatome. Its modular organization encompasses both lattice and core codes.

This thesis work mainly focuses on the self-shielding module of the APOLLO3® lattice code.

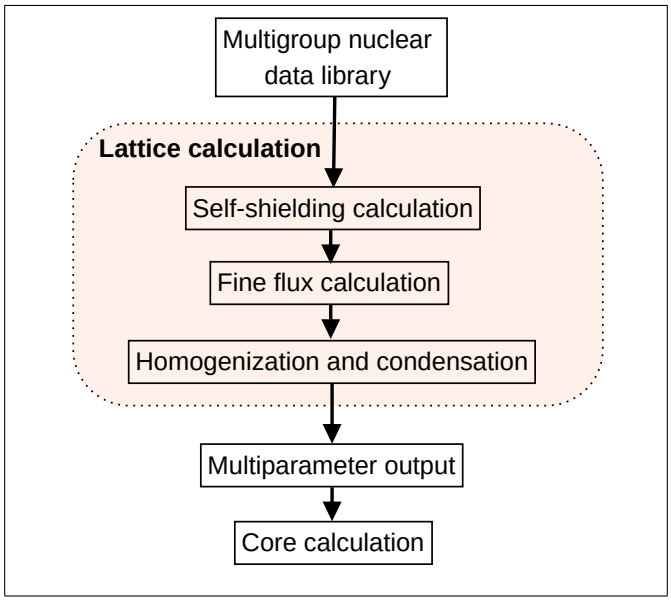

Figure 2.3: APOLLO3® two-step computational scheme for thermal reactor calculations

Multigroup nuclear data libraries

The APOLLO3® code does not take as input data the point-wise cross sections themselves, but the multigroup nuclear data libraries generated by the GALILEE processing system [17]. The creation of these multigroup libraries is actually realized once and for all for a given energy mesh and nuclear data evaluation. The input libraries for an APOLLO3® lattice calculation are:

- The multigroup cross sections computed using an approximated and geometry-independent weight function. They are called infinitely-diluted cross sections, or unself-shielded cross sections, as they do not take into account the local variations of the neutron flux in the vicinity of resonances.
- The mathematical probability tables per isotope per energy group. They provide the knowledge of the statistical variations of the resonant cross sections within an energy group.

- The mathematical probability tables per isotope on an ultra-fine group energy mesh, used to compute on-the-fly the mixture probability tables on the calculation multigroup mesh. This library also contains the correspondence between the ultra-fine group mesh and the energy mesh employed for the lattice calculation.
  The calculation and the role of the probability tables are further explained in Chapter 3.

- Some self-shielding methods, such as the fine-structure method (see Chapter 3 for a description of the self-shielding methods in APOLLO3®), require isotopic reference reaction rates tabulated on the temperature and the background dilution.

The multigroup nuclear data libraries are stored in an HDF5 file, where the cross sections are stored as array or matrices. They are generated for a list of temperatures ranging usually from 273K to 2974K; the data are read by interpolating between the two closest temperatures.

Lattice calculation

The lattice calculation consists of solving the neutron transport equation on a finely discretized heterogeneous geometry. Because this is a time expensive computation, the calculation is often carried out on a small portion of the core geometry, such as a fuel pin or a fuel assembly, and reflective boundary conditions are applied in all boundaries to simulate an infinite lattice of the same configuration, hence the name of this calculation step. Effective cross sections are derived from the lattice calculation and utilized to generate space-homogenized and energy-condensed cross sections preserving the reaction rates, stored in an external library to be used as input data for the core calculation.

The APOLLO3® lattice calculations are traditionally carried out on the SHEM-281 group energy structure [30] [31] or the LWR-383 group energy mesh, derived from the improved SHEM-361 group structure [32].

The existing self-shielding methods in the APOLLO3® code, all implemented in C++, are the subject of a more detailed inventory in the next chapter. For thermal reactor calculations, three main methods are implemented: the equivalence fine-structure method [2], inherited from the APOLLO2 lattice code, and the more recent fine-structure subgroup method [18] and Equivalent Dancoff-factor Cell method [19].

The flux solvers available for the lattice calculation are mainly implemented in C++ and Fortran 90. The IDT solver [33] [34] [35] relies on the method of short characteristics for Cartesian cells. The TDT-MOC solver applies the method of long characteristics for unstructured geometry meshes (TDT [25] [36]). The NYMO solver combines spherical harmonics and discontinuous Galerkin methods [37] to solve the transport equation on any type of geometry; it is worth noting that it can be used for both the lattice and the core calculations.

Homogenization and condensation

Despite the improvements of computer technologies, it is still not plausible today to carry out a precise transport calculation on a large and detailed three-dimensional geometry with a fine energy mesh and spatial discretization. Output cross sections undergo a space-homogenization and an energy-condensation process [38] in order to replace the heterogeneous components of the reactor

by homogeneous ones. The calculation of the homogeneous system results in accurate mean values, while the information on the heterogeneous system is lost.

Condensed and homogenized cross sections are stored in external files called Multiparameter Output (MPO). In practice, the MPO are not generated for a sole operating point; the lattice calculation is repeated for a selection of parameters (burn-up, boron concentration, moderator density and temperature, fuel temperature, etc.) in order to gather a description of the possible states of the reactor. The core calculation code then interpolates through the input MPO to obtain its entry data. The advantage of this technique is the great reduction in CPU time when carrying a full core calculation. Indeed, the lattice calculation is by far the limiting element in terms of computational time, but once the MPO is created, it does not need to be run again, leaving only the second step of the two-step computational scheme, namely the core calculation.

Core calculation

The core calculation solves the transport equation or its approached form (such as the diffusion equation) on the whole three dimensional core geometry. Because of the consequent size of the problem, the discretization in space and energy can not be as fine as in the lattice calculations. The use of the homogenized and condensed cross section library provided by the lattice calculation enables to erase any detail smaller than a fuel assembly or a fuel pin, while preserving the local reaction rates. The core calculation is often coupled to a thermal hydraulics solver to take into account the temperature and density feedbacks.

The choice of the core solver depends on the specificity of the problem. MINOS [39] solves the SP_N or diffusion approximations on a three dimensional geometry discretized with a structured mesh (cartesian or hexagonal). MINARET [40] solves the SP_N or P_N formulation of the neutron transport equation on an unstructured cylindrical geometry.

3 - State of the Art of the Self-shielding Methods for Thermal Reactor Calculations in the APOLLO3® Code

This chapter offers an overview of the existing self-shielding methods for thermal reactor calculations in APOLLO3®, highlighting the main advantages and weaknesses of each one of them. The methods for fast reactor calculations are not treated in this chapter, but an interested reader may refer to Reference [41] [42] for the subgroup method based on the ECCO [43] formalism, and to References [41] [5] for the Tone's method.

In the first section, the concept of Mathematical Probability Table (MPT) is described. Currently, all the APOLLO3® self-shielding methods are based on the MPTs. Quadrature formulas are derived from them to compute group-integrated quantities, such as the multigroup cross sections or reaction rates. The second section describes the fine-structure equation solvers of APOLLO3®, for heterogeneous and homogeneous geometries. The two subsequent sections present the self-shielding methods of APOLLO3® for thermal reactor calculations. The equivalence-based self-shielding method of APOLLO3® [44] [45], inherited from the APOLLO2 [26] fine-structure method [2] [3], and improved by taking into account the up-scattering and interference effects. Another class of self-shielding methods rely on the use of probability tables to represent the variations of resonant cross sections within an energy group. All the self-shielding methods are accompanied by a Superhomogenization (SPH) correction or a multigroup equivalence to fix the angular dependence of the cross section created by the multigroup approximation. The last section is a summary of the chapter.

3.1 . Mathematical Probability Tables

Probability tables are a manner of representing the fluctuations of the cross sections within an energy group g, using a discrete set of values $\{p_k^g, \sigma_k^g, \sigma_{\rho,x,k}^g\}_{k=1,\dots,K}$, with p_k^g being the probability for the cross section to be equal to σ_k^g, and for the partial cross section to be equal to $\sigma_{\rho,x,k}^g$. K is called the order of the probability table. The higher the order, the finer the representation of the cross section. To simplify the reading, the group index will be dropped from the notations in this section.

The development of the so-called mathematical probability tables in France was originally initiated by Pierre Ribon [13] in the CALENDF [46] code, based on the theory of the Padé approximants and of the Gauss quadrature formula. Considering a function whose dependence in lethargy is through the intermediary of the total cross section $\sigma(u)$, the following Riemann integral can be transformed into a Lebesgue integral:

$$\frac{1}{\Delta u^g}\int_g f(\sigma(u))\,du = \int_{D_g} p(\sigma)\,f(\sigma)\,d\sigma, \tag{3.1}$$

where $p(\sigma)$ is the cross section probability density in the group g, as shown in Figure 3.1, and $D_g = \{\sigma(u),\, u \in g\}$ is the notation employed to described the set of values reached by the cross section. The probability density can be approximated by a series of Dirac functions

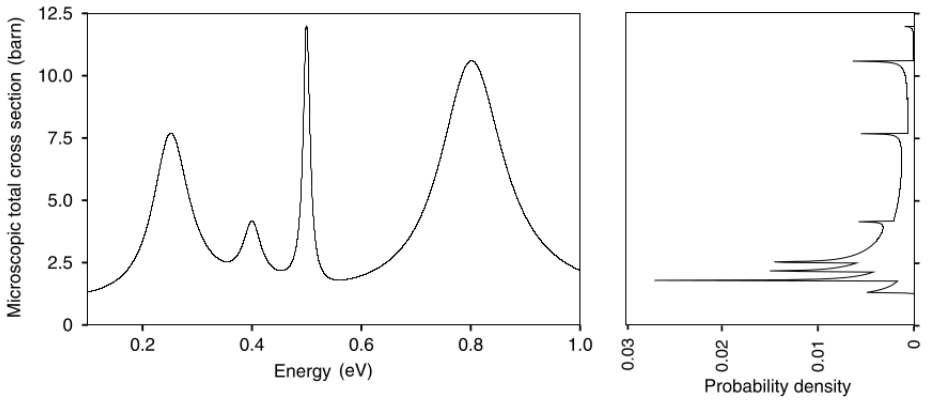

Figure 3.1: Probability density of a resonant total cross section (from [14])

$$p(\sigma) \approx \sum_{k=1}^{K} p_k \delta(\sigma - \sigma_k), \tag{3.2}$$

enforcing the criteria $\sum_{k=1}^{K} p_k = 1$. The integral in Equation (3.1) can be reformulated as:

$$\begin{aligned} \int_{D_g} p(\sigma)\, f(\sigma)\, d\sigma &\approx \sum_{k=1}^{K} p_k \int_{D_g} f(\sigma)\delta(\sigma - \sigma_k)\, d\sigma \\ &= \sum_{k=1}^{K} p_k f(\sigma_k). \end{aligned} \tag{3.3}$$

In short, we have established the following quadrature formula of order K to numerically compute the group-averaged value of f, whose dependence in lethargy is only operated through the value of σ:

$$\frac{1}{\Delta u^g} \int_g f(\sigma(u))\, du \approx \sum_{k=1}^{K} p_k f(\sigma_k). \tag{3.4}$$

Subsequently, we present the calculation of the parameters for this type of integrals, using the formalism of the MPTs. The calculation of the MPT parameters, first for a single isotope, then for a resonant mixture, is detailed.

3.1.1 . Calculation of the mathematical probability table for a single isotope

The computation process of a MPT of order K is divided into two distinct steps [13] [3]. The first one consists in finding the probabilities p_k and base points σ_k of expression (3.4) for the total cross section. The MPT is then completed by adding the base points for the partial cross sections $\sigma_{\rho,x,k}$.

Mathematical probability table for the total cross section

The MPTs are meant to preserve a mathematical property of the total cross section within an energy group g, namely the n^{th} moments $\mathcal{M}_n$ of the point-wise cross section, defined as

$$\mathcal{M}_n = \int_{D_g} p(\sigma)\sigma^n \, d\sigma, \tag{3.5}$$

where n is an integer. With a MPT of order K, this integral can be approximately computed as a discrete sum:

$$\mathcal{M}_n \approx \sum_{k=1}^{K} p_k \sigma_k^n, \tag{3.6}$$

with the weight p_k and base points σ_k being unknowns at this point. This represents $2K$ unknowns to be determined. By writing the relation (3.6) for $2K$ values of $\mathcal{M}_n$, a non linear system of equations is constructed. In Reference [13], it is suggested that both negative and positive values of n should be employed in order to represent accurately both the peaks and sinks of the cross section. The integer n is chosen to take all the values between L and $2K + L - 1$, with L being the first moment preserved. In Reference [3], L is taken equal to $1 - K$. The moment of order 0, that is to say for $n = 0$, is associated to the probability density normalization criteria

$$\mathcal{M}_0 = \int_{D_g} p(\sigma) \, d\sigma = 1. \tag{3.7}$$

The moment of order 1 translates the preservation of the averaged value of the total cross section in the group g:

$$\mathcal{M}_1 = \frac{1}{\Delta u^g} \int_g \sigma(u) \, du = \langle \sigma \rangle^g. \tag{3.8}$$

The non linear system is not directly solved for the unknown probabilities and base points. The generating function of the moments can be expanded around $z = 0$ using a Maclaurin series:

$$\begin{aligned} F_L(z) &= \int_{D_g} \frac{p(\sigma)\sigma^L}{1 - z\sigma} d\sigma \\ &= \int_{D_g} p(\sigma)\sigma^L \left[1 + z\sigma + (z\sigma)^2 + ... + (z\sigma)^{2K-1} + \mathcal{O}(z^{2K})\right] d\sigma \\ &= \sum_{k=0}^{2K-1} z^k \mathcal{M}_{L+k} + \mathcal{O}(z^{2K}) \end{aligned} \tag{3.9}$$

The Taylor polynomial is represented by a Padé approximant, which basically is a fraction of two polynomials, with $2K - 2$ unknown coefficients:

$$\sum_{k=0}^{2K-1} z^k \mathcal{M}_{L+k} = \frac{a_0 + a_1 z + ... + a_{K-1} z^{K-1}}{b_0 + b_1 z + ... + b_{K-1} z^{K-1} + z^K} + \mathcal{O}(z^{2K}). \tag{3.10}$$

Two linear systems of equations can be derived from Equation (3.10), by multiplying both sides of the equation by the denominator of the Padé approximant, and by neglecting all the terms with power of z greater than $2K - 1$. The first one

$$\begin{cases} 0 &= b_0\,\mathcal{M}_{L+K} + b_1\,\mathcal{M}_{L+K-1} + ... + b_{K-1}\,\mathcal{M}_{L+1} + \mathcal{M}_L \\ 0 &= b_0\,\mathcal{M}_{L+K+1} + b_1\,\mathcal{M}_{L+K} + ... + b_{K-1}\,\mathcal{M}_{L+2} + \mathcal{M}_{L+1} \\ & ... \\ 0 &= b_0\,\mathcal{M}_{L+2K-1} + b_1\,\mathcal{M}_{L+2K-2} + ... + b_{K-1}\,\mathcal{M}_{L+K} + \mathcal{M}_{L+K-1} \end{cases} \tag{3.11}$$

can be solved for the coefficients $\{b_k\}_{k=0,...,K-1}$, which are then replaced in the following system

$$\begin{cases} a_0 &= b_0\,\mathcal{M}_L \\ a_1 &= b_0\,\mathcal{M}_{L+1} + b_1\,\mathcal{M}_L \\ & ... \\ a_{K-1} &= b_0\,\mathcal{M}_{L+K-1} + b_1\,\mathcal{M}_{L+K-2} + ... + b_{K-1}\,\mathcal{M}_L \end{cases} \tag{3.12}$$

to retrieve the coefficients $\{a_k\}_{k=0,...,K-1}$.

It can be shown, denoting $\{z_k\}_{k=1,...,K}$ the roots of the polynomial at the denominator of (3.10), that the base points for the total cross sections are given by the relation:

$$\sigma_k = \frac{1}{z_k}, \quad \text{for } k = 1, ..., K. \tag{3.13}$$

The theory of Gaussian quadrature and orthogonal polynomials actually ensures that the z_i are all simple roots [47]. It is also established that the σ_k all lie in the support of the total cross section, meaning that all σ_k belong to D_g. Using these newly computed σ_k to write Equation (3.6) for the $2K$ values of n, a linear system of equations is obtained, with the probabilities p_k as unknowns. There are $2K$ equations for only K unknowns. Because the Gauss quadrature associated to a weight function is unique, it is assured that this linear system possesses an unique solution. It can either be obtained by using a least square method, or by selecting K independent equations.

Mathematical probability table for the partial cross sections

The definition of MPTs for the partial cross sections is not as straightforward as for the total cross section. It needs to enforce that the sum of all the partial cross sections is equal to the total cross section

$$\sigma_k = \sum_\rho \sigma_{\rho,k}, \quad \text{for } k = 1, ..., K. \tag{3.14}$$

and would share the same probabilities p_k as the total cross section. As Paul Reuss observed in [48], the partial cross sections always intervene linearly in neutronics, in integrals of the form

$$\frac{1}{\Delta u^g} \int_g \sigma_\rho(u)\, f(\sigma(u))\, du = \int_{D_g} \int_{D_{\rho,g}} \sigma_\rho\, f(\sigma)\, \Pi(\sigma_\rho, \sigma)\, d\sigma_\rho d\sigma, \tag{3.15}$$

where $D_{\rho,g} = \{\sigma_\rho(u),\, u \in g\}$ and $\Pi(\sigma_\rho, \sigma)$ is the conditional probability density of σ and σ_ρ. Using this conditional probability density will lead to the calculation of base points $\sigma_{\rho,k}$ defined in such a way that σ_ρ will be approximately equal to $\sigma_{\rho,k}$, knowing that σ is approximately equal to σ_k, with a probability p_k. Integrals such as (3.15) would be discretized by means of a quadrature formula:

$$\frac{1}{\Delta u^g}\int_g \sigma_\rho(u)\, f(\sigma(u))\, du \approx \sum_{k=1}^{K} p_k\, \sigma_{\rho,k}\, f(\sigma_k). \tag{3.16}$$

Similarly to the calculation procedure of the MPT for the total cross section, the moments of the partial cross sections are defined:

$$\mathcal{P}_{\rho,n} = \frac{1}{\Delta u^g}\int_{D_{\rho,g}} \sigma_\rho(u)\, \sigma^n(u)\, du \tag{3.17}$$

A linear system of equations can be constructed by writing the quadrature formula corresponding to (3.17) for K values of the integer n:

$$\mathcal{P}_{\rho,n} = \sum_{k=1}^{K} p_k \sigma_{\rho,k}\, \sigma_k^n. \tag{3.18}$$

This time, only K values of moments are required because only the K base points of the partial cross sections have to be calculated. The selected values of n are located between J and $J+K-1$, with J an integer that has to be chosen between $L-1$ and $L-1+K$ for the criteria (3.14) to be valid. In practice, J is set to $\lfloor -\frac{N}{2} \rfloor$ [3], where $\lfloor x \rfloor$ designates the floor function applied to the real number x. The probabilities p_k being already known at this stage of the computation, the only unknowns of Equation (3.18) are the $\sigma_{\rho,k}$.

3.1.2 . Mathematical probability tables for a resonant mixture

In the previous subsection, the parameters of the MPT for a single resonant isotope are derived. In this subsection, we will now assume that the material is composed of a mixture of different resonant isotopes, indexed with the letter x, ranging from 1 to X. We will demonstrate the computation of the weights and base points of the MPT by treating the mixture as a single isotope. The total cross section in this subsection therefore designates the whole mixture total cross section, expressed as the sum of the absorption and scattering cross sections of every isotope, weighted by their proportions a_x:

$$\sigma = \sum_x a_x \left(\sigma_{a,x} + \sigma_{s,x}\right). \tag{3.19}$$

The quantities $a_x \sigma_{\rho,x}$ will be treated as partial cross sections of this composing isotope.

It is supposed that the single-isotope MPTs are known for each isotope present in the resonant mixture. They are noted $\{p_{x,k}, \sigma_{x,k}, \sigma_{\rho,x,k}\}_{k=1,...,K_x}$, for $x = 1, ..., X$. Let us point out that they may not share the same order, as K_x is an integer specific to the isotope x.

The moments of the point-wise total cross section of the resonant mixture, within an ultra-fine energy group g, are defined with the relation

$$\mathcal{M}_n = \frac{1}{\Delta u^g}\int_g \sigma^n(u)\, du, \tag{3.20}$$

with n being an integer. Denoting $\sigma_x = \sum_\rho a_x \sigma_{\rho,x}$ the total cross section of isotope x (but still a partial cross section of the mixture), this integral can be expressed through a change of variable as a Lebesgue integral

$$\mathcal{M}_n = \int_{D_g} \left(\vec{a}^T . \vec{\sigma}\right)^n \Pi(\vec{\sigma})\, d\vec{\sigma}, \tag{3.21}$$

where the following notation has been used:

$$\vec{\sigma} = \begin{pmatrix} \sigma_1 \\ \vdots \\ \sigma_x \\ \vdots \\ \sigma_X \end{pmatrix}, \quad \vec{a} = \begin{pmatrix} a_1 \\ \vdots \\ a_x \\ \vdots \\ a_X \end{pmatrix}, \quad D_g = \{D_{g_1} \times ... \times D_{g_X}\},$$

where D_{g_x}, for x between 1 and X, is the support of the total cross section of the isotope x, and $\Pi(\vec{\sigma})$ is the conditional probability density of the total cross sections of all the isotopes of the mixture. This probability density can be simplified as the product of the marginal distribution of the total cross section of each isotope, under the assumption that they are independent of each other:

$$\Pi(\vec{\sigma}) = \prod_{x=1}^{X} p(\sigma_x). \tag{3.22}$$

This hypothesis, known as the "statistical hypothesis", is only valid on a very fine energy discretization. When this assumption is valid, the expression of the point-wise moment (3.21) can be re-written in an approximate discrete form as:

$$\mathcal{M}_n \approx \sum_{k_1=1}^{K_1} ... \sum_{k_X=1}^{K_X} \left(\sum_{x=1}^{X} a_x \sigma_{x,k_x} \right)^n \prod_{x=1}^{X} p_{x,k_x}. \tag{3.23}$$

From Equation (3.23), the moment of order n of the total cross section of the resonant mixture can be calculated. It is then utilized as a regular total point-wise moment to compute the corresponding MPT of the mixture, according to the process described in the first subsection.

The treatment for the partial cross sections of the resonant mixture requires to define a partial moment, expressed with the single-isotope MPTs parameters. The partial moment of order n for the resonant mixture in an ultra-fine energy group g is

$$\mathcal{P}^n_{\rho,x} = \frac{1}{\Delta u^g} \int_g a_x\, \sigma_{\rho,x}(u)\, \sigma^n(u)\, du. \tag{3.24}$$

Similarly as for the mixture total cross section, and under the same assumption of "statistical hypothesis", a discrete relation can be derived:

$$\mathcal{P}^n_{\rho,x} \approx \sum_{k_1=1}^{K_1} ... \sum_{k_X=1}^{K_X} a_x \sigma_{\rho,x,k_x} \left(\sum_{x=1}^{X} a_x \sigma_{x,k_x} \right)^n \prod_{x=1}^{X} p_{x,k_x}. \tag{3.25}$$

This equation provides a relation to compute the partial moments of order n of the resonant mixture using the single-isotope MPTs. Then the partial moments can be employed to compute the partial cross sections base points for the mixture MPT, as was shown in the previous subsection.

3.2 . Fine-Structure Equation Solvers

This section describes the theory of the solvers of the APOLLO3® code utilized to compute reaction rates in either a heterogeneous or a homogeneous geometry, by solving the fine-structure equation. The solution is obtained by means of a subgroup method based on the mixture mathematical probability tables, and of a model to approximate the resonant scattering operator. The solvers account for the up-scattering treatment, and the resonance interference treatment is accounted for by the use of the mixture MPTs to compute group-integrated quantities. The reaction rates can be computed with this heterogeneous solver for any energy discretization.

3.2.1 . Description of the heterogeneous fine-structure equation solver

For a heterogeneous problem, the collision probability equation reads

$$\Sigma_i V_i \Phi_i(u) = \sum_j P_{ij} V_j \left[R_{0j} \Phi_j(u) + R_{1j} \Phi_j(u) \right] \tag{3.26}$$

where i and j are region indexes, P_{ij} is the collision probability, and V_i is the volume of the region i. The indexes 0 and 1 designate the resonant isotopes and moderator isotopes, respectively. $R_{0j}\Phi_j$ and $R_{1j}\Phi_j$ are therefore the resonant and moderating scattering operators in the region j, respectively. Φ_i is the scalar neutron flux in the region i. The flat flux approximation is applied to each self-shielding region α, containing the regions having a similar resonant mixture and localization, leading to the relation:

$$\Phi_i = \Phi_\alpha \text{ if } i \in \alpha. \tag{3.27}$$

It is assumed that the flux can be factorized as the product of two functions. The first one, called the macroscopic flux χ, is a smooth and regular function of lethargy. It is defined as

$$\chi_i(u) = \frac{R_{1i}\Phi_i}{\Sigma_{s1i}}, \tag{3.28}$$

where Σ_{s1i} is the macroscopic scattering cross section of the moderator isotopes in the region i. The second function is called the fine-structure factor φ and contains the resonant shape of the flux. The neutron flux can then be expressed as

$$\Phi_i = \chi_i(u)\varphi_i(u). \tag{3.29}$$

The fine-structure approximation consists of supposing that the macroscopic flux can be extracted from the resonant scattering operator

$$R_{0i}\left[\chi_i(u)\varphi_i(u)\right] \approx \chi_i(u) R_{0i}\varphi_i(u). \tag{3.30}$$

It is also supposed to be space-independent

$$\chi_i(u) \approx \chi(u). \tag{3.31}$$

Inserting Equation (3.29) into Equation (3.26), and applying the assumptions (3.30) and (3.31), the following fine-structure equation for a heterogeneous geometry is obtained:

$$\Sigma_i V_i \varphi_i(u) = \sum_j P_{ij} V_j \left[N_{0j} r_{0j} \varphi_j(u) + \Sigma_{s1j} \right], \tag{3.32}$$

where N_{0j} is the density of resonant isotopes in the region j, and r_{0j} is the microscopic resonant scattering operator in the same region. In the first implementation of the FSM in the APOLLO3® code, the fine-structure equation (3.32) was solved using the Direct Method developed by Coste [27] [3]; the Improved Direct Method (IDM) [45] was later implemented, leading to a decrease of the size of the matrices to be stored in memory and inverted during the calculation. The IDM requires to write the fine-structure equation in a matrix-vector form:

$$\vec{\varphi}(u) = C(u) r_0 \vec{\varphi}(u) + \vec{S}(u), \tag{3.33}$$

where $\vec{\varphi}$ and $r_0\vec{\varphi}$ are vectors of dimension N_α, the number of self-shielding regions. $\vec{S}$ is also a vector of the same dimension, with its elements being:

$$S_\alpha(u) = \frac{\sum_{i\in\alpha} \sum_j P_{ij}(u) V_j \Sigma_{s1j}}{\sum_{i\in\alpha} V_i \left[\Sigma_{1i} + \sum_x N_{0x,i} \sigma_{0x,i} \right]}. \tag{3.34}$$

$N_{0x,i}$ is the density of the resonant isotope x in the region i, and $\sigma_{0x,i}$ is its microscopic total cross section. The $(N_\alpha \times N_\alpha)$ matrix C is defined as

$$C_{\alpha\beta}(u) = \frac{\sum_{i\in\alpha} \sum_{j\in\beta} P_{ij}(u) V_j N_{0j}}{\sum_{i\in\alpha} V_i \left[\Sigma_{1i} + \sum_x N_{0x,i} \sigma_{0x,i} \right]}. \tag{3.35}$$

The constant source approximation is applied to the scattering source within each energy group g:

$$\begin{aligned} r_0\vec{\varphi}(u) &\approx \langle r_0\vec{\varphi} \rangle^g \quad \text{if } u \in g \\ &= \frac{1}{\Delta u^g} \int_g r_0 \vec{\varphi}(u) du. \end{aligned} \tag{3.36}$$

Consequently, the General Resonance (GR) model [3] is applied:

$$\begin{aligned} \langle r_0\vec{\varphi} \rangle^g &\approx r_0 \vec{\varphi}^{\,GR,g} \\ &= \sum_x \sum_{g'} A_x P_x^{g'\to g} \langle \vec{\tau}_{s,0x}^{GR} \rangle^{g'}, \end{aligned} \tag{3.37}$$

with A_x being a diagonal matrix containing the proportions of the resonant isotope x in the resonant mixture in each self-shielding region $a_{0x,\alpha} = \frac{N_{0x,\alpha}}{N_{0,\alpha}}$. $P_x^{g'\to g}$ is a diagonal matrix whose elements are the $p_{0x}^{g'\to g}$, defined as the probability for a neutron to scatter from a group g' to the group g by

colliding on a resonant isotope x.

In the Equation (3.37), let us separate the contributions of the groups g' with respect to their position to the group g:

$$r_0\vec{\varphi}^{\,GR,g} = \sum_x A_x \left[\sum_{g'<g} P_x^{g'\to g} \langle \vec{\tau}_{s,0x}^{\,GR} \rangle^{g'} + P_x^{g\to g} \langle \vec{\tau}_{s,0x}^{\,GR} \rangle^{g} + \sum_{g'>g} P_x^{g'\to g} \langle \vec{\tau}_{s,0x}^{\,GR} \rangle^{g'} \right] \tag{3.38}$$

During the self-shielding calculation, the orders are treated from high energy to low energy, that is to say in the order of increasing g, meaning that the down-scattering sources (for $g' < g$) are known. The contribution due to the self-scattering source have to be calculated. The mean scattering rate in the group g is expressed as

$$\langle \vec{\tau}_{s,0x}^{\,GR} \rangle^{g} = \frac{1}{\Delta u^g} \int_g \sigma_{s,0x}(u) \vec{\varphi}^{\,GR}(u) du, \tag{3.39}$$

where $\sigma_{s,0x}(u)$ is also a diagonal matrix, with $\sigma_{s,0x,\alpha}(u)$ as coefficients. Inserting Equations (3.33) and (3.37) in (3.39), the expression of the scattering rate in the group g can be derived:

$$\begin{aligned} \langle \vec{\tau}_{s,0x}^{\,GR} \rangle^{g} = & \left[I - \sum_x A_x P_x^{g\to g} \frac{1}{\Delta u^g} \int_g \sigma_{s,0x}(u) C(u)\, du \right]^{-1} \\ & \times \left[\sum_x A_x P_x^{g\to g} \frac{1}{\Delta u^g} \int_g \sigma_{s,0x}(u) C(u) \sum_{g'\neq g} P_x^{g'\to g} \langle \vec{\tau}_{s,0x}^{\,GR} \rangle^{g'}\, du \right. \\ & \left. + \sum_x A_x P_x^{g\to g} \frac{1}{\Delta u^g} \int_g \sigma_{s,0x}(u) \vec{S}(u)\, du \right] \end{aligned} \tag{3.40}$$

with I being the identity matrix. Equation (3.40) gives the contribution of the self-scattering source. The up-scattering term (for $g' > g$) are not known when the group g is being computed. The use of another resonant scattering model to decouple the sources is thus necessary. The Statistical (ST) model [3] [44] is chosen to approximate the scattering rates in the concerned energy groups:

$$\begin{aligned} \langle r_0\vec{\varphi} \rangle^{g'} &\approx r_0\vec{\varphi}^{\,ST,g'} \quad \text{if } g' > g \\ &= \sum_x A_x \langle \vec{\tau}_{s,0x}^{\,ST} \rangle^{g'}. \end{aligned} \tag{3.41}$$

The ST model is a special case of the GR model, where the contributions coming from other energy groups are supposed to be zero. The expression of the scattering rate using this model is:

$$\begin{aligned} \langle \vec{\tau}_{s,0x}^{\,ST} \rangle^{g} = & \left[I - \sum_x A_x \frac{1}{\Delta u^g} \int_g \sigma_{s,0x}(u) C(u)\, du \right]^{-1} \\ & \times \left[\sum_x A_x \frac{1}{\Delta u^g} \int_g \sigma_{s,0x}(u) \vec{S}(u)\, du \right]. \end{aligned} \tag{3.42}$$

In Equations (3.40) and (3.42), the quadrature formulas derived from the MPTs presented in section 3.1 of this chapter are employed to compute the group-averaged quantities

$$\frac{1}{\Delta u^g}\int_g \sigma_{s,0x}(u)C(u)\,du = \sum_{k=1}^{K} p_k^g \sigma_{s,x,k}^g C_k^g, \tag{3.43}$$

$$\frac{1}{\Delta u^g}\int_g \sigma_{s,0x}(u)\vec{S}(u)\,du = \sum_{k=1}^{K} p_k^g \sigma_{s,x,k}^g \vec{S}_k^g, \tag{3.44}$$

where C_k^g and $\vec{S}_k^g$ are the values of the matrix C and of the vector $\vec{S}$ when replacing the microscopic total cross section in the expression of their coefficients with the base point for the total cross section σ_k^g. The scattering operator ${r_0\vec{\varphi}}^{GR,g}$ can be computed by inserting Equations (3.40) and (3.42) in (3.38). It is then used in Equation (3.33) to retrieve the flux ${\vec{\varphi}}^{GR}(u)$. The reaction rates are then computed as

$$\vec{\tau}_{\rho,0x}^g = \int_g \sigma_{\rho,0x}(u){\vec{\varphi}}^{GR}(u)\,du, \tag{3.45}$$

where $\sigma_{\rho,0x}(u)$ is a diagonal matrix containing the resonant cross sections for a nuclear reaction ρ in every self-shielding region $\sigma_{\rho,0x,\alpha}(u)$. This integral is also calculated using a quadrature formula derived from the MPTs.

3.2.2 . Description of the homogeneous fine-structure equation solver

This subsection gives a description of the solver of APOLLO3® utilized to solve the fine-structure equation and compute the reaction rates of an IHM. The up-scattering is accounted for. This homogeneous solver is also based on the subgroup formalism, as the group-integrated quantities are calculated with the mixture MPTs.

Let us consider an IHM, in which the slowing-down equation is written:

$$\left[\Sigma_0(u) + \Sigma_1\right]\Phi(u) = R_0\Phi(u) + R_1\Phi(u), \tag{3.46}$$

with Σ_0 and Σ_1 being the macroscopic total cross section for the resonant isotopes and moderating isotopes, respectively. Similarly as in the heterogeneous case previously described, the fine-structure approximation is applied, leading to the fine-structure equation for an IHM:

$$\left[\sigma_0(u) + \sigma_b\right]\varphi(u) = {\vec{a_0}}^T r_0\vec{\varphi}(u) + \gamma_b\sigma_b, \tag{3.47}$$

where σ_0 is the microscopic total cross section of the resonant mixture, $\sigma_b = \dfrac{\Sigma_1}{N_0}$ is the background dilution, and $\gamma_b = \dfrac{\Sigma_{s1}}{\Sigma_1}$ is a parameter characterizing the scattering power of the moderator, with Σ_{s1} being its macroscopic scattering cross section, and ${\vec{a_0}}^T$ is the vector $(a_{01}, ..., a_{0x}, ...)$ containing the proportions of each resonant isotope in the mixture, with $a_{0x} = \dfrac{N_{0x}}{N_0}$. The same model as for the heterogeneous geometry is employed to approximate this resonant scattering operator, that is to say the GR model:

$$\begin{aligned} r_0\vec{\varphi}(u) &\approx \langle r_0\vec{\varphi}\rangle^g \quad \text{for } u \in g \\ &\approx {r_0\vec{\varphi}}^{GR,g} \end{aligned} \tag{3.48}$$

with

$$\begin{aligned} r_0\vec{\varphi}^{\,GR,g} &= \sum_{g'} P^{g'\to g}\langle\vec{\tau}_{s0}^{\,GR}\rangle^{g'} \\ &= \sum_{g'<g} P^{g'\to g}\langle\vec{\tau}_{s0}^{\,GR}\rangle^{g'} + P^{g\to g}\langle\vec{\tau}_{s0}^{\,GR}\rangle^{g} + \sum_{g'>g} P^{g'\to g}\langle\vec{\tau}_{s0}^{\,GR}\rangle^{g'} \end{aligned} \tag{3.49}$$

$P^{g'\to g}$ is a diagonal matrix, with the probabilities of transfer per isotope $p_x^{g'\to g}$ on its diagonal, and $\langle\vec{\tau}_{s0}^{\,GR}\rangle^{g}$ is the scattering rate in the group g:

$$\langle\vec{\tau}_{s0}^{\,GR}\rangle^{g} = \frac{1}{\Delta u^g}\int_g \vec{\sigma_{s0}}(u)\varphi^{GR}(u)du, \tag{3.50}$$

with $\vec{\sigma}_{s0}(u)$ is the vector containing the scattering cross sections per isotope $\sigma_{s,0x}(u)$. From Equations (3.47), (3.48), (3.49) and (3.50), the expression of the scattering rate can be derived:

$$\langle\tau_{s0}^{GR}\rangle^{g} = \langle\vec{I}_{s0}\rangle^{g} \times \frac{\sum_{g'\neq g}\vec{a}_0^{\,T}P^{g'\to g}\langle\vec{\tau}_{s0}^{\,GR}\rangle^{g'} + \gamma_b\sigma_b}{1-\vec{a}_0^{\,T}P^{g\to g}\langle\vec{I}_{s0}\rangle^{g}}, \tag{3.51}$$

where the following notation has been employed:

$$\langle\vec{I}_{s0}\rangle^{g} = \frac{1}{\Delta u^g}\int_g \frac{\vec{\sigma}_{s0}(u)}{\sigma_0(u)+\sigma_b}\,du. \tag{3.52}$$

Since the groups are treated in increasing order, the down-scattering terms of Equation (3.49) are known. The self-scattering term is deduced from the expression of the scattering term given in Equation (3.51). Only the up-scattering term is left to compute. The contributions from the up-scattering are determined using the ST model, as it has been done in the heterogeneous solver:

$$\begin{aligned} r_0\vec{\varphi}^{\,GR,g} &\approx r_0\vec{\varphi}^{\,ST,g} \quad \text{if } g'>g. \\ &= \langle\vec{\tau}_{s0}^{\,ST}\rangle^{g'} \end{aligned} \tag{3.53}$$

The expression of the scattering source in the group g' becomes:

$$\langle\vec{\tau}_{s0}^{\,ST}\rangle^{g'} = \langle\vec{I}_{s0}\rangle^{g'} \times \frac{\gamma_b\sigma_b}{1-\vec{a}_0^{\,T}\langle\vec{I}_{s0}\rangle^{g'}}. \tag{3.54}$$

The resonant scattering operator is then calculated combining Equations (3.54), (3.51) and (3.49). It is then inserted in the fine-structure equation (3.47) to derive the flux φ^{GR}. This flux can then be substituted in the expression of partial reaction rates

$$\tau_{\rho,0x}^{g} = \int_g \sigma_{\rho,0x}(u)\varphi^{GR}(u)\,du \tag{3.55}$$

and the integral is computed using a quadrature formula derived from the MPTs.

3.3 . Equivalence-based Fine-Structure Method

The Fine-Structure Method (FSM) of APOLLO3® [44] [45] is based on a double equivalence procedure derived from the legacy Livolant-Jeanpierre self-shielding method [2] [3] of APOLLO2. The reaction rates of a heterogeneous geometry are computed in the first step, called the heterogeneous-homogeneous equivalence. The multigroup equivalence then iteratively computes the multigroup cross sections preserving those reaction rates.

3.3.1 . Heterogeneous-homogeneous equivalence

Let us consider a heterogeneous geometry, divided into self-shielding regions denoted with the index α. The objective of the heterogeneous-homogeneous equivalence is to compute, for each region α and each resonant energy group g the multigroup reaction rate

$$\tau^g_{\rho,x,\alpha} = \int_g \sigma_{\rho,x}(u)\phi_\alpha(u)du \tag{3.56}$$

where ρ designates the type of nuclear reaction, and x the resonant isotope. Because approximations are employed in the heterogeneous multigroup calculation, the equivalence with an Infinite Homogeneous Medium (IHM) where the reaction rates are known without approximations is required.

This first equivalence procedure is divided into three calculation steps. First, approximated reaction rates are computed on the coarse energy structure in the heterogeneous geometry, by using a resonant scattering model and a rather coarse energy discretization, from 172 up to 281 groups, to solve the fine-structure equation. For each self-shielding region, the fine-structure equation in an IHM is then solved using the same energy mesh and resonant scattering model. The background dilution of this IHM is adjusted to preserve the heterogeneous reaction rates; this equivalent dilution is finally employed to read by interpolation an external library containing reference homogeneous rates tabulated in an ultra-fine-group mesh without any approximation of the resonant scattering operator, provided by the GALILEE nuclear data processing system [17].

Equivalence between a heterogeneous region and an infinite homogeneous medium

In the first step of the self-shielding calculation, the multigroup reaction rates are computed in the heterogeneous geometry, using the heterogeneous fine-structure equation solver of section 3.2.1. They are approximated rates, as they have been obtained through the use of the GR model for the resonant scattering source and on a coarse energy mesh. They are noted $\tau^{GR,g,het}_{\rho,x,\alpha}$.

For each self-shielding region of the heterogeneous geometry, a series of IHM calculations is carried out with the homogeneous fine-structure solver of section 3.2.2 for a set of background dilutions $\{\sigma_{b,m}\}_{m=1,..,M}$. The homogeneous solver renders the rates $\{\tau^{GR,g,hom}_{\rho,x}(\sigma_{b,m})\}_{m=1,..,M}$.

The heterogeneous-homogeneous equivalence procedure enforces the preservation of the absorption rates, that is to say that for each resonant energy group g and each resonant isotope x, an equivalent background dilution $\sigma^g_{b,x,\alpha}$ has to be found so that

$$\tau^{GR,g,hom}_{a,x}(\sigma^g_{b,x,\alpha}) = \tau^{GR,g,het}_{a,x,\alpha}. \tag{3.57}$$

The equivalent background dilution is found by the secant method. It is then used to read by interpolation an external library containing "exact" reaction rates calculated in an IHM without any

modelization of the resonant scattering operator. In the case of a resonant mixture, the reaction rates are calculated on-the-fly by using the homogeneous fine-structure equation solver with an ultra-fine-group mesh for the dilution $\sigma^g_{b,x,\alpha}$. These reaction rates, noted $\tau^{g,hom}_{\rho,x}(\sigma^g_{b,x,\alpha})$, are then considered to be the solutions of the self-shielding region α of the heterogeneous geometry:

$$\tau^g_{\rho,x,\alpha} = \tau^{g,hom}_{\rho,x}(\sigma^g_{b,x,\alpha}). \tag{3.58}$$

Up-scattering treatment in the tabulations of the rates for a mixture

The use of the fine-structure equivalence self-shielding method requires that reference reaction rates per isotope are tabulated for different background dilutions and temperatures in an IHM. But because the composition of the resonant mixture may not be known in advance, it is not possible to calculate a priori these rates for the mixture in an IHM and store them in an external file to be extracted by interpolation, as it is typically done for a single isotope.

The on-the-fly tabulation of the reaction rates was first implemented by employing the homogeneous fine-structure solver of the subsection 3.2.2 with an ultra-fine-group energy mesh [3]. But this method relies on the use of the asymptotic transfer probabilities, which are not compatible with the up-scattering treatment and may introduce large errors [45]. An adapted Resonance Interference Factor (RIF) method [45] [49] [50] has been implemented to exploit the isotope-wise reference rates of an IHM tabulated in an external file by the GALILEE nuclear data processing system [17]. This allows the consideration of the up-scattering in a mixture treatment.

The RIF is defined, for a nuclear reaction ρ, a resonant isotope x and a self-shielding region α, as the ratio between the reaction rate $\tau_{\rho,x,\alpha}(\sigma_{b,x,\alpha})$ accounting for the mixture treatment, and the reaction rate $\tau_{\rho,x,\alpha}(\tilde{\sigma}_{b,x,\alpha})$ calculated by considering that only the isotope x is resonant, all the others isotopes being part of the moderator. $\sigma_{b,x,\alpha}$ and $\tilde{\sigma}_{b,x,\alpha}$ are the equivalent background dilutions with and without the mixture treatment, respectively. It is assumed that the RIF is geometry-independent, meaning that it can be computed in an IHM, using the ST model:

$$RIF^g_{\rho,x,\alpha} = \frac{\tau^g_{\rho,x,\alpha}(\sigma_{b,x,\alpha})}{\tau^g_{\rho,x,\alpha}(\tilde{\sigma}_{b,x,\alpha})} \approx \frac{\tau^{ST,g,hom}_{\rho,x}(\sigma_{b,x,\alpha})}{\tau^{ST,g,hom}_{\rho,x}(\tilde{\sigma}_{b,x,\alpha})}, \tag{3.59}$$

In the calculation of the reaction rate in the IHM without mixture treatment, the total cross sections of all the isotopes except for x take the values of their potential cross section σ_p. The dilution $\tilde{\sigma}_{b,x,\alpha}$ can thus be computed with the following relation:

$$\tilde{\sigma}_{b,x,\alpha} = \frac{\sigma_{b,x,\alpha} + \sum_{y \neq x} a_{0y}\sigma_{p,y}}{a_{0x}} - \sigma_{p,x}. \tag{3.60}$$

The expression of the averaged scattering rate in an IHM using the ST model is given in Equation (3.54). Similarly, the expression of a nuclear reaction ρ is

$$\langle \vec{\tau}^{ST}_{\rho 0} \rangle^g = \langle \vec{I}_{\rho 0} \rangle^g \times \frac{\gamma_b \sigma_b}{1 - \vec{a}_0^T \vec{I}^g_{s0}}, \tag{3.61}$$

where the same notations have been used as in the previous subsections. Once the RIF has been calculated, the reaction rates of the heterogeneous geometry are corrected:

$$\tau^g_{\rho,x,\alpha}(\sigma_{b,x,\alpha}) = RIF^g_{\rho,x,\alpha} \times \tau^g_{\rho,x,\alpha}(\tilde{\sigma}_{b,x,\alpha}), \tag{3.62}$$

where the quantity $\tau^g_{\rho,x,\alpha}(\tilde{\sigma}_{b,x,\alpha})$ is read by interpolation in the table of the "exact" reaction rates of the isotope x in an IHM.

3.3.2 . Multigroup equivalence

The second equivalence procedure of the fine-structure self-shielding method consists in the determination of the self-shielded cross sections in the resonant domain, by preserving the multigroup reaction rates $\tau^g_{\rho,x,\alpha}$ obtained in the previous heterogeneous-homogeneous equivalence step. The following equation has to be solved

$$\sigma^g_{\rho,x,\alpha}\varphi^g_\alpha = \tau^g_{\rho,x,\alpha}. \tag{3.63}$$

The flux depends on the lethargy solely through the total cross sections of the regions $\vec{\Sigma}^g$. The self-shielded cross section is

$$\sigma^g_{\rho,x,\alpha} = \frac{\tau^g_{\rho,x,\alpha}}{\varphi^g_\alpha(\vec{\Sigma}^g)}. \tag{3.64}$$

In Equation (3.64), the reaction rate is known from the heterogeneous-homogeneous equivalence, but the neutron flux has to be determined by solving the following multigroup equation:

$$\varphi^g_\alpha(\vec{\Sigma}^g) = \frac{1}{\Delta u^g}\sum_\beta C^g_{\alpha\beta}(\vec{\Sigma}^g)\sum_{g'} p^{g'\to g}_{0\alpha}\langle\tau_{s0\alpha}\rangle^{g'} + S^g_\alpha(\vec{\Sigma}^g), \tag{3.65}$$

where the following notation has been employed

$$C^g_{\alpha\beta}(\vec{\Sigma}^g) = \frac{\displaystyle\sum_{i\in\alpha}\sum_{j\in\beta} P_{ij}(\vec{\Sigma}^g)V_j N_{0j}}{\displaystyle\sum_{i\in\alpha} V_i\left[\Sigma^g_{1i} + \sum_x N_{0x,i}\sigma^g_{0x,i}\right]}, \tag{3.66}$$

and

$$S^g_\alpha(\vec{\Sigma}^g) = \frac{\displaystyle\sum_{i\in\alpha}\sum_{j} P_{ij}(\vec{\Sigma}^g)V_j \Sigma^g_{s1j}}{\displaystyle\sum_{i\in\alpha} V_i\left[\Sigma^g_{1i} + \sum_x N_{0x,i}\sigma^g_{0x,i}\right]}. \tag{3.67}$$

The multigroup resonant scattering operator in a self-shielding region α is known from the solution of the heterogeneous-homogeneous equivalence. The multigroup equivalence is an iterative solution of (3.64). Starting from an initial value for the flux in all the self-shielding regions, the microscopic multigroup cross sections are derived from Equation (3.64). In every region i, the total macroscopic cross section is deduced from

$$\Sigma^g_i = \sum_x N_{0x,\alpha}\sigma^g_{0x,\alpha} + \Sigma^g_{1i} \text{ if } i \in \alpha. \tag{3.68}$$

The collision probabilities are computed for this new value of macroscopic total cross section, and the value of the flux is updates by solving Equation (3.65).

This process is repeated until convergence.

3.3.3 . Discussion on the use of the fine-structure method

The FSM described in this section is currently the most commonly used in APOLLO3® calculations for thermal reactors. It is efficient, thanks to the heterogeneous-homogeneous equivalence that enables the use of a reduced number of groups, such as the XMAS 172-group [51] or the SHEM 281-group structures [30], and to the definition of self-shielding regions, which decreases the effective number of regions to be computed. It has also been extensively tested on numerous numerical benchmarks, and benefits from the experience from the APOLLO2 code.

However, because the heterogeneous rates are replaced by the ones computed in an IHM, the FSM fails to accurately represent the spatial distribution of the reaction rates. In the reference [18], Mao et al. showed on the Rowland UO_2 pin-cell benchmark [52] that although a good multiplication factor was obtained, the absorption in the outer ring of the discretized pin-cell was overestimated. The accuracy of the FSM is limited by the distorted heterogeneous reaction rates.

Recent developments in the APOLLO3® self-shielding methods have led to the development of a subgroup method, based on the same formalism as the FSM. In fact, the calculation of the heterogeneous reaction rates in section 3.2.1 are comparable to a subgroup method, as the energy-integrated quantities are computed with the use of probability tables. The subgroup method of APOLLO3® is different because it uses a fine energy discretization in the resolved energy domain in order to skip the heterogeneous-homogeneous equivalence step.

3.4 . Fine-structure Equation based Subgroup Method

A recent work has led to the implementation in APOLLO3® of a subgroup method [18] in order to improve the precision of the fine-structure method previously described.

3.4.1 . Fine-structure heterogeneous solver

In a heterogeneous geometry, the evolution of the neutron flux is described by the equation (3.32), based on the fine-structure approximation. This equation is solved using the already described heterogeneous fine-structure equation solver of the section 3.2.1 on a fine energy mesh of 383 groups. It is assumed that this energy discretization is fine enough to not require a heterogeneous-homogeneous equivalence.

Because this subgroup method relies on the use of the GR model to approximate the resonant scattering sources of the fine-structure equation, it will be called “SG-GR” in this manuscript.

3.4.2 . Application of the SPH correction

The self-shielded cross sections obtained through the previous subgroup calculation are generally not able to preserve reaction rates in a multigroup solution [53] [12] . A multigroup equivalence procedure is therefore necessary to enforce that criteria; this is the role of the SPH correction [18]. It is a group and region-dependent correction, the same SPH factor is applied to all the resonant isotopes in the same region. The cross sections of moderating isotopes are not modified by this procedure, even

though they are mixed with resonant isotopes. The SPH factor μ_i^g, where i is a region index and g an energy group, is determined by iterating on a low order equation (multigroup equation) to converge towards a reference solution, obtained by solving a high order equation (subgroup equation).

The high order equation is the heterogeneous subgroup equation, whose solutions are the fluxes:

$$\phi_i^g = \phi_\alpha^g \text{ if } i \in \alpha, \tag{3.69}$$

as well as the reference arrival source in g:

$$Q_i^g = N_{0i}\langle r_0 \varphi_\alpha^{GR}\rangle^g + \Sigma_{s1i} \text{ if } i \in \alpha, \tag{3.70}$$

the reference total reaction rate:

$$\tau_i^g = \sum_x a_{0x,\alpha}\left(\tau_{s,0x,\alpha}^g + \tau_{a,0x,\alpha}^g\right) \text{ if } i \in \alpha, \tag{3.71}$$

and the total macroscopic cross section:

$$\Sigma_i^g = \frac{N_{0i}\tau_i^g}{\phi_i^g} + \Sigma_{1i}. \tag{3.72}$$

The low order equation is the following multigroup collision probability equation, where the low order quantities actualized at each iteration are the macroscopic total cross section $\tilde{\Sigma}$ and the flux $\tilde{\phi}$:

$$\tilde{\Sigma}_i^g V_i \tilde{\phi}_i^g = \sum_j P_{ij}^g V_j Q_j^g \tag{3.73}$$

The SPH factor is defined as the ratio of the high order reference flux from Equation (3.69) and of the the low order flux from Equation (3.73):

$$\mu_i^g = \frac{\phi_i^g}{\tilde{\phi}_i^g} \tag{3.74}$$

The SPH factor is computed through the subsequent iterative procedure:

1. Set $\mu_i^{g,(0)} = 1$ in all the fuel regions.
2. At the n^{th} iteration, solve the multigroup low order equation (3.73) for the low order flux $\tilde{\phi}_i^{g,(n)}$.
3. Compute the new SPH factor:
$$\mu_i^{g,(n)} = \frac{\phi_i^g}{\tilde{\phi}_i^{g,(n)}}. \tag{3.75}$$
4. Check for the convergence criteria:
$$\max_i \left| \frac{\mu_i^{g,(n)}}{\mu_i^{g,(n-1)}} \right| < \varepsilon, \tag{3.76}$$

where ε is set by default to 10^{-5}. Stop the iterations if the convergence criteria is met or the maximum number of iterations is reached. Otherwise, actualize the value of the macroscopic total cross section:

$$\tilde{\Sigma}_i^{g,(n+1)}(\vec{r}) = \mu_i^{g,(n)} \Sigma_i^g \tag{3.77}$$

and go back to step 2.

Once the SPH factor has been determined in every region i and energy group g, the self-shielded microscopic cross section $\sigma_{\rho,x}^{g,\text{eff}}$ can be computed for the reaction ρ and isotope x:

$$\sigma_{\rho,x,i}^{g,\text{eff}} = \mu_i^g \frac{\tau_{\rho,x,i}^g}{\phi_i^g}. \tag{3.78}$$

The multigroup cross sections preserving the reaction rates are thus obtained by the application of the SPH correction.

3.4.3 . Discussion on the use of the SG-GR method

The SG-GR method implemented in APOLLO3® renders very good multiplication factors and reaction rates on typical thermal reactor calculations, with less than 60 pcm of difference on the multiplication factor of the Rowlands UO_2 and MOX pin-cell benchmarks, compared with a TRIPOLI-4® calculation [18]. Its main drawback resides in its prohibitively expensive computational time for its application to depletion calculations or large geometries. Three main causes have been identified as being primarily responsible for the long computational time [19]:

1. A significant proportion of the lattice calculation time is spent in the mixture MPTs calculation. This time increases with both the number of mixtures present in the geometry, and with the number of resonant isotopes contained in the mixtures. In practice, the online computation of mixture MPTs becomes inadequately long when the number of isotopes exceeds five or six.

2. The SG-GR method is used conjointly with a fine energy mesh of a few hundred groups, e.g. 383 groups, in order to not resort to the heterogeneous-homogeneous equivalence procedure as it is done in the FSM. The use of a fine energy structure implies a large number of groups in the flux calculation.

3. The calculation of thousands of two-dimensional collision probabilities on the whole lattice geometry, to take into account the shadowing effects of neighboring fuel rods, is known to be a tediously long process, even when employing approximations such as the Multi-Cell Approximation [54].

The reduction of the time spent in calculating the collision probabilities has been the subject of a recent effort, with the development of the Equivalent Dancoff-factor Cell (EDC) Method.

3.5 . Equivalent Dancoff-factor Cell Method

A method consisting of transforming a two-dimensional lattice calculation into a set of independent one-dimensional cylindrical fuel cell calculations, by preserving the Dancoff factor of the fuel rod in the lattice geometry has been proposed in the NECP-X code [21], where it is called the "global–local self-shielding calculation scheme", and coupled to the Pseudo-Resonant-Nuclide Subgroup Method

[12]. The name of "Equivalent Dancoff-factor Cell" was mentioned in the GALAXY code, where it is employed with an ultra-fine-group resonance treatment [55]. Since the collision probability calculation is much faster for one-dimensional cylindrical cells than for a two-dimensional geometry, it leads to significant improvement in the computational time.

The EDC method has been implemented in APOLLO3® and coupled to the SG-GR method [19].

3.5.1 . Definition of the Dancoff factor

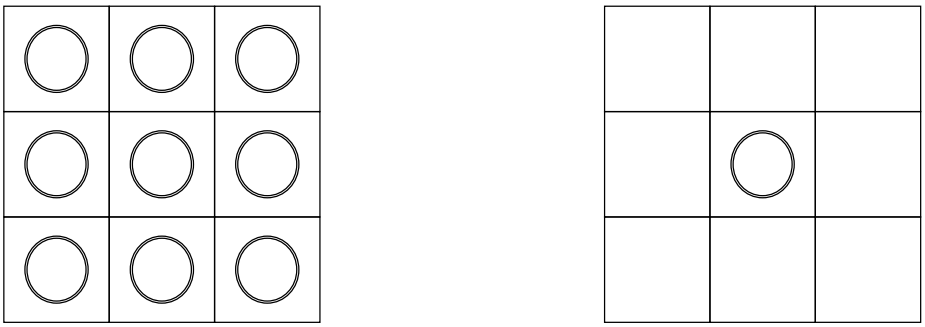

(a) Lattice of fuel rods (b) Isolated rod

Figure 3.2: Two-dimensional lattice of fuel rods (left) and isolated rod surrounded by moderator (right)

Let us consider a two-dimensional heterogeneous system, as represented in Figure 3.2. The escape probability P_{esc} of a neutron born uniformly in the a fuel rod is defined as its probability to undergo its first collision in the cladding or the moderator. In the case where the fuel rod is isolated and surrounded by an infinite moderator medium, this escape probability is noted $P_{esc}^{isolated}$. In the case where it is part of a lattice of identical fuel rods, the escape probability is lower, since the neutron can re-enter another rod and collide in the fuel of that neighboring rod. The corresponding escape probability is noted $P_{esc}^{lattice}$. The Dancoff factor is a measurement of that shadowing effect in the black limit, where the total cross section of the fuel approaches infinity:

$$D = \lim_{\Sigma_{fuel} \to +\infty} \frac{P_{esc}^{lattice}}{P_{esc}^{isolated}}. \tag{3.79}$$

3.5.2 . Calculation of the Dancoff factor

Let us consider a two-dimensional lattice composed of a set of L fuel rods $\{F_l, l = 1, ..., L\}$. In each cell, the macroscopic total cross section of the fuel medium is set to the arbitrary large value of 10^5 cm^{-1}. The cross sections of the moderator and of the cladding are set to their potential scattering cross sections. The Dancoff factor of a pin F_l in this two-dimensional lattice system is, according to the definition (3.79):

$$D_l^{2D} = \frac{P_{esc,l}^{lattice}}{P_{esc,l}^{isolated}}. \tag{3.80}$$

Figure 3.3 shows that for every cell of the two-dimensional lattice, an equivalent one-dimensional cylindrical cell is created with the exact same fuel rod F_l at the center, and with a white reflective

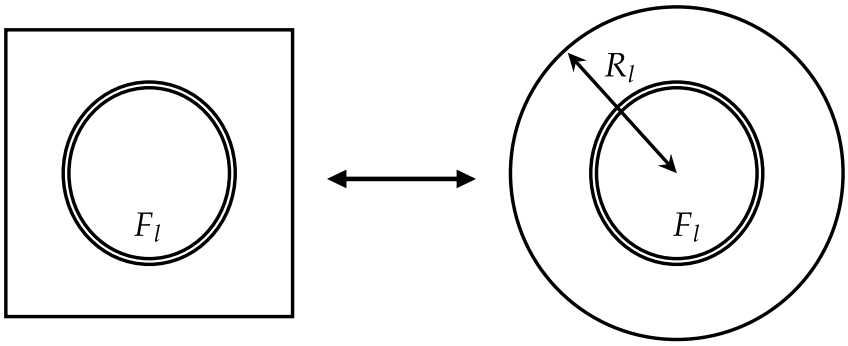

Figure 3.3: Equivalent Dancoff-factor cell

boundary condition. The radius R_l of the cylindrical cell is adjusted so that the Dancoff factor of the cylindrical cell D_l^{1D} is equal to D_l^{2D}, where

$$D_l^{1D}(R_l) = \frac{P_{esc,l}^{cylinder}(R_l)}{P_{esc,l}^{isolated}}. \tag{3.81}$$

One can notice that the denominator $P_{esc,l}^{isolated}$ is the same in the expression of the Dancoff factor in the two-dimensional lattice in Equation (3.80), and in the one-dimensional cylindrical reflected cell in Equation (3.81). The equality of the Dancoff factor is therefore equivalent to the equality of the following escape probabilities:

$$D_l^{1D}(R_l) = D_l^{2D} \iff P_{esc,l}^{cylinder}(R_l) = P_{esc,l}^{lattice}. \tag{3.82}$$

The escape probability $P_{esc,l}^{lattice}$ corresponds to the event where a neutron born in the pin F_l exits the pin, and undergoes a collision in the moderator medium. In other words, it is the opposite event of colliding in a fuel pin, which happens with a probability $P_{l\to F}^{lattice}$, where F designates the complete set of fuel pins. The expression of the escape probability in the two-dimensional lattice becomes

$$P_{esc,l}^{lattice} = 1 - P_{l\to F}^{lattice}, \tag{3.83}$$

where $P_{l\to F}^{lattice}$ is computed with the collision probability method. In the case where the fuel pins are divided into rings, the lattice collision probability for the fuel pin in the cell l is given by the formula:

$$P_{l\to F}^{lattice} = \frac{\sum_{j\in F}\sum_{i\in l} P_{ji}^{lattice} V_i}{\sum_{i\in l} V_i}, \tag{3.84}$$

where V_i is the volume of the fuel region i, and $P_{ji}^{lattice}$ designates the first-flight collision probability for a neutron born uniformly in the region i to undergo its first collision in the region j. Similarly, the escape probability in the cylindrical cell can be expressed as

$$P_{esc,l}^{cylinder}(R_l) = 1 - P_{l\to l}^{cylinder}(R_l). \tag{3.85}$$

This time, the fuel pin F_l is the only one of the set F. The fuel to fuel collision probability is a function of the researched radius R_l:

$$P_{l\to l}^{cylinder}(R_l) = \frac{\sum_{j\in l}\sum_{i\in l} P_{ji}^{cylinder}(R_l)V_i}{\sum_{i\in l} V_i}. \tag{3.86}$$

In Equations (3.84) and (3.86), the collision probabilities are computed using the collision probability method with the multi-cell approximation [41]. Finally, the radius of the cylindrical cell is calculated by solving the equation

$$P_{l\to l}^{cylinder}(R_l) = P_{l\to F}^{lattice}. \tag{3.87}$$

This is done by binary search. Once the radii R_l of all the cells l have been computed, the SG-GR method is applied independently to every one-dimensional cylindrical cell.

3.5.3 . Discussion on the use of the EDC-GR method

The EDC method of APOLLO3® has led to a reduction of the computational time by a factor up to 50 in the self-shielding of PWR assembly calculations, compared with the SG-GR method [19] and with the FSM method [56]. It represents more accurately the spatial distribution of the reaction rates than the FSM, and contrary to the SG-GR, it does not rely on the use of the Same Material Approximation. The latter has been known to introduce errors in the calculation of assemblies composed of materials significantly different [56], but having some resonant isotopes in common, such as UO_2 and Gadolinium-UO_2 materials.

The preliminary tests on the EDC method show that it is a very promising self-shielding method, capable of combining both accuracy and fast execution. However its computational time is still heavily burdened by the on-the-fly calculation of the mixture MPTs, which make up for more than half the time of the total self-shielding calculation [56]. In order to improve that aspect, the calculation of the mixture MPTs has been parallelized, as well as the self-shielding of the one-dimensional cylindrical cells.

Extensive numerical tests still have to be carried out in order to validate the EDC method of APOLLO3®, as this method is still recent and does not benefit from many feedbacks from the users.

3.6 . Summary

This chapter presents the self-shielding methods of APOLLO3® for the calculation of thermal reactors.

Section 3.1 summarizes the principle of the calculation of the mathematical probability tables, for single isotopes and for resonant mixtures. These probability tables are employed as input data from which quadrature formulas are derived for the self-shielding methods of APOLLO3®.

Section 3.2 presents the two subgroup solver existing in APOLLO3® to solve the fine-structure equation in a heterogeneous or homogeneous solver. These solvers are utilized in sections 3.3 and 3.4 for the descriptions of the self-shielding methods of APOLLO3®.

The fine-structure method, inherited from APOLLO2, is introduced in the section 3.3. It is based on a double equivalence: first, the heterogeneous-homogeneous equivalence is carried out on

a coarse energy mesh to compute the multigroup reaction rates that have to be preserved in the subsequent multigroup equivalence. The self-shielded cross sections are obtained after this second equivalence step. Because the reaction rates of the heterogeneous geometry are calculated in an infinite homogeneous medium, the fine-structure method is unable to precisely represent the spatial distribution of the reaction rates in the cell. Although the multiplication factor obtained with this method is often satisfying, most of the time it is due to the compensation of errors between the regions of the calculation.

A subgroup method, also based on the fine-structure approximation, was implemented in APOLLO3® in order to obtain a better depiction of the spatial reaction rates. It is presented in the section 3.4. The use of a fine-group energy structure enables to skip the heterogeneous-homogeneous equivalence from which the errors of the fine-structure method originated. This subgroup method is time expensive, for various reasons. The use of a finer energy mesh results in a longer flux calculation than with a coarser mesh, because more multigroup fluxes have to be computed. The calculation of the mixture mathematical probability tables is also time expensive. But the most time consuming part of the subgroup method is the calculation of hundreds of collision probabilities for a two-dimensional geometry.

The Equivalent Dancoff-factor Cell method, detailed in section 3.5, was developed to mitigate the time spent in the calculation of the collision probabilities. The two-dimensional lattice calculation is divided into independent one-dimensional cylindrical cell calculations, thus greatly accelerating the self-shielding calculation.

All the subgroup methods of APOLLO3® require a very fine energy discretization of almost 400 groups, making the flux calculation laboriously long. An evident axis of improvement to reduce the computational time of the lattice calculation is to decrease the number of energy groups.

4 - Numerical Benchmarks Used in this Work

The numerical evaluation of the methods implemented throughout this thesis work have required the creation of a numerical benchmark database for testing purpose. The various benchmarks selected are representative of typical thermal reactor calculations, and more specifically of Pressurized Water Reactor (PWR). They vary in terms of geometry and composition, and are defined in the order of increasing complexity. This chapter gives a description of all the test cases used throughout this work.

This thesis work can be divided into two main axis. The first axis is the calculation of physical probability tables on a coarse group structure, and all the preliminary steps required to carry out this development. The second axis focuses on the performance of different subgroup methods when coupled to the physical probability tables. These two parts of the thesis have their own dedicated list of benchmarks, that will be subsequently described.

4.1 . Benchmarks for the Validation of the Physical Probability Tables

The physical probability tables calculated in this work are based on reference cross sections obtained by an ultra-fine-group slowing-down calculation in an infinite homogeneous medium (IHM). For this reason, the validation of the physical probability tables has been carried out in infinite homogeneous media only. Only their compositions differ; mixtures with an increasing number of resonant isotopes have been selected.

Tables 4.1 and 4.2 show the composition of resonant mixtures corresponding to a simplified UO_2 and a typical UO_2 fuel materials with an enrichment of about 3.7%. In the next chapters, these two benchmarks will be designated by the names of "IHM-U8U5-3.7" and "IHM-UO_2 -3.7", respectively. Table 4.3 gives the composition of a MOX mixture, taken from the Mosteller [57] benchmark; it corresponds to an enrichment of 4 wt.% in PuO_2. This test case will be called "IHM-MOX".

Because the resonant mixtures are placed in an IHM, there is no spatial discretization associated to these numerical test cases.

Table 4.1: Composition of the benchmark "IHM-U8U5-3.7"

Isotope	Density (10^{24} at./cm^3)
^{238}U	2.2E-02
^{235}U	8.56E-04

4.2 . Benchmarks for the Evaluation of the Subgroup Methods

The numerical test cases selected for this second part of the thesis work will be used for the evaluation of the subgroup methods. Various geometries, from a simple IHM to a fuel assembly, enable to verify the accuracy of the subgroup methods in geometries of increasing complexity. The compositions of the resonant mixtures in these numerical tests are taken from the Yamamoto's benchmark [58] for light water reactors.

Table 4.2: Composition of the benchmark "IHM-UO_2 -3.7"

Isotope	Density (10^{24} at./cm^3)
^{234}U	7.38E-06
^{235}U	8.56E-04
^{236}U	1.37E-06
^{238}U	2.2E-02

Table 4.3: Composition of the benchmark "IHM-MOX"

Isotope	Density (10^{24} at./cm^3)	Isotope	Density (10^{24} at./cm^3)
^{235}U	1.59387E-4	^{240}Pu	2.74749E-4
^{238}U	2.19768E-2	^{241}Pu	1.37374E-4
^{239}Pu	4.12123E-4	^{242}Pu	9.15830E-5

In a lattice calculation, the self-shielding procedure is followed by a transport calculation using the computed self-shielded cross sections. The flux solver employed in this work is the two-dimensional TDT MOC solver of APOLLO3® [36]. The tracking parameters are set to 32 azimuthal angles, 4 polar angles and a transversal integration step of 0.01 cm. The anisotropic scattering order is fixed to P3.

4.2.1 . Infinite homogeneous medium

The first benchmark used for the evaluation of the subgroup methods is an IHM composed of a mixture of ^{238}U, ^{235}U and H_2O, in proportions described in 4.4. This composition corresponds to a simplified UO_2 mixture with a high enrichment of 6.5 wt% in ^{235}U.

Table 4.4: Composition of the benchmark "IHM-U8U5-6.5"

Isotope	Density (10^{24} at./cm^3)
^{238}U	2.1477E-02
^{235}U	1.5122E-03
H_2O	2.2074E-02

4.2.2 . Fuel-pin cells

Two kinds of pin-fuel cells are used in the study of the performance of the subgroup methods. The first one is a typical PWR cell, called "Cell-UO_2 ", whose composition, dimensions and temperatures are indicated in Table 4.5.

In order to be able to distinguish the errors due to the self-shielding of the cladding from the self-shielding of the fuel material, another cell benchmark is defined. This numerical test, called "Cell-UO_2 -noClad", is almost identical to the previous one, except for the cladding that has been replaced with moderator.

For the self-shielding calculation, the fuel-pins are divided into 10 rings, corresponding to percentages of 20, 20, 10, 10, 10, 10, 5, 5, 5, and 5, respectively, of the total fuel volume. For the flux

Table 4.5: Composition of the "Cell-UO_2 " benchmark

Material	Isotope	Density (10^{24} at./cm^3)	Temperature (K)	Radius / Pitch (cm)
Fuel	^{238}U	2.1477E-02	974	0.412
	^{235}U	1.5122E-03		
	^{16}O	4.5945E-02		
Cladding	^{90}Zr	2.2200E-02	574	0.476
	^{91}Zr	4.8280E-03		
	^{92}Zr	7.3713E-03		
	^{94}Zr	7.5006E-03		
	^{96}Zr	1.2070E-03		
Moderator	H_2O	2.2074E-02	574	1.265

calculation, each ring has been divided into 8 sectors. The spatial meshes used are shown in Figure 4.1.

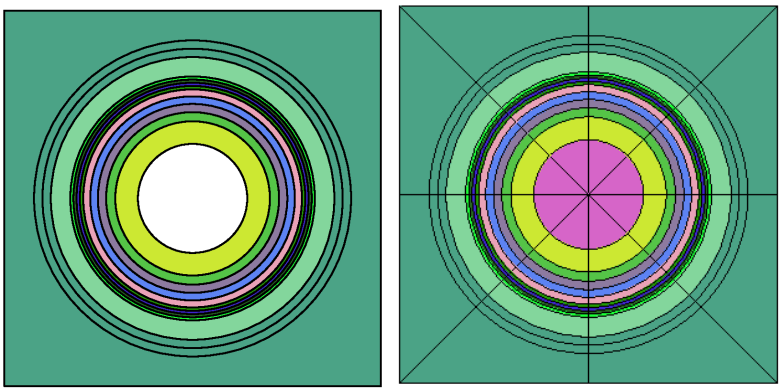

(a) Self-shielding calculation (b) Flux calculation

Figure 4.1: Spatial meshes employed in the pin-cell calculations

4.2.3 . Motif of 3×3 cells

Two motifs of 3×3 cells are employed in the evaluation of the subgroup methods. In the "3×3-Tube" test case, the central cell is occupied by a guide tube. In the "3×3-Gd" test case, the central cell is a fuel-pin with a UO_2 -Gadolinium bearing fuel.

Because of the symmetry of the geometry of the 3×3 cluster of cells, the calculation is carried out on a reduced geometry shown in Figure 4.2, with reflective boundary conditions. The spatial discretizations of each cell are the same as those shown in Figure 4.1. The guide tube of the "3×3-Tube" test case is only divided in 8 sectors for the flux calculation.

In both the "3×3-Tube" and the "3×3-Gd" benchmarks, the composition of the UO_2 fuel-pins is identical to the single pin-cell numerical test case, detailed in Table 4.5. Table 4.6 and Table 4.7 describe the composition, the temperature and the dimensions of the guide-tube cell and of the Gd-UO_2 pin cell, respectively. The Gd-UO_2 fuel corresponds to an enrichment of 4.0 wt% in ^{235}U and 10.0 wt% in Gd_2O_3.

Table 4.6: Composition of the guide-tube cell in the "Motif 3×3 Water-hole" benchmark

Material	Isotope	Density (10^{24} at./cm^3)	Temperature (K)	Radius / Pitch (cm)
Moderator	H_2O	2.2074E-02	574	0.570
Cladding	^{90}Zr	2.2200E-02	574	0.610
	^{91}Zr	4.8280E-03		
	^{92}Zr	7.3713E-03		
	^{94}Zr	7.5006E-03		
	^{96}Zr	1.2070E-03		
Moderator	H_2O	2.2074E-02	574	1.265

Table 4.7: Composition of the Gd-UO_2 pin-cell in the "Motif 3×3-Gd" benchmark

Material	Isotope	Density (10^{24} at./cm^3)	Temperature (K)	Radius / Pitch (cm)
Gd-UO_2 fuel	^{238}U	1.9268E-2	974	0.412
	^{235}U	8.1312E-4		
	^{16}O	4.5130E-2		
	^{154}Gd	7.1289E-5		
	^{155}Gd	4.8938E-4		
	^{156}Gd	6.8028E-4		
	^{157}Gd	5.2077E-4		
	^{158}Gd	8.2650E-4		
	^{160}Gd	7.2761E-4		
Cladding	^{90}Zr	2.2200E-02	574	0.476
	^{91}Zr	4.8280E-03		
	^{92}Zr	7.3713E-03		
	^{94}Zr	7.5006E-03		
	^{96}Zr	1.2070E-03		
Moderator	H_2O	2.2074E-02	574	1.265

4.2.4 . PWR fuel assembly

For the last category of test cases, two fuel assemblies with a configuration similar to a 17×17 PWR fuel design were selected. Only $1/8^{\text{th}}$ of assembly, with reflective boundary conditions, is represented in the calculation, as in the Figure 4.3. The "Gd-UO_2 assembly" test case of the Figure 4.3b is directly taken from the Yamamoto's benchmark. The "UO_2 assembly" benchmark of Figure 4.3a is a simplified case where the Gd-UO_2 pin cells have been replaced with UO_2 pin cells.

The compositions are the same as the ones presented for the cluster of 3×3 cells, given in Table 4.5, 4.6 and 4.7. The same spatial discretization as in Figure 4.1 is employed for the self-shielding and flux calculations.

4.3 . Summary

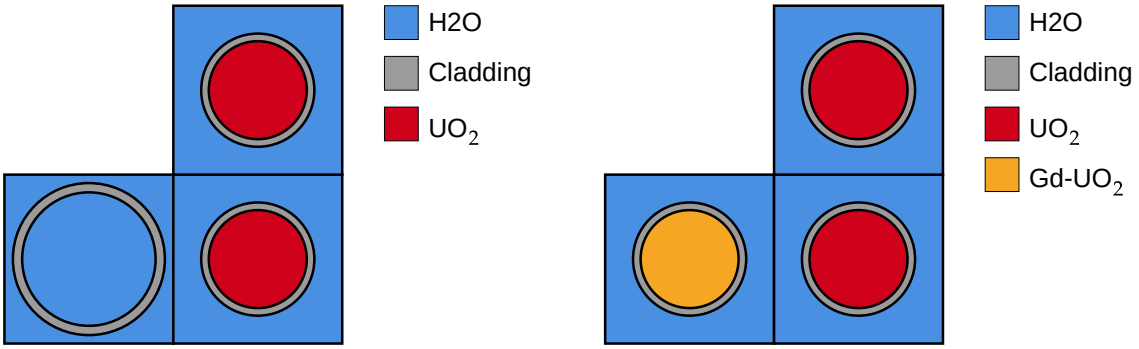

(a) "Motif 3×3 Water-hole" (b) "Motif 3×3-Gd"

Figure 4.2: Geometry of the 3×3 cells test cases

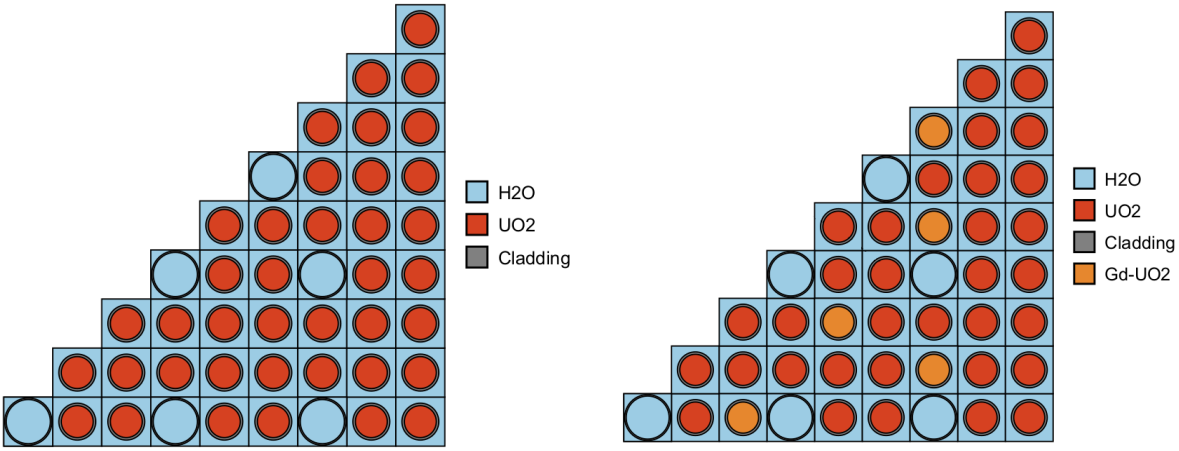

(a) UO_2 assembly (b) Gd-UO_2 assembly

Figure 4.3: PWR fuel assemblies

In this chapter, the numerical benchmarks utilized throughout the thesis work for the verification and evaluation of the implemented methods were presented. They have been separated in two categories, according to their utilisation case: either the validation of the physical probability tables, or the evaluation of the subgroup self-shielding methods. For both categories, benchmarks of increasing complexity have been selected.

In the rest of this thesis manuscript, the complete description of the benchmarks will not be repeated. The numerical benchmarks will be referred to with the names introduced in this chapter.

5 - Verification of an Ultra-Fine Group Slowing-down Solver in an Infinite Homogeneous Medium

This chapter describes the theory and the validation of the ultra-fine group slowing-down solver for the computation of the effective multigroup cross sections in an infinite homogeneous medium, in the APOLLO3® lattice code. The cross sections can be computed for any number of energy groups, but in the context of this PhD we are mostly interested in the ability of the solver to provide coarse multigroup effective cross sections. A coarse 69 group energy mesh was adapted from the open source 69 group energy structure of the WIMS-D library [59].

5.1 . Description of the UFG-IHM slowing-down equation solver

Let us consider an IHM composed of a mixture of resonant isotopes denoted x, whose effective multigroup cross sections have to be computed on a coarse energy mesh $\{G_k\}_{k=1,...,NG}$.

In order to obtain the reference cross sections for the resonant mixture on this coarse energy mesh, the UFG-IHM solver presently described solves Equation (3.47) on an ultra-fine-group energy structure $\{g_k\}_{k=1,...,ng}$. The fine reactions rates and neutron flux are then be condensed and used to compute the coarse reference cross sections.

Existing literature shows that reference cross sections are typically obtained by solving the elastic slowing-down equation on ultra fine energy meshes of more than one million energy groups [12]. Currently, the finest energy mesh available in the bank of APOLLO3® nuclear data libraries is the MUSCLET energy mesh [60], made of 23317 energy groups. It was selected for this work. The multigroup library of the MUSCLET energy mesh is based on the CEA V512 multigroup library, based on the JEFF-3.1 nuclear data evaluation [22].

In Section 3.2.2 of Chapter 3, the solution of the fine-structure equation (3.47) by the subgroup method was detailed. It relies on the application of the General Resonance (GR) model [3] in every fine group to approximate the resonant scattering source and on the use of the mixture MPTs [61] to compute group-integrated quantities. This same fine-structure solver is employed with the MUSCLET ultra-fine-group energy structure, in order to retrieve the fine neutron flux ϕ^g and reaction rates $\tau^g_{\rho 0x}$ for a reaction ρ and a resonant isotope x. Specifically, the nuclear reactions of interest for this work are the absorption, fission and elastic scattering reactions.

The fine neutron flux and reaction rates are then condensed onto the coarse energy mesh, by adding the contribution of each fine group to the large group to which it belongs:

$$\phi^G = \sum_{g \in G} \phi^g \tag{5.1}$$

$$\tau^G_{\rho 0x} = \sum_{g \in G} \tau^g_{\rho 0x} \tag{5.2}$$

The coarse effective multigroup cross section for reaction ρ of isotope x can then be simply obtained as the ratio of these two quantities:

$$\sigma_{\rho 0x}^{G} = \frac{\tau_{\rho 0x}^{G}}{\phi^{G}} \ . \tag{5.3}$$

For now, the up-scattering is not taken into account in the solution of the fine-structure equation with the UFG-IHM solver, as the transfer probabilities accounting for the up-scattering are presently not available in the MUSCLET library.

5.2 . Validation of the UFG-IHM Solver on the Coarse 69-Group Energy Structure

Numerical tests are presented in this section for the validation of the UFG-IHM solver for the generation of multigroup effective cross sections on the coarse 69 group energy structure. Given a resonant mixture of density N_0, the solver is called for twelve values of background dilutions and three temperatures, shown in Table 5.1. In the chosen list of temperatures, 974K is the one corresponding to the typical fuel-pin temperature in PWR reactor calculations. It is therefore critical to ensure that the accuracy of the solver is satisfying for this temperature in particular. The other two temperatures, 294K and 2274K, are meant to observe the behavior of the computed cross sections with extreme temperature variations.

The computed cross sections are compared to the Monte Carlo reference values, obtained by running the TRIPOLI-4® CEA stochastic code [62] in its "PROTECTION" mode. In the Monte Carlo simulation, the background dilution σ_b of the infinite homogeneous medium is adjusted by adding hydrogen atoms, with a density N_1, to the resonant mixture:

$$N_1 = N_0 \frac{\sigma_b}{\sigma_{pot,H1S}}, \tag{5.4}$$

where $\sigma_{pot,H1S} = 20.478003$ barns is the potential scattering of hydrogen, and $H1S$ is the notation adopted to represent the modified version of hydrogen whose only non-null cross section is its potential scattering cross section. The use of $H1S$ instead of regular ^{1}H allows the adjustment of the background dilution without modifying the absorbing properties of the medium, enabling an accurate comparison between the APOLLO3® and TRIPOLI-4® slowing-down calculations.

Table 5.1: Parameters for the validation of the UFG-IHM solver

Parameter	Values
Temperature (K)	294, 974, 2274
Background dilutions (barns)	1, 10, 28, 40, 45, 52, 80, 100, 200, 400, 600, 1000

For each benchmark of the section 4.1, the relative error (in percent) on the cross sections computed with the UFG-IHM solver is computed, in the resonant energy groups indexed from 15 to 27 in the 69 group energy mesh. If $\sigma_{\rho 0x}^{G}$ is the cross section of the resonant isotope x for the nuclear reaction ρ in the coarse group G computed using the UFG-IHM deterministic solver, and $\bar{\sigma}_{\rho 0x}^{G}$ is its corresponding Monte Carlo reference value, the relative error is:

$$\varepsilon^G_{\rho,x} = 100 \times \frac{\sigma^G_{\rho 0x} - \bar{\sigma}^G_{\rho 0x}}{\bar{\sigma}^G_{\rho 0x}}. \tag{5.5}$$

The relative error is also computed on the total cross section of the resonant mixture σ^G_0, which is obtained by summing the absorption and scattering cross sections of each resonant isotope, multiplied by their proportion in the mixture:

$$\sigma^G_0 = \sum_x a_{0x} \left(\sigma^G_{a0x} + \sigma^G_{s0x}\right). \tag{5.6}$$

5.2.1 . Single ^{238}U isotope

This first numerical test is a preliminary calculation, not introduced in Chapter 4 describing the benchmarks. The simplest resonant mixture that one can solve is a mixture made of a single isotope, diluted with $H1S$ isotopes, as there is no interference effect to take into account. The most important resonant isotope for thermal reactor calculations is ^{238}U; it is therefore the natural candidate for this first numerical test. The total and partial cross sections of ^{238}U are computed when it is alone in an IHM, for different temperatures and background dilutions. Figures 5.1 to 5.3 represent the relative errors on the computed total and absorption cross sections with respect to the TRIPOLI-4® reference value for different temperatures and background dilutions.

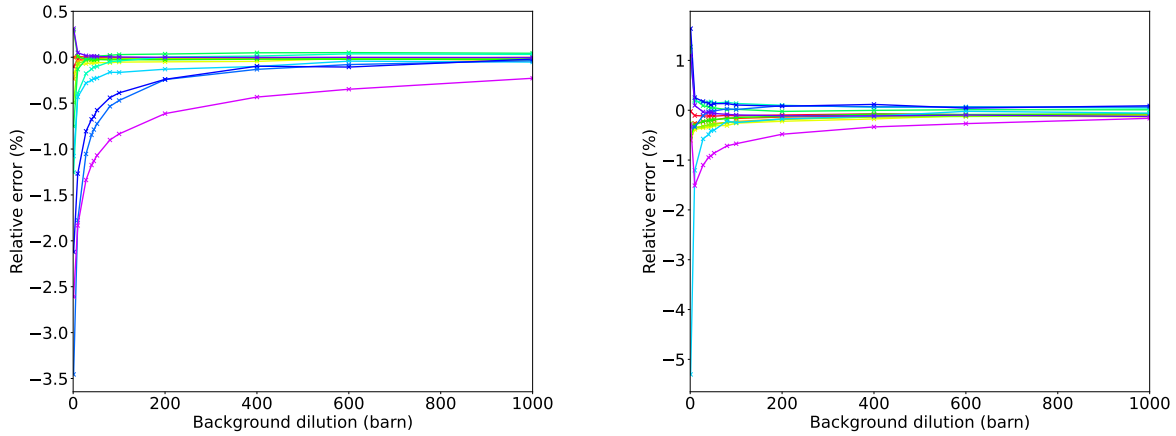

(a) ^{238}U total cross section

(b) ^{238}U absorption cross section

Figure 5.1: Relative errors on the ^{238}U cross sections at 294K

It can be observed that the relative error follows the same trend for the total cross section and the absorption cross section. The results obtained at 294K and 2274K are not significantly different from the 974K calculation. However they are highly dependent on the background dilution, as the absolute

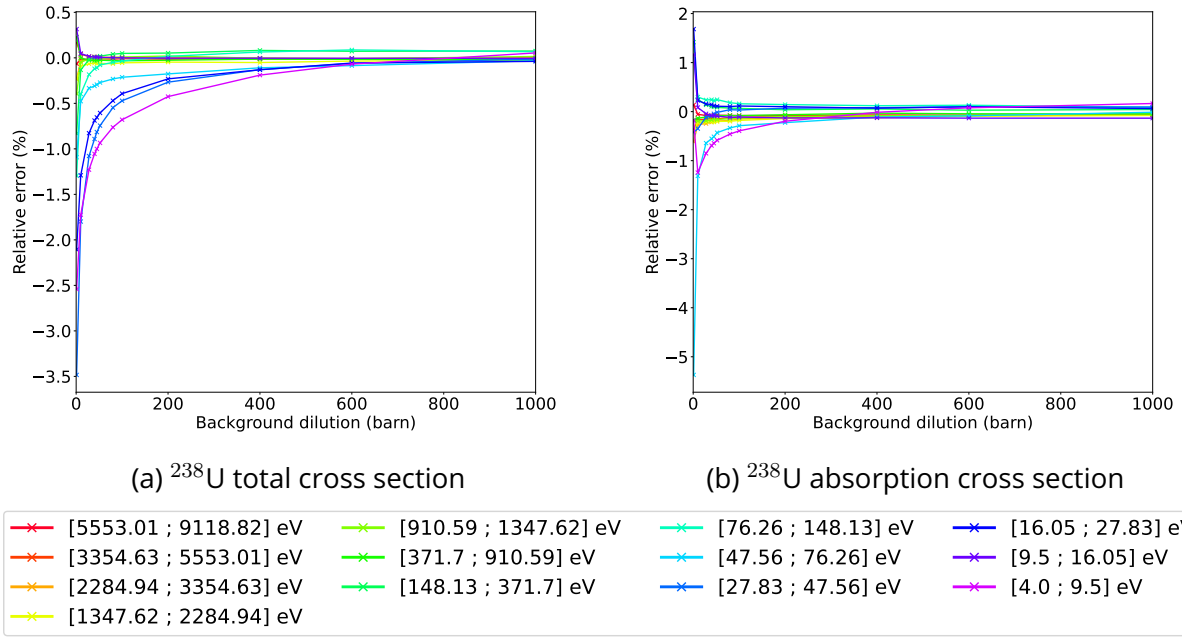

(a) ^{238}U total cross section (b) ^{238}U absorption cross section

Figure 5.2: Relative errors on the ^{238}U cross sections at 974K

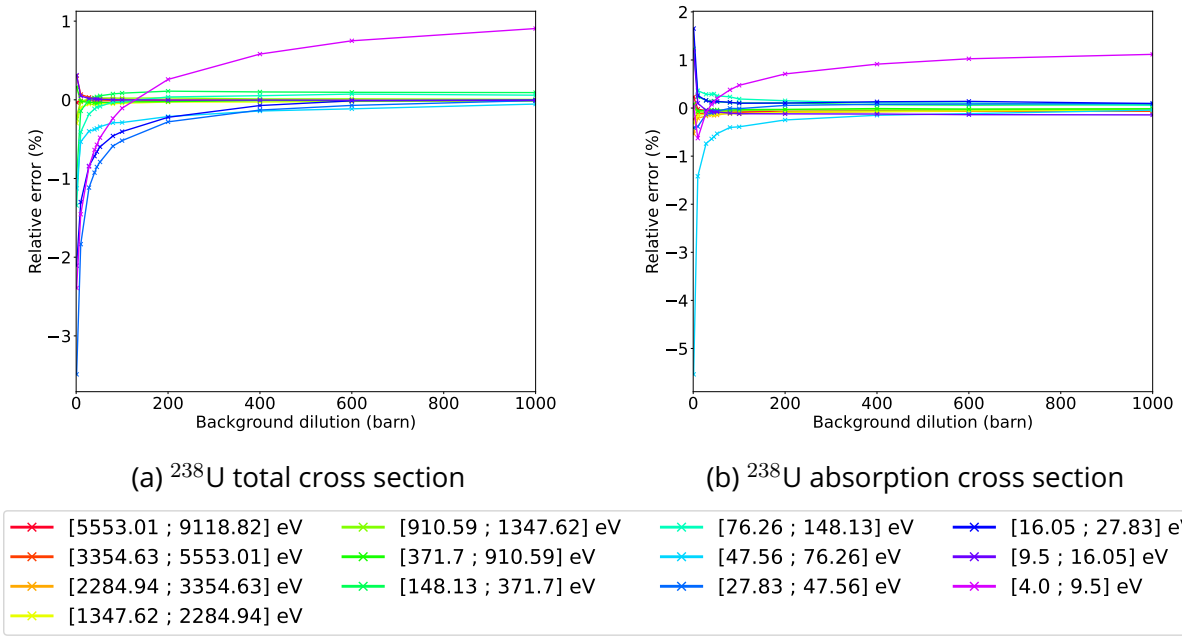

(a) ^{238}U total cross section (b) ^{238}U absorption cross section

Figure 5.3: Relative errors on the ^{238}U cross sections at 2274K

value of the error increases when the background dilution gets smaller. At low dilutions where the error is maximum, it remains under 5%. For most energy groups shown in the Figures, the relative

error converges towards a very small value under 1% when the background dilution approaches high values, except for Group 27, located between 4 eV and 9.5 eV. The diverging trend in this specific energy group is mostly visible at 974K and 2274K. Let us note that a large resonance of ^{238}U, located around 6.67 eV, is in this group, which may explain the difficulty to compute this specific energy range.

Overall, this first numerical test showed the ability of the UFG-IHM solver to compute the cross sections for the ^{238}U with an error of the order of a few percents. It is not yet possible to conclude if this accuracy is satisfying or not, since its impact in a global self-shielding calculation remains to be quantified.

5.2.2 . ^{238}U - ^{235}U resonant mixture

The second test case presented to evaluate the UFG-IHM solver is a resonant mixture composed of two isotopes, ^{238}U and ^{235}U, in proportions representative of a UO_2 fuel material with low enrichment. It corresponds to the "IHM-U8U5-3.7" of Chapter 4.

Figures 5.4 and 5.5 represent the relative error on the total and absorption cross sections of the mixture, and the error on the absorption cross sections of each isotope, for a temperature of 974K. This test case also has been carried out at 294K and 2274K, but no significant difference has been observed from the 974K results.

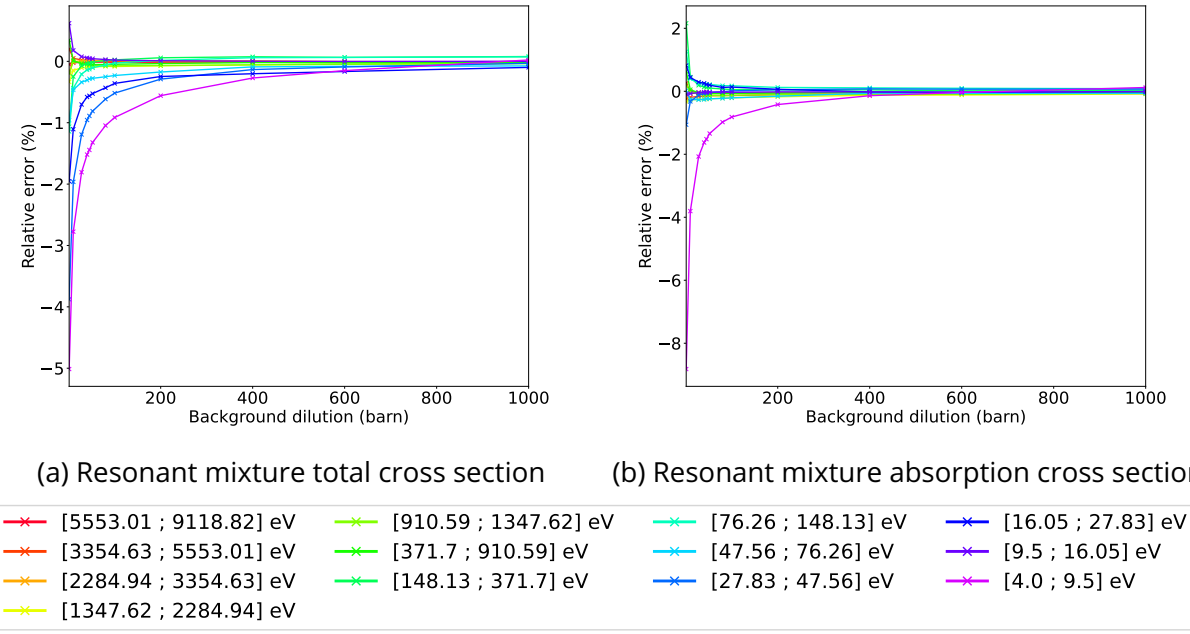

(a) Resonant mixture total cross section (b) Resonant mixture absorption cross section

Figure 5.4: Relative errors on the ^{238}U-^{235}U mixture cross sections at 974K

As was already observed with the previous single isotope case, the relative error converges at high dilutions around a small value of the order of 1%. It is larger for low values of dilutions, especially for the absorption cross section of ^{235}U in the group located between 4.0 and 9.5 eV, where it exceeds -15%. This specific group had already been signaled in the previous test case to show significant errors for the treatment of ^{238}U alone; the addition of ^{235}U in the mixture and the overlapping of the

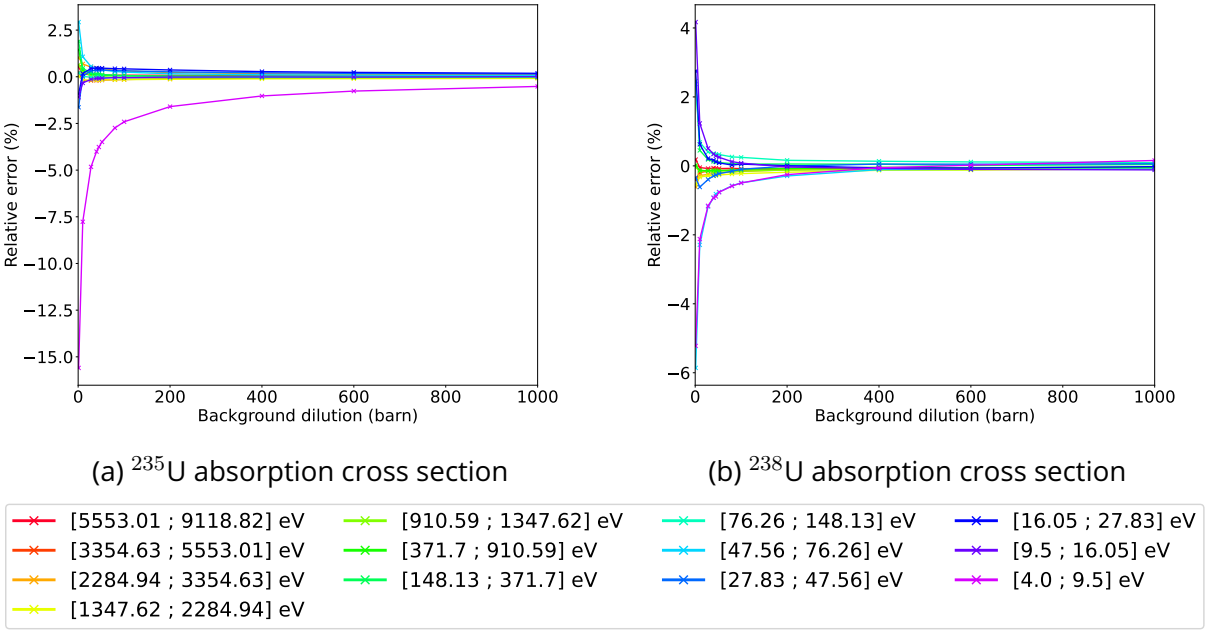

(a) ^{235}U absorption cross section (b) ^{238}U absorption cross section

Figure 5.5: Relative errors on the ^{238}U and ^{235}U absorption cross sections at 974K

resonances of those two isotopes adds complexity to the calculation of this group. It was questioned whether the resonance interference effect could be improved, in order to decrease the error observed on the cross section of ^{235}U.

In the implementation of this UFG-IHM solver, the mixture treatment is operated through the online calculation of mixture MPTs, and through the use of an ultra-fine-group energy structure. We conjectured that the MUSCLET energy mesh was not refined enough in the 4.0 to 9.5 eV energy range to properly take into account interference effects between large resonances. It was decided to create an even finer energy structure by refining each group located between 4.0 eV and 9.5 eV, raising the total number of energy groups from 23317 to 25966 [63], and see if the error on the ^{235}U absorption cross section was diminished. The results of this test, on Figure 5.6 for a temperature of 974K, show no clear sign of improvement. It was therefore concluded that it was not necessary to use a refined version of the MUSCLET energy structure in the UFG-IHM solver, as this would only result in a higher computational time without any proof of a better precision.

The correction of the error measured on the resonant cross sections for low values of background dilutions is still under investigation. Meanwhile, it is expected that the errors observed here may be the source of errors when using these cross sections to generate physical probability tables later on, and thus propagate through the self-shielding calculation to impact the global calculation. We will pay attention to this in the analysis of further numerical results.

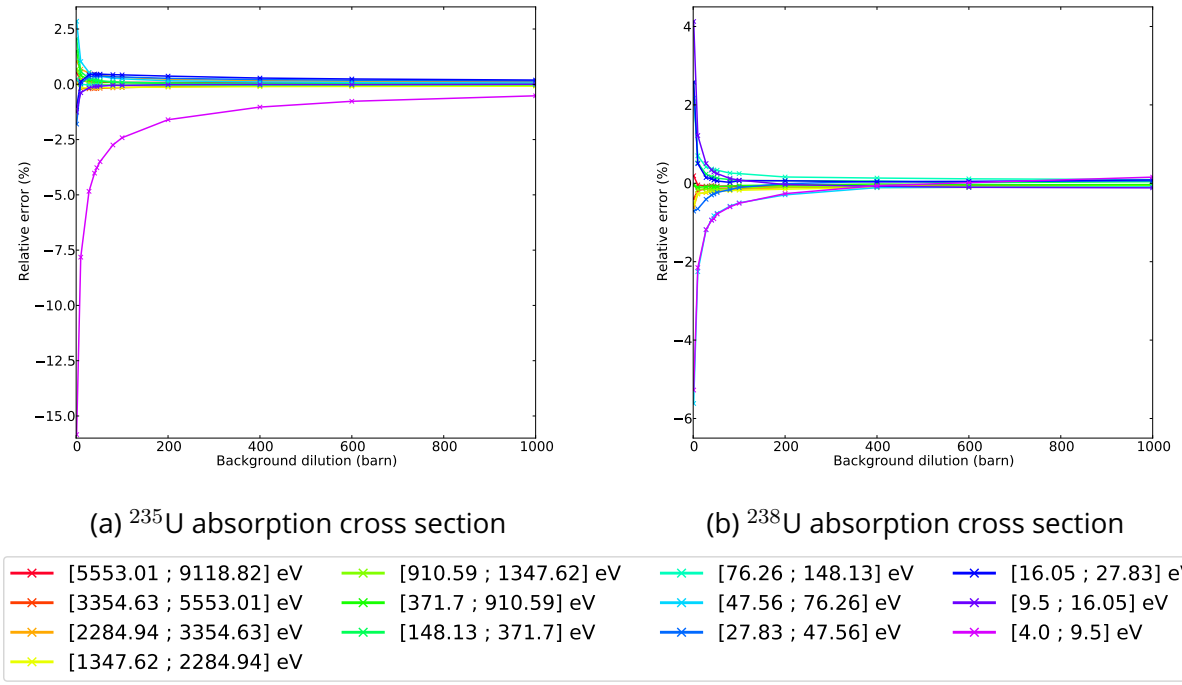

(a) ^{235}U absorption cross section

(b) ^{238}U absorption cross section

Figure 5.6: Relative errors on the ^{238}U and ^{235}U absorption cross sections at 974K, when using the refined 25966-group MUSCLET energy structure in the UFG-IHM solver

5.2.3 . UO_2 mixture

The third numerical test carried out for the validation of the UFG-IHM solver is a resonant mixture containing four different isotopes of uranium, as it is often encountered in calculations with UO_2 fuels. It corresponds to the "IHM-UO_2-3.7" benchmark of Chapter 4.

As in the previous test case, the graphs are presented for the temperature of 974K, as no significant difference was observed at 294K or 2274K.

Figure 5.7 display the relative error on the total and absorption cross sections of the UO_2 mixture. It is similar to the errors shown for in the ^{238}U-^{235}U case, showing that these two isotopes are responsible for most of the error in the UO_2 calculation.

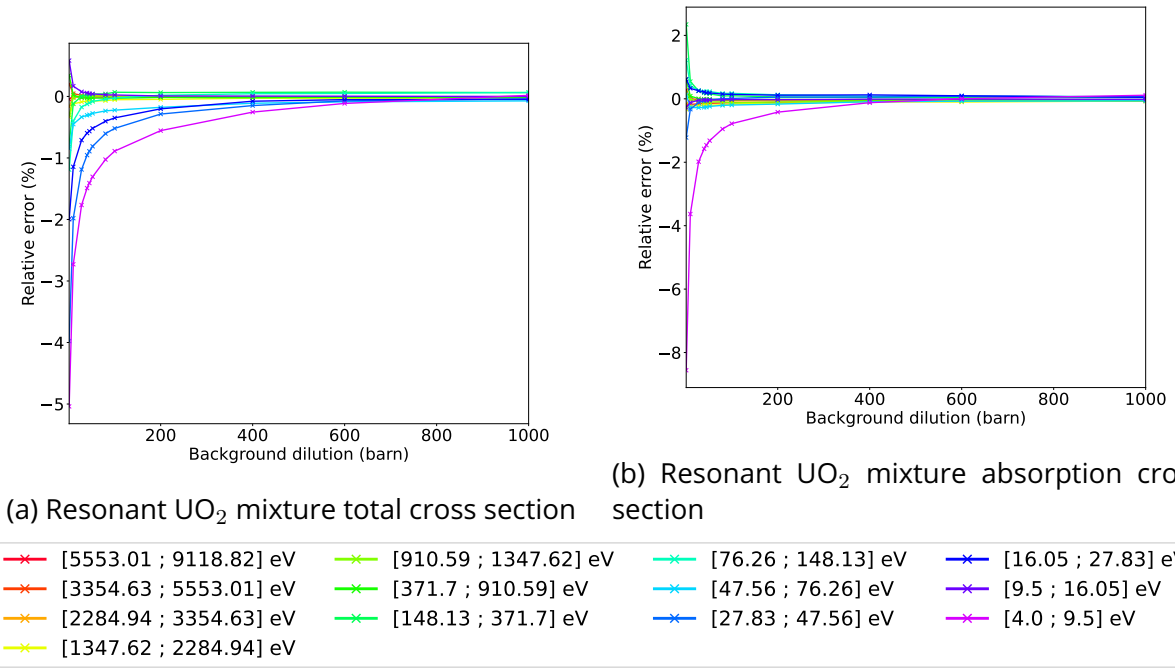

(a) Resonant UO_2 mixture total cross section

(b) Resonant UO_2 mixture absorption cross section

Figure 5.7: Relative errors on the UO_2 mixture cross sections at 974K

The detail on the absorption cross section for each isotope is given in the Figure 5.8. Although the ^{234}U isotope displays particularly high relative errors in some energy groups that do not shrink as much as expected when the background dilution increases, its contribution to the global error of the mixture is in fact almost negligible because it only makes up for a very small proportion of the whole mixture. The same statement can be applied to ^{236}U; although it can be seen that its absorption cross section is not well calculated in the [4.0 ; 9.5] eV and [2284.94 ; 3354.63] eV energy groups, it does not significantly impact the error on the absorption of the whole mixture.

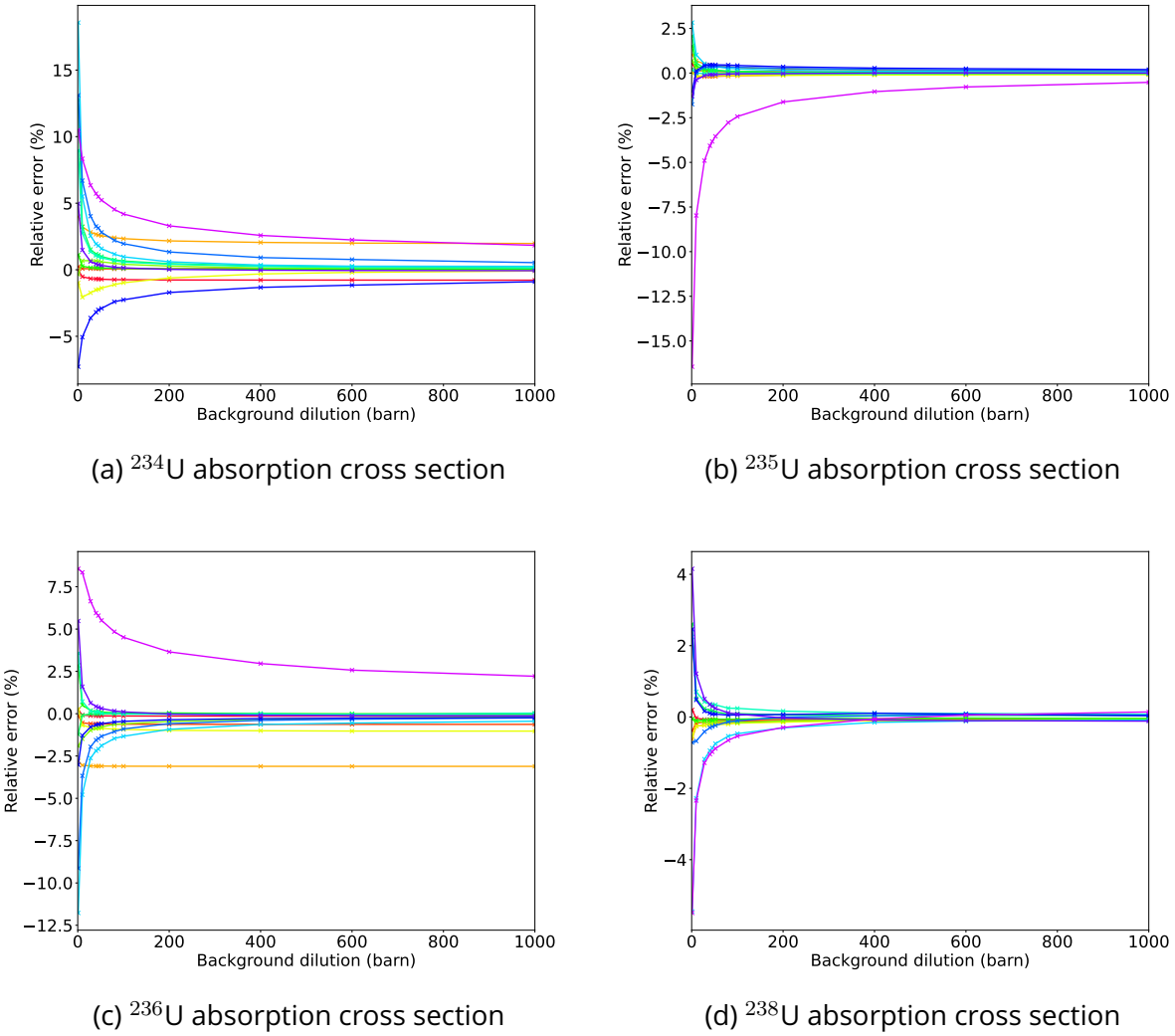

(a) ^{234}U absorption cross section

(b) ^{235}U absorption cross section

(c) ^{236}U absorption cross section

(d) ^{238}U absorption cross section

Figure 5.8: Relative errors on the ^{234}U, ^{235}U, ^{236}U and ^{238}U absorption cross sections at 974K

5.2.4 . MOX mixture

The last mixture calculated to verify the solver is a MOX fuel, corresponding to the "IHM-MOX" test case of Chapter 4. This benchmark is particularly interesting because of the strong resonance interference effect expected between the isotopes of Plutonium and the isotopes of Uranium.

The relative errors on the total and absorption cross sections of the mixture, presented in the Figure 5.9, is converging at high values of background dilutions toward a very small value, under 1% in absolute value. Even for very small dilutions, the error remains quite small, under 5% for the total cross section and 3% for the absorption cross section, which shows that the whole mixture is well calculated by the UFG-IHM solver in all the energy groups of the resonant domain.

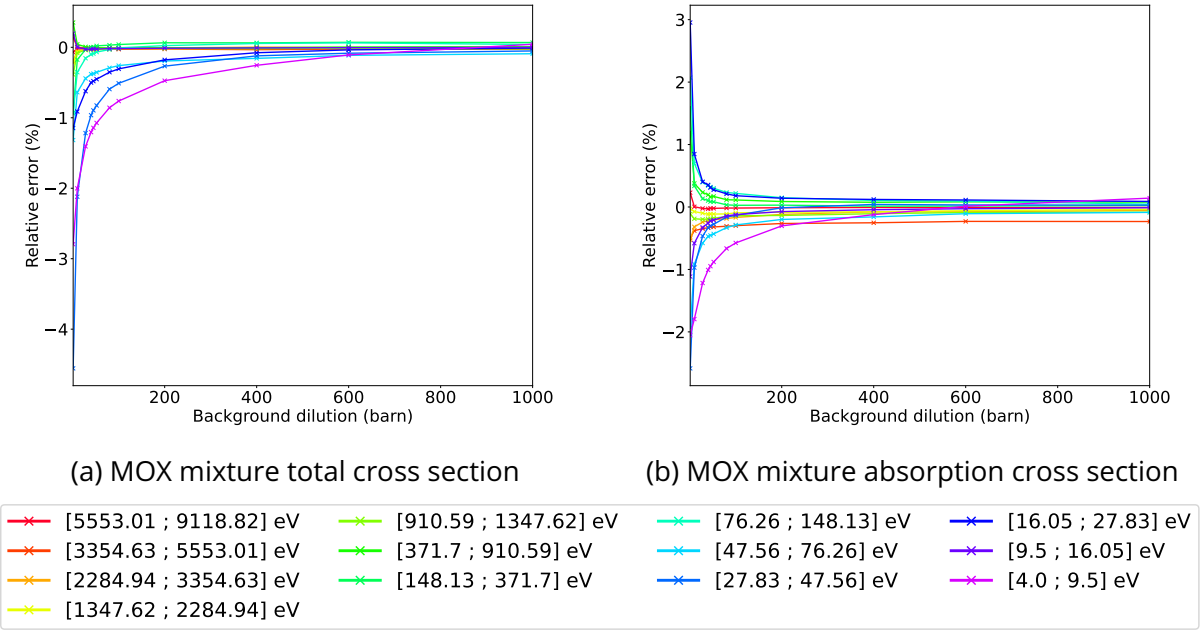

(a) MOX mixture total cross section

(b) MOX mixture absorption cross section

Figure 5.9: Relative errors on the MOX mixture cross sections at 974K

Figure 5.10 displays the relative errors on the absorption cross section of each isotope composing the MOX mixture. The graphs of the ^{235}U and ^{238}U absorption cross sections are similar to the ones previously detailed in the ^{235}U-^{238}U and UO_2 test cases.

The errors on the isotopes of Plutonium are bigger than for the Uranium isotopes, in almost all the energy groups. In some energy groups, the error quickly reaches a plateau and does not decrease anymore with the background dilution. Fortunately this plateau is almost always under the threshold of 5%, in absolute value, except for the ^{242}Pu which presents larger errors, between 5% and 10%, in two energy groups. These two groups are adjacent and cover the energy domain between 910.59 eV and 2284.94 eV. This again could be explained by the resonance overlapping of cross sections in the concerned energy groups, denoting a problem in the online calculation of the mixture mathematical probability tables.

5.3 . Conclusions

In this chapter, we described the verification of a deterministic UFG-IHM solver in APOLLO3®. The quasi-exact resolution of the fine-structure equation relies on a very fine discretization of the energy domain thanks to the use of an ultra fine energy mesh called MUSCLET, which is composed of 23317 groups. In each fine group, the resonant scattering operator is approximated with the "General Resonance" model, and the integrals in energy are computed with the quadrature formula derived from the mixture mathematical probability tables. The resonance interference effects are taken into account thanks to the on-the-fly calculation of mixture MPTs by the GALILEE code. The outcome of this UFG-IHM solver are multigroup cross sections per isotope, condensed onto a coarse energy mesh of 69 groups.

Numerical comparisons with the TRIPOLI-4® code have shown the ability of this solver to compute the cross sections for different values of background dilutions, temperature, and energy groups, and for different kind of resonant mixtures, with a relative error under 5% for most cases, except for low values of dilutions where the error noticeably increases. We observed some significant errors for a few isotopes in specifics energy groups, that could be explained by an insufficiency of the interference effect accounted for by the mixture MPTs.

This should be further investigated in order not to propagate these errors in the calculation of the physical probability tables, and then in the global self-shielding calculation.

Another axis of improvement would be the computation of group-averaged quantities using quadrature formulas that are not derived from the mixture MPTs. Indeed, mixture MPTs can be very time expensive to generate, especially when the mixture is composed of many different resonant isotopes. In practice, there is a limitation on the number of isotopes (around 6) that can be treated using that technique, because the MPTs of more complex mixtures are prohibitively long to compute, especially for industrial purposes. This difficulty could be bypassed using more basic quadrature formula in the ultra-fine-group calculations, such as a rectangle rule, instead of the MPTs. The validation work should then make sure that the overlapping of resonances from different isotopes is well rendered.

Finally, this solver could take into account the up-scattering phenomenon, by slightly changing the expression of the General Resonance model, as is detailed in Reference [45]. In the GR model, the contributions of all the energy groups should be summed, not only the contributions from higher energy. This would require to iterate to converge the sources. This implementation would be straightforward, and would enable to account for the up-scattering in the reference cross section calculation.

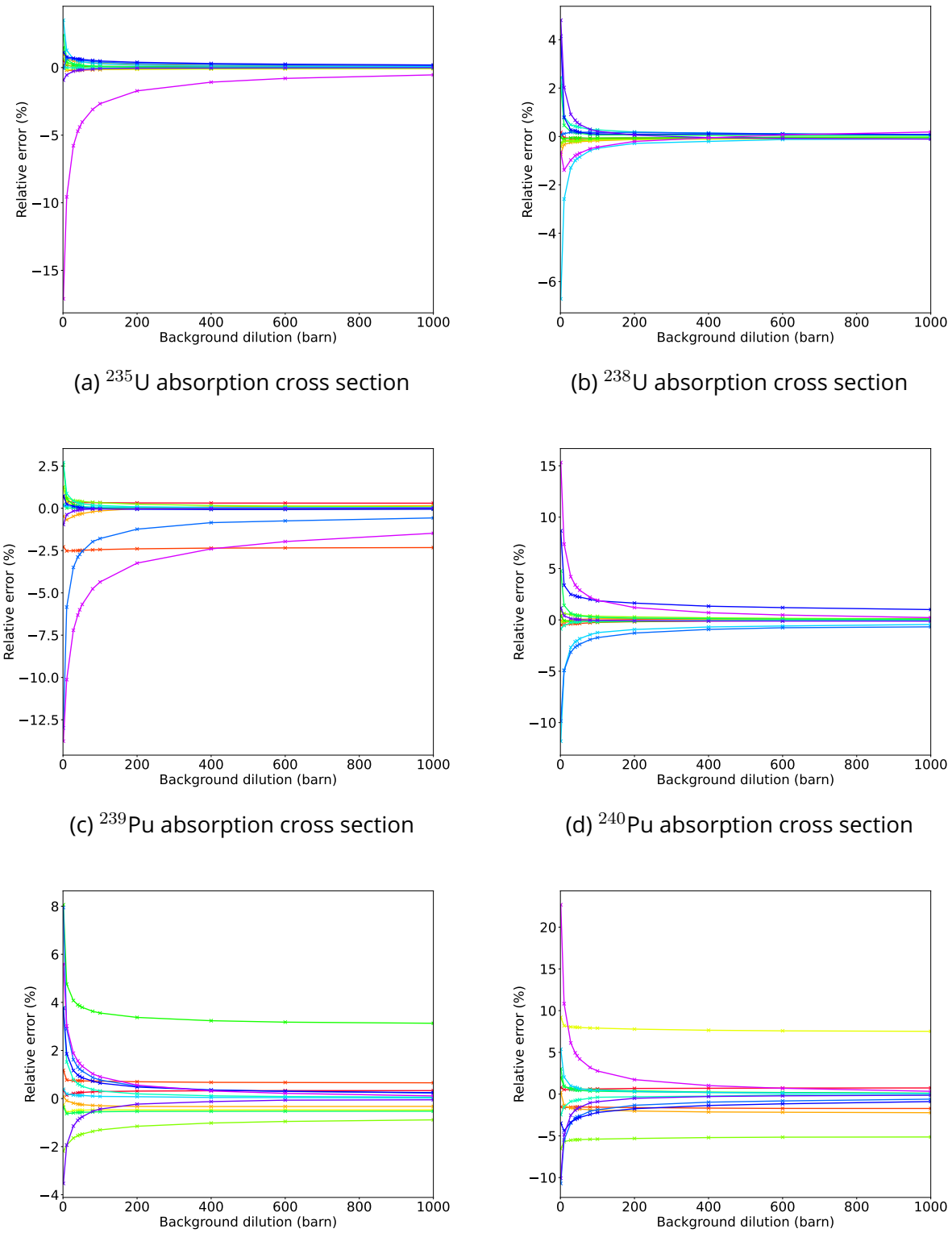

(a) ^{235}U absorption cross section

(b) ^{238}U absorption cross section

(c) ^{239}Pu absorption cross section

(d) ^{240}Pu absorption cross section

(e) ^{241}Pu absorption cross section

(f) ^{242}Pu absorption cross section

Figure 5.10: Relative errors on the absorption cross sections of the isotopes composition the MOX mixture at 974K

6 - On-the-fly Calculation of Physical Probability Tables in APOLLO3®

This chapter describes the calculation of the parameters $\{\omega_k^g, \sigma_k^g, \sigma_{\rho,x,k}^g\}_{\rho,x,k=1,...,K}$ of a Physical Probability Table (PPT) of order K for a resonant energy group g. To facilitate the reading in this chapter, the notations have been lightened by dropping the group index g. It is to be understood that the PPTs are group-dependent.

The fitting procedure of the effective cross sections obtained with an ultra-fine-group slowing-down calculation in an infinite homogeneous medium is described in the first section. It relies on the use of a rational fraction, whose coefficients are obtained by solving a linear system. Two methods have been tested to construct and solve this linear system. In the second section, the determination of the PPT parameters, i.e. the subgroup probabilities and cross sections, serving as quadrature weights and base points, is detailed. The validation of the PPTs is carried out in the third section on several numerical tests, representing resonant mixtures of interest for PWR simulation. The last section of this chapter synthesizes the conclusions of this work, and gives some perspectives on future improvements.

6.1 . Fitting Procedure of the Effective Cross Sections using a Rational Fraction

Let us consider a mixture composed of resonant isotopes, denoted by x, for which we seek to compute a PPT of order K. The UFG-IHM solver, described in Chapter 5, is utilized to generate the reference cross sections of the resonant mixture for M values of background dilutions. They will be denoted $\{\bar{\sigma}(\sigma_{b,m}), m = 1, ..., M\}$ for the total cross section of the whole resonant mixture, and $\{\bar{\sigma}_{\rho,x}(\sigma_{b,m}), m = 1, ..., M\}$ for each of its partial cross sections. The nuclear reactions considered during the calculation of the PPTs are absorption, scattering and fission. In Table 6.1, we selected a list of 13 dilutions ranging from 1 to 1×10^{10} barns, the last one being considered as infinite, from which the M values are picked.

Table 6.1: List of background dilutions employed to generate the reference multigroup cross sections

m	$\sigma_{b,m}$ (barn)	m	$\sigma_{b,m}$ (barn)	m	$\sigma_{b,m}$ (barn)
1	1	6	52	11	600
2	10	7	80	12	1×10^3
3	28	8	100	13	1×10^{10} *
4	40	9	200		
5	45	10	400		

* this value corresponds to the infinite dilution

The fitting procedure of the reference cross sections relies on the use of a Padé approximant, which is a form of rational fraction, leading to the expression

$$\bar{\sigma}(\sigma_b) = \frac{c_0 + c_1\sigma_b + c_2\sigma_b^2 + ... + c_{K-1}\sigma_b^{K-1}}{d_0 + d_1\sigma_b + d_2\sigma_b^2 + ... + d_{K-1}\sigma_b^{K-1}} \tag{6.1}$$

for the total cross section, and

$$\bar{\sigma}_{\rho,x}(\sigma_b) = \frac{e_{\rho,x,0} + e_{\rho,x,1}\sigma_b + e_{\rho,x,2}\sigma_b^2 + ... + e_{\rho,x,K-1}\sigma_b^{K-1}}{d_0 + d_1\sigma_b + d_2\sigma_b^2 + ... + d_{K-1}\sigma_b^{K-1}} \tag{6.2}$$

for the partial cross sections. All the coefficients $\{c_k\}_{k=1,...,K-2}$, $\{d_k\}_{k=1,...,K-2}$ and $\{e_{\rho,x,k}\}_{k=1,...,K-2}$ are unknowns and have to be determined. The coefficients of order $K-1$ are actually known in advance because in order to ensure the preservation of the cross section at infinite dilution, we have to set $c_{K-1} = \bar{\sigma}(\sigma_{b,\infty})$, $e_{\rho,x,K-1} = \bar{\sigma}_{\rho,x}(\sigma_{b,\infty})$ and $d_{K-1} = 1$. Let us also remark that the polynomial at the denominator of the fraction is identical in both relations, decreasing the total number of unknowns to be computed to $2K-2$ for the total cross section, and $K-1$ for each of the partial cross sections. This is accomplished by constructing a linear system of equations, where the number of equations has to be at least equal to the number of unknowns. The size of the linear system can therefore be different for the total and partial cross sections. We will thus distinguish $M \geq 2K-2$ and $M' \geq K-1$, the number of dilutions used for the determination of the unknown coefficients of the total cross section and the partial cross sections respectively.

Two methods, hereafter denominated as Direct Resolution (DR) method and Orthogonal Polynomials (OP) method, are presented to construct and solve the linear system, in order to retrieve the unknow coefficients of the rational fractions of Equations (6.1) and (6.2).

6.1.1 . Direct Resolution method

The DR method is similar to the one presented in the section IV.A. of the Reference [53]. It is quickly recapped in this subsection, separating the calculation stage for the mixture total cross section and the stage for its partial cross sections.

Fitting procedure of the total cross section

The fitting process of the reference mixture total cross section using the DR method is rather straightforward. It consists of writing Equation (6.1) for all of the $M \geq 2K-2$ values of background dilutions, leading to the construction of a linear system of the form $A\vec{x} = \vec{b}$, where $\vec{x}$ is a vector containing all the unknown coefficients:

$$\begin{bmatrix} 1 & \sigma_{b1} & \dots & \sigma_{b1}^{K-2} & -\bar{\sigma}(\sigma_{b1}) & -\bar{\sigma}(\sigma_{b1})\sigma_{b1} & \dots & -\bar{\sigma}(\sigma_{b1})\sigma_{b1}^{K-2} \\ 1 & \sigma_{b2} & \dots & \sigma_{b2}^{K-2} & -\bar{\sigma}(\sigma_{b2}) & -\bar{\sigma}(\sigma_{b2})\sigma_{b2} & \dots & -\bar{\sigma}(\sigma_{b2})\sigma_{b2}^{K-2} \\ \vdots & \vdots & & \vdots & \vdots & & \vdots & \\ 1 & \sigma_{b,M} & \dots & \sigma_{b,M}^{K-2} & -\bar{\sigma}(\sigma_{b,M}) & -\bar{\sigma}(\sigma_{b,M})\sigma_{b,M} & \dots & -\bar{\sigma}(\sigma_{b,M})\sigma_{b,M}^{K-2} \end{bmatrix} \begin{pmatrix} c_0 \\ \vdots \\ c_{K-2} \\ d_0 \\ \vdots \\ d_{K-2} \end{pmatrix} = \begin{pmatrix} \sigma_{b1}^{K-1}\left[\bar{\sigma}(\sigma_{b1}) - \bar{\sigma}(\sigma_{b,\infty})\right] \\ \vdots \\ \vdots \\ \vdots \\ \sigma_{b,M}^{K-1}\left[\bar{\sigma}(\sigma_{b,M}) - \bar{\sigma}(\sigma_{b,\infty})\right] \end{pmatrix}. \tag{6.3}$$

This system is solved using the QR factorization of the LAPACK fortran library with the routines DGEQRF and DORGQR. The size of the system is conditioned by the number M, which is the number of equations used to compute the coefficients. For the total cross section, M has to be at least $2K-2$, the number of coefficients to be determined, but it can be larger. In this case, the solution of the system is not exact but corresponds to the least square solution.

Fitting procedure of the partial cross sections

The fitting procedure of the partial cross sections using the DR method is almost identical as the one described for the total cross section. The main difference lies in the reduced number of unknowns, as the coefficients of the denominator of the rational fraction in Equation (6.2) have already been determined in the previous stage of the calculation. Writing Equation (6.2) for at least $M' \geq K-1$ values of background dilutions, another linear system of equations is formed:

$$\begin{pmatrix} 1 & \sigma_{b1} & \dots & \sigma_{b1}^{K-2} \\ \vdots & \vdots & & \vdots \\ 1 & \sigma_{b,M'} & \dots & \sigma_{b,M'}^{K-2} \end{pmatrix} \begin{pmatrix} e_{\rho,x,0} \\ \vdots \\ e_{\rho,x,K-2} \end{pmatrix} = \begin{pmatrix} Q(\sigma_{b,1})\bar{\sigma}_{\rho,x}(\sigma_{b,1}) - \bar{\sigma}_{\rho,x}(\sigma_{b,\infty})\sigma_{b,1}^{K-1} \\ \vdots \\ Q(\sigma_{b,M'})\bar{\sigma}_{\rho,x}(\sigma_{b,M'}) - \bar{\sigma}_{\rho,x}(\sigma_{b,\infty})\sigma_{b,M'}^{K-1} \end{pmatrix}, \tag{6.4}$$

where $Q(\sigma_{b,m}) = d_0 + d_1\sigma_{b,m} + d_2\sigma_{b,m}^2 + ... + d_{K-1}\sigma_{b,m}^{K-1}$, for $m = 1, ..., M'$. This linear system of equation is solved directly using the QR decomposition of the LAPACK library.

6.1.2 . Orthogonal Polynomials method

The idea behind the development of the OP method stems from the intent to simplify the matrix A involved in the linear system of equations [64]. An ideal pre-conditionment of the problem would lead to the resolution of a diagonal or triangular system, as they can be solved effortlessly.

Determination of the unknown coefficients for the total cross section

A family of orthogonal polynomials can be generated using the following three terms recurrence relation [65]:

$$\begin{cases} P_{-1}(x) = 0 \\ P_0(x) = 1 \\ P_k(x) = (x - \alpha_k)P_{k-1}(x) - \beta_k P_{k-2}(x). \end{cases} \tag{6.5}$$

The coefficients α_k and β_k are deduced from the orthogonality condition, that is specific to the set of dilutions $\{\sigma_{b,m}, m = 1, ..., M\}$:

$$\langle P_i, P_j \rangle = \sum_{m=1}^{M} P_i(\sigma_{b,m}) P_j(\sigma_{b,m}) = 0 \text{ if } i \neq j. \tag{6.6}$$

The coefficients α_k and β_k appearing in the recurrence relation can be deduced from Equations (6.5) and (6.6):

$$\alpha_k = \frac{\sum_{m=1}^{M} \sigma_{b,m} P_{k-1}^2(\sigma_{b,m})}{\sum_{m=1}^{M} P_{k-1}^2(\sigma_{b,m})}, \tag{6.7}$$

$$\beta_k = \frac{\sum_{m=1}^{M} \sigma_{b,m} P_{k-1}(\sigma_{b,m}) P_{k-2}(\sigma_{b,m})}{\sum_{m=1}^{M} P_{k-2}^2(\sigma_{b,m})} = \frac{\sum_{m=1}^{M} P_{k-1}^2(\sigma_{b,m})}{\sum_{m=1}^{M} P_{k-2}^2(\sigma_{b,m})}. \tag{6.8}$$

For a PPT of order K, all the polynomials from P_0 to P_{K-1} have to be generated, to be able to reformulate (6.1) using the newly defined orthogonal polynomials:

$$\bar{\sigma}(\sigma_b) = \frac{c'_0 P_0(\sigma_b) + ... + c'_{K-1} P_{K-1}(\sigma_b)}{d'_0 P_0(\sigma_b) + ... + d'_{K-1} \times P_{K-1}(\sigma_b)}. \tag{6.9}$$

Equations (6.9) and (6.1) should actually represent the same rational fraction, the only difference being the way the terms are organized. Determining the coefficients $\{c'_k\}_{k=1,...,K-1}$ and $\{d'_k\}_{k=1,...,K-1}$ should therefore allow to find, by matching the coefficients between the two equivalent expressions, the coefficients $\{c_k\}_{k=1,...,K-1}$ and $\{d_k\}_{k=1,...,K-1}$ of Equation (6.1). One can already deduce that the coefficients of highest order should be identical, because they are the only ones multiplying the terms in σ_b^{K-1}. This leads to setting $c'_{K-1} = c_{K-1} = \bar{\sigma}(\sigma_{b,\infty})$ and $d'_{K-1} = d_{K-1} = 1$ in order to preserve the infinite dilution value.

An error function is defined, so that its minimization provides the linear system of equations to solve in order to retrieve the unknowns coefficients of the rational fraction (6.9):

$$\varphi(c'_0, ..., c'_{K-2}, d'_0, ..., d'_{K-2}) = \sum_{m=1}^{M} \left[\sum_{i=0}^{K-1} c'_i P_i(\sigma_{b,m}) - \bar{\sigma}(\sigma_{b,m}) \sum_{i=0}^{K-1} d'_i P_i(\sigma_{b,m}) \right]^2. \tag{6.10}$$

Enforcing that the gradient of this error function should be null leads to the following set of linear equations:

$$c'_j W_{jj} - \sum_{i=0}^{K-2} d'_i U_{ij} = U_{K-1,j} \quad \text{for} \quad j = 0, ..., K-2, \tag{6.11}$$

$$\sum_{i=0}^{K-2} c'_i U_{ij} - \sum_{i=0}^{K-2} d'_i V_{ij} = -\bar{\sigma}(\sigma_{b,\infty}) U_{K-1,j} + V_{K-1,j} \quad \text{for} \quad j = 0, ..., K-2. \tag{6.12}$$

where the following notations were employed

$$W_{ij} = \langle P_i, P_j \rangle = \sum_{m=1}^{M} P_i(\sigma_{b,m}) P_j(\sigma_{b,m}) = W_{ji}, \tag{6.13}$$

$$U_{ij} = \langle \bar{\sigma} P_i, P_j \rangle = \sum_{m=1}^{M} \bar{\sigma}(\sigma_{b,m}) P_i(\sigma_{b,m}) P_j(\sigma_{b,m}) = U_{ji}, \tag{6.14}$$

$$V_{ij} = \langle \bar{\sigma} P_i, \bar{\sigma} P_j \rangle = \sum_{m=1}^{M} \bar{\sigma}^2(\sigma_{b,m}) P_i(\sigma_{b,m}) P_j(\sigma_{b,m}) = V_{ji}\ , \tag{6.15}$$

with $W_{ij} = 0$ if $i \neq j$. The first set of Equations (6.11) is diagonal on the $\{c'_k\}_{k=0,...,K-2}$ unknowns and, therefore, can be used to eliminate these unknowns from the second system of equations in (6.12). When the linear system is put into a matrix-vector form $A\vec{x} = \vec{b}$, it can be observed that the matrix A is composed of a diagonal bloc in its upper left part, but that it is not completely diagonal. The announced objective of simplifying the linear system using orthogonal polynomials was consequently not successfully completed; but, the interest of the OP method will appear clearly in the calculation of the coefficients for the partial cross sections hereafter.

Determination of the unknown coefficients for the partial cross sections

Because the definition of the scalar product in Equation (6.6) is dependent on the number and values of the background dilutions, a new family of orthogonal polynomials has to be created if any other set of dilutions is chosen to compute the coefficients of the partial cross sections. In the case where the exact same set of dilutions is employed, then the same family of polynomials can be re-used.

As for the fitting process of the total cross section, the use of the OP method for the partial cross sections consists in re-writing Equation (6.2) using the set of orthogonal polynomials P:

$$\bar{\sigma}_{\rho,x}(\sigma_{b,m}) = \frac{e'_0 P_0(\sigma_{b,m}) + ... + e'_{K-1} P_{K-1}(\sigma_{b,m})}{d'_0 P_0(\sigma_{b,m}) + ... + d'_{K-1} P_{K-1}(\sigma_{b,m})}\ , m = 1, ..., M', \tag{6.16}$$

To determine the unknown coefficients of the numerator, the following error function is minimized:

$$\varphi_{\rho,x}(e'_0, ..., e'_{K-2}) = \sum_{m=1}^{M'} \left[\sum_{i=0}^{K-2} e'_i P_i(\sigma_{b,m}) - f_{\rho,x}(\sigma_{b,m}) \right]^2 , \tag{6.17}$$

where $f_{\rho,x}(\sigma_{b,m}) = \bar{\sigma}_{\rho,x}(\sigma_{b,m}) \sum_{i=0}^{K-1} d'_i P_i(\sigma_{b,m}) - \bar{\sigma}_{\rho,x}(\sigma_{b,\infty}) \sigma_{b,m}^{K-1}$. It leads to a direct relation to compute each of the unknown coefficient of the numerator, without having to resolve any linear system of equations:

$$e'_i = \frac{\sum_{m=1}^{M'} f_{\rho,x}(\sigma_{b,m}) P_i(\sigma_{b,m})}{\sum_{m=1}^{M'} P_i^2(\sigma_{b,m})}. \tag{6.18}$$

The main advantage of the OP methods is evident: the absence of any system to solve in order to determine the coefficients for the partial cross sections may lead to a gain of computational time, especially when the number of isotopes is large.

6.2 . Calculation of the Physical Probability Table Parameters

For reminder, a PPT of order K is composed of K subgroup weights ω_k, K subgroup total cross sections σ_k and K subgroup partial cross sections $\sigma_{\rho,x,k}$ for each nuclear reaction ρ, and each resonant isotope x in the mixture. These are all the parameters we need to compute, for each resonant energy group.

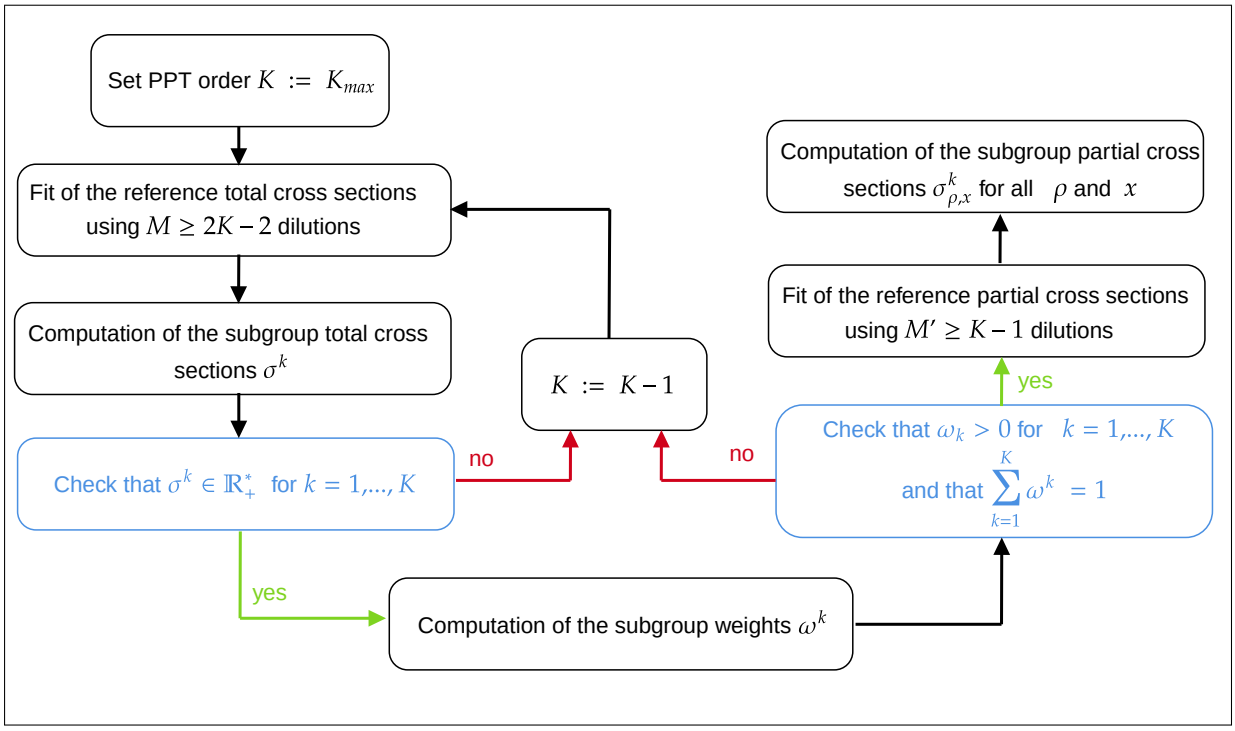

Figure 6.1: Calculation steps of a physical probability table

In practice, the operations are carried out in the order indicated in the diagram of Figure 6.1. A maximal PPT order K_{max} is set depending on the number of reference cross sections available after the quasi-exact slowing-down calculation. Because at least $2K-2$ values of dilutions are required to fit the total cross section with both the DR and OP methods, in addition of the infinite value, and because 13 values were selected in Table 6.1, K_{max} is maximum equal to 7 in our case.

In this section, the computation of the PPT parameters is described, using the rational approximations obtained in the last section.

The relation to determine the subgroup total cross sections, σ_k, is obtained by enforcing the following criteria:

$$\bar{\sigma}(\sigma_b) = \sigma(\sigma_b), \tag{6.19}$$

for each value of background dilution listed in Table 6.1. This criteria translates the preservation of the reference effective cross sections for certain values of background dilutions, as $\sigma(\sigma_b)$ designates the cross sections reconstructed using the PPT parameters:

$$\sigma(\sigma_b) = \frac{\sum_{k=1}^{K} \frac{\omega_k \sigma_k}{\sigma_k + \sigma_b}}{\sum_{k=1}^{K} \frac{\omega_k}{\sigma_k + \sigma_b}}. \tag{6.20}$$

Equation (6.19) can be expressed in an equivalent form:

$$\bar{\sigma}(\sigma_b) = \frac{\sum_{k=1}^{K} \omega_k \sigma_k \prod_{\substack{l=1 \\ l \neq k}}^{K} (\sigma_l + \sigma_b)}{\sum_{k=1}^{K} \omega_k \prod_{\substack{l=1 \\ l \neq k}}^{K} (\sigma_l + \sigma_b)}. \tag{6.21}$$

By taking $\sigma_b = -\sigma_n$, where σ_n is supposed to be one of the K subgroup base point, it becomes:

$$\bar{\sigma}(-\sigma_n) = \frac{\sum_{k=1}^{K} \omega_k \sigma_k \prod_{\substack{l=1 \\ l \neq k}}^{K} (\sigma_l - \sigma_n)}{\sum_{k=1}^{K} \omega_k \prod_{\substack{l=1 \\ l \neq k}}^{K} (\sigma_l - \sigma_n)}, \tag{6.22}$$

where one may notice that the term $\prod_{\substack{l=1 \\ l \neq k}}^{K} (\sigma_l - \sigma_n)$ is always equal to 0, except when $n = k$. The sum at both the numerator and the denominator of the fraction therefore contains only one term each, and the global expression can be resumed to:

$$\begin{aligned} \bar{\sigma}(-\sigma_n) &= \frac{\omega_n \sigma_n}{\omega_n} \\ &= \sigma_n. \end{aligned} \tag{6.23}$$

Combining Equations (6.1) and (6.23), we obtain:

$$\begin{aligned} \sigma_n &= \frac{c_0 + c_1(-\sigma_n) + c_2(-\sigma_n)^2 + ... + c_{K-1}(-\sigma_n)^{K-1}}{d_0 + d_1(-\sigma_n) + d_2(-\sigma_n)^2 + ... + d_{K-1}(-\sigma_n)^{K-1}} \\ \iff 0 &= c_0 + (c_1 + d_0)(-\sigma_n) + ... + (c_{K-1} + d_{K-2})(-\sigma_n)^{K-1} + d_{K-1}(-\sigma_n)^K \end{aligned} \tag{6.24}$$

This relation is true for every subgroup base point. In other words, the researched base points are the roots of the following polynomial of order K:

$$P(-\sigma) = c_0 + (c_1 + d_0)(-\sigma) + ... + (c_{K-1} + d_{K-2})(-\sigma)^{K-1} + d_{K-1}(-\sigma)^K. \tag{6.25}$$

A wide variety of algorithms exist to solve for the roots of a polynomial. It was chosen to implement the Aberth method [66] to compute simultaneously all the roots of this polynomial in the complex plan. A first guess is necessary to initialize the set of roots $\{z_k^{(0)},\ k = 1, ..., K\}$. The Cauchy bound [67] of polynomial (6.25) is calculated and used to limit a disk in the complex plane, in which the initial values of the roots are drawn randomly. Each iteration then converges the set of complex roots

$$z_k^{(n+1)} = z_k^{(n)} - \frac{\dfrac{P(z_k^{(n)})}{P'(z_k^{(n)})}}{1 - \dfrac{P(z_k^{(n)})}{P'(z_k^{(n)})} \displaystyle\sum_{i \neq k} \frac{1}{z_k^{(n)} - z_i^{(n)}}}, \quad k = 1, ..., K, \tag{6.26}$$

where n is the iteration index. When the convergence is reached, the roots are checked in order to ensure that they all are real and positive. If that is not the case, then the computation of a PPT of order K fails. The order of the probability is decreased of one, and the PPT calculation is restarted, until all the subgroup total cross sections are found real and positive.

In the case where the PPT order is 2 and a complex or negative subgroup total cross section is found, the order of the PPT is decreased to 1. In that case, it is not necessary to go through the whole fitting process again, as the probability table of order 1 is just composed of a single base point with an associated weight of 1. The base point is simply the mean value of all the reference cross sections for the resonant group.

When all the subgroup base points for the total cross section are found real and positive, the subgroup weights are computed using the direct relation:

$$\omega_k = \frac{d_0 + ... + d_{K-1}(-\sigma_k)^{K-1}}{\displaystyle\prod_{\substack{l=1 \\ l \neq k}}^{K} (\sigma_l - \sigma_k)}, \quad k = 1, ..., K. \tag{6.27}$$

The determination of the base points for the subgroup partial cross sections, for every reaction ρ and resonant isotope x, consists in enforcing the fitting criteria

$$\bar{\sigma}_{\rho,x}(\sigma_b) = \sigma_{\rho,x}(\sigma_b),\ m = 1, ..., M' \tag{6.28}$$

where

$$\sigma_{\rho,x}(\sigma_b) = \frac{\displaystyle\sum_{k=1}^{K} \frac{\omega_k \sigma_{\rho,x,k}}{\sigma_k + \sigma_b}}{\displaystyle\sum_{k=1}^{K} \frac{\omega_k}{\sigma_k + \sigma_b}}. \tag{6.29}$$

From Equation (6.2) can be derived a direct relation for the determination of the subgroup base points for the partial cross sections:

$$\sigma_{\rho,x,k} = \frac{\displaystyle\sum_{l=0}^{K-1} e_{\rho,x,l}(-\sigma_k)^l}{\displaystyle\sum_{l=0}^{K-1} d_l(-\sigma_k)^l}, \; k = 1, ..., K. \tag{6.30}$$

6.3 . Numerical Validation of the Physical Probability Tables on the Coarse 69 Group Energy Mesh

In the previous section, the online generation of physical probability tables in APOLLO3® was described, using as entry data the reference cross sections of a resonant mixture in an infinite homogeneous medium tabulated for different values of background dilutions. In this section, we will now present numerical tests carried out on resonant mixtures of various complexity to ensure that the computed PPTs are capable of correctly fitting the input reference cross sections.

Given a mixture composed of x resonant isotopes, whose reference cross sections are known for a list of background dilutions σ_b, and denoted $\bar{\sigma}(\sigma_b)$ and $\bar{\sigma}_{\rho,x}(\sigma_b)$ for the total and partial cross sections respectively, the relative error (in percent) on the computed PPT is given by the relation:

$$\varepsilon(\sigma_b) = 100 \times \frac{\sigma(\sigma_b) - \bar{\sigma}(\sigma_b)}{\bar{\sigma}(\sigma_b)} \tag{6.31}$$

and

$$\varepsilon_{\rho,x}(\sigma_b) = 100 \times \frac{\sigma_{\rho,x}(\sigma_b) - \bar{\sigma}_{\rho,x}(\sigma_b)}{\bar{\sigma}_{\rho,x}(\sigma_b)}, \tag{6.32}$$

where $\sigma(\sigma_b)$ and $\sigma_{\rho,x}(\sigma_b)$ are the reconstructed cross sections using the PPT parameters, as defined in relations (6.20) and (6.29). The PPTs were calculated using a total of 13 dilutions, listed in Table 6.1, but for this numerical validation, the reference cross sections were calculated for an extended set of 53 background dilutions, one of them being the infinite dilution $\sigma_{b,\infty} = 10^{10}$ barns.

6.3.1 . UO_2 mixture

Because it was observed in Chapter 5 that the effective cross sections calculated with the UFG-IHM solver were so similar in the "IHM-U8U5-3.7" and in the "IHM-UO_2-3.7" benchmarks, only the latter is presented in the current chapter. The errors are displayed in the energy group located between 4.0 eV and 9.5 eV because there is a significant overlapping of a very large resonance of ^{238}U with smaller and more numerous resonances of ^{235}U.

Figure 6.2 shows the difference in the relative error for the total cross section of the UO_2 mixture and the ^{238}U absorption cross section for both the DR and OP method, depending on the number of dilutions employed in the fitting procedure. In these graphs, the errors on PPTs of order 5 are presented. The errors are found to be nearly identical for the two fitting methods; this is actually to be expected since the OP method is just a reformulation of the fitting problem directly solved in the DR method; given the same set of input effective cross sections, they should effectively provide the same rational fraction, and so the same subgroup parameters. The slight differences observed on the Figure 6.2 for a PPT of order 5 are mostly due to accumulated numerical errors in the OP method. Indeed, this method has been found to be more prone to numerical instability. It could maybe be improved by defining another scalar product to generate the set of orthogonal polynomials used in the fitting procedure; also, a naive evaluation of the polynomials was implemented in APOLLO3®, and it could most likely be improved to reduce the errors of this method.

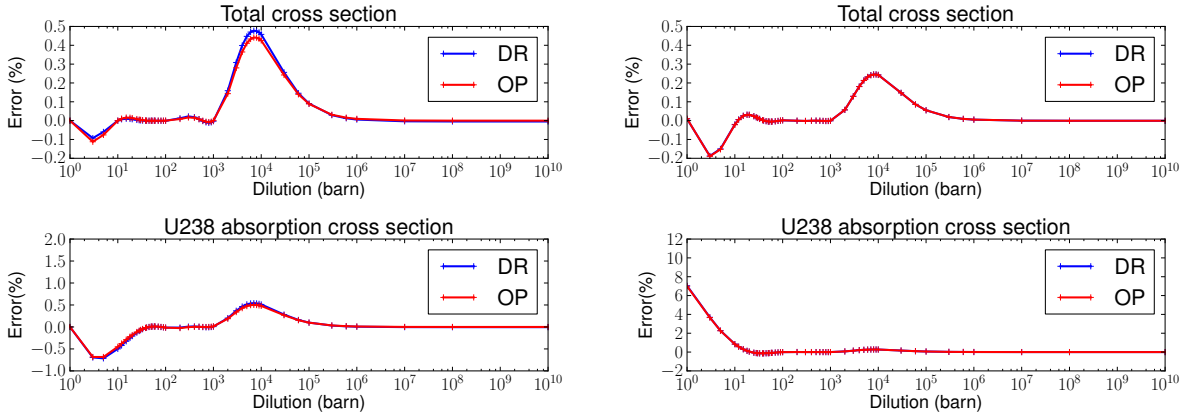

(a) $(2K-2)$ dilutions (b) 12 dilutions

Figure 6.2: Comparison of the DR and OP methods in the [4.0 ; 9.5] eV energy group ($K=5$)

Figures 6.3 to 6.7 focus on the relative error for different order K of PPT on the total cross section of the whole mixture and on the absorption cross section of each of the resonant isotope composing the mixture, when the PPT has been generated according to the DR method using $2K-2$ background dilutions in the fitting procedure, in addition of the infinite dilution. The errors obtained when calculating the PPT with 13 dilutions, or with the OP method, are not displayed because Figure 6.2 shows that they are very similar.

As can be expected, the difference observed between the reference cross section and the reconstructed one is tightly linked to the PPT order. The lower the PPT order K, the higher the relative error.

The relative error for a PPT of order 5 is under 1% on all the dilution range and does not present the typical oscillating behavior observed with lower orders, showing that a very satisfying level of precision has already been reached. In practice, although the theoretical maximum PPT order reachable with a list of 13 reference cross sections is 7, we never managed to obtain PPTs with an order superior to 5. For $K=6$ and $K=7$, at least one of the base points for the total cross section was found either negative or complex, leading to the failure of the PPT calculation process and the

decrease of the order.

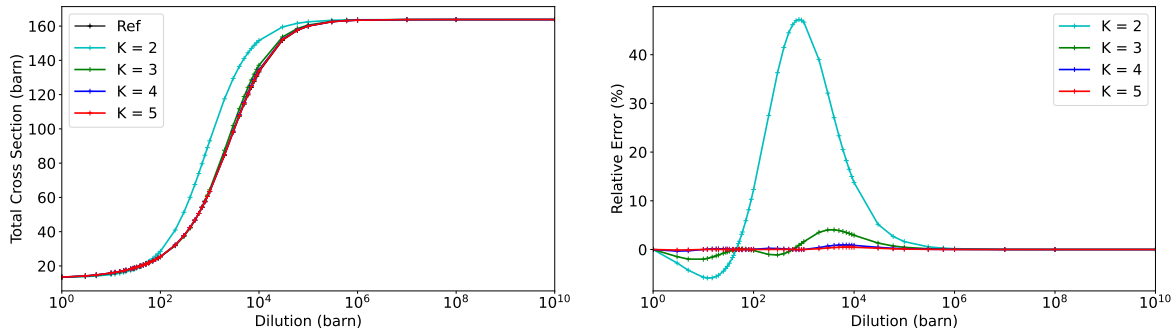

Figure 6.3: Error on the UO_2 mixture total cross section using the DR method, for different order K of PPT, in the [4.0 ; 9.5] eV energy group

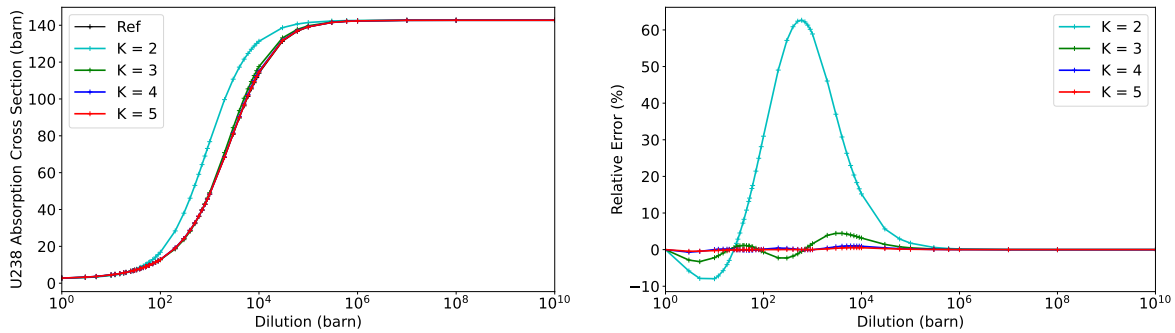

Figure 6.4: Error on the ^{238}U absorption cross section using the DR method, for different order K of PPT, in the [4.0 ; 9.5] eV energy group

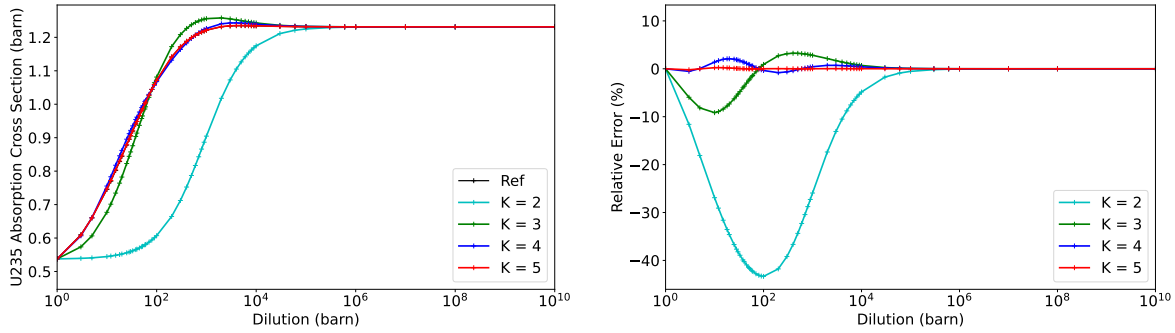

Figure 6.5: Error on the ^{235}U absorption cross section using the DR method, for different order K of PPT, in the [4.0 ; 9.5] eV energy group

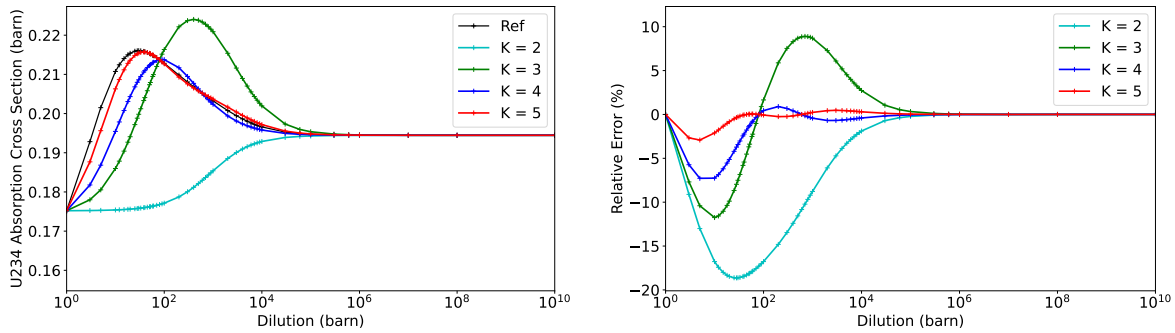

Figure 6.6: Error on the ^{234}U absorption cross section using the DR method, for different order K of PPT, in the [4.0 ; 9.5] eV energy group

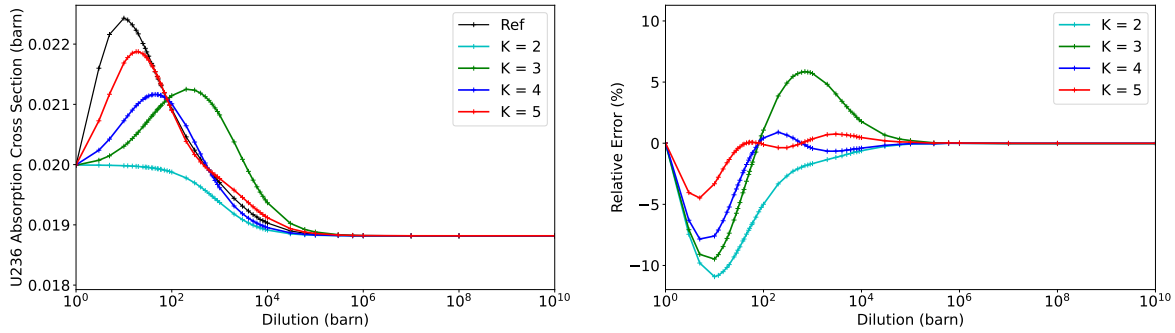

Figure 6.7: Error on the ^{236}U absorption cross section using the DR method, for different order K of PPT, in the [4.0 ; 9.5] eV energy group

6.3.2 . MOX mixture

The second test case presented in this section of numerical validation is representative of a MOX fuel calculation, the mixture being composed of six resonant isotopes of both uranium and plutonium. The resonant mixture is described in Chapter 4 under the name of "IHM-MOX". The results are displayed in the group between 27.8 eV and 47.5 eV, because both the isotopes of Uranium and Plutonium display significant resonances in this range.

Figures 6.8 and 6.9 present the relative error on the constructed total cross section of the whole MOX mixture, and of the absorption cross section of ^{238}U. The DR method has been selected for the fitting procedure, using $2K-2$ values of background dilutions for the calculation of a PPT of order K, in addition of the infinite dilution $\sigma_{b,\infty}$. The conclusions drawn from the study of these graphs are identical to the ones of the previous test cases:

1. The higher the PPT order, the more precise the reconstructed cross sections are.

2. A PPT of order 5 already yields a very satisfying level of precision for both the total cross section of the mixture, and its partial cross sections.

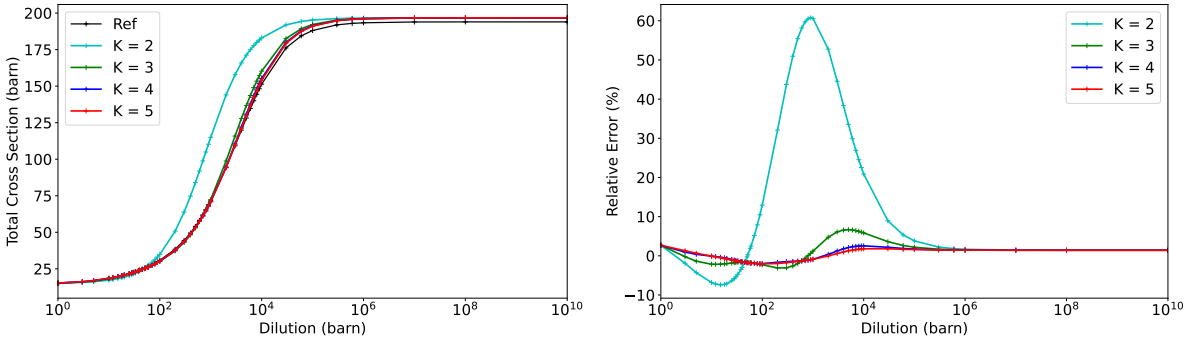

Figure 6.8: Error on the total cross section using the DR method, for different order K of PPT, in the [27.8 ; 47.5] eV energy group

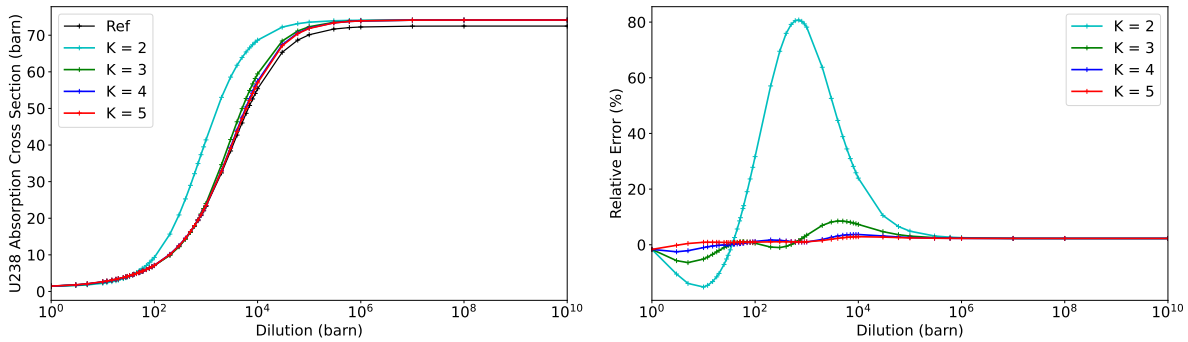

Figure 6.9: Error on the ^{238}U absorption cross section using the DR method, for different order K of PPT, in the [27.8 ; 47.5] eV energy group

6.4 . Conclusions

In this section, we described the routines that were implemented in APOLLO3® to fit a list of reference cross sections using rational fractions. Two methods were proposed: the "Direct Resolution" method which consists of solving the linear system of equations for the unknown coefficients of the rational fraction, without any form of pre-conditioning. The "Orthogonal Polynomial" method is based on the reformulation of the linear system, using orthogonal polynomials calculated online, in order to simplify the system of equations before solving it. In theory, the OP method is particularly interesting for the fitting of the partial cross sections because it provides an analytical expression for the computation of the unknown coefficients. Nonetheless, very few studies have been conducted on the OP approach and it has not yet been coupled to the APOLLO3® self-shielding methods. In the rest of this thesis work, the DR method is selected to calculate the PPTs.

The numerical tests to validate the cross sections calculated with the newly developed PPTs have shown a very satisfying precision, for simple and more complex resonant mixtures. In particularly, a PPT of order 5 was demonstrated to be enough to have a relative error of less than 1% on all the dilution domain. The difficulties we encountered to calculate PPTs of higher orders should be investigated.

At this point, it is important to note that while it is crucial that the calculated PPTs should accurately reproduce the reference cross sections, the accuracy of the global self-shielding will be

restricted by the precision of the reference cross sections themselves. In Chapter 5, some errors in the mixture treatment have been identified that will be propagated through the calculation process of the PPTs. Only a global lattice calculation will put into evidence the impact of the miscalculation of the reference cross sections. This is the subject of the next chapters.

7 - Evaluation of the GR-based Subgroup Method coupled with the Physical Probability Tables

In this chapter, the subgroup method of APOLLO3®, based on the use of the General Resonance (GR) model and of the mixture mathematical probability tables (MPTs), is coupled to the newly computed physical probability tables (PPTs). It is hoped that the use of the PPTs will enable to carry out calculations on a coarse energy mesh without too much loss of accuracy compared with a standard SG-GR calculation relying on the use of the MPTs. In the first section, numerical tests are carried out to test the impact of the number of groups on the accuracy of the PPT-based SG-GR method. The results are discussed in a subsequent section, and suggestions of improvement for this work are proposed.

7.1 . Impact of the Energy Mesh Refinement on the Accuracy of the Physical Probability Table based Subgroup Method

In the second section of Chapter 4, benchmarks representative of thermal reactor calculations have been selected for the evaluation of the subgroup methods. The lattice calculation is performed using the multigroup nuclear data library readily available as input external file for the APOLLO3® calculation; this enables us to study the impact of the number of energy groups on the accuracy of the calculation, by comparing the results obtained with the existing 383, 281, 172 and 69 energy group libraries. For each resonant energy group, a PPT of order K is calculated on-the-fly using the Direct Resolution method detailed in Chapter 6, with $2K-2$ values of background dilutions to carry out the fitting procedure, in addition of the infinite dilution.

The accuracy of the PPT-based SG-GR method is evaluated by comparing the multiplication factor k_{eff} , the multigroup absorption and production rates of the resonant mixture as well as the multigroup absorption rates of the ^{238}U isotope, with reference values obtained with a TRIPOLI-4® [62] calculation. They are also compared with the 383-group MPT-based SG-GR calculation.

7.1.1 . UO_2 mixture in an infinite homogeneous medium

The first numerical test is the "IHM-U8U5-6.5" benchmark. The study of an infinite homogeneous medium enables to quantify the errors due to the self-shielding in energy only, as this problem is space-independent.

Table 7.1 provides the difference on the multiplication factor k_{eff} obtained with the PPT-SG-GR subgroup method for different energy discretization, and with the 383-group MPT-SG-GR calculation, compared with the Monte Carlo reference value.

The first observation is that the lattice calculation run by using the 383 group MPT-based SG-GR calculation yields a significant error of the order of 150 pcm. This is more than the expected accuracy for this method, as it has been shown that the difference on the multiplication factor for a more complex heterogeneous UO_2 pin-cell calculation is typically around 10 pcm [18], so much less than this simpler test case. The subgroup method coupled with the PPTs also renders a large difference

even for the fine energy meshes of 383 and 281 groups. The error is of the same magnitude as for the fine MPTs, but with an opposite sign. When decreasing the number of energy groups down to 172 and 69, the absolute value of the difference is diminished.

Table 7.1: Difference on the multiplication factor for the "IHM-U8U5-6.5" benchmark

Calculation	k_{eff}	Δ k_{eff} (pcm)
TRIPOLI-4®	1.26490 $\pm$ 3 pcm	-
MPT - 383g	1.26642	152
PPT - 383g	1.26340	-150
PPT - 281g	1.26367	-123
PPT - 172g	1.26542	52
PPT - 69g	1.26554	64

Because the value of the k_{eff} is a global result encompassing various local effects, it is not sure that an improvement of the calculated k_{eff} effectively denotes an improvement of the self-shielding method. Figure 7.1 and Figure 7.2 provide the detail of the errors in the multigroup absorption and production rates of the resonant mixture, and in the multigroup absorption rates of each isotope, respectively.

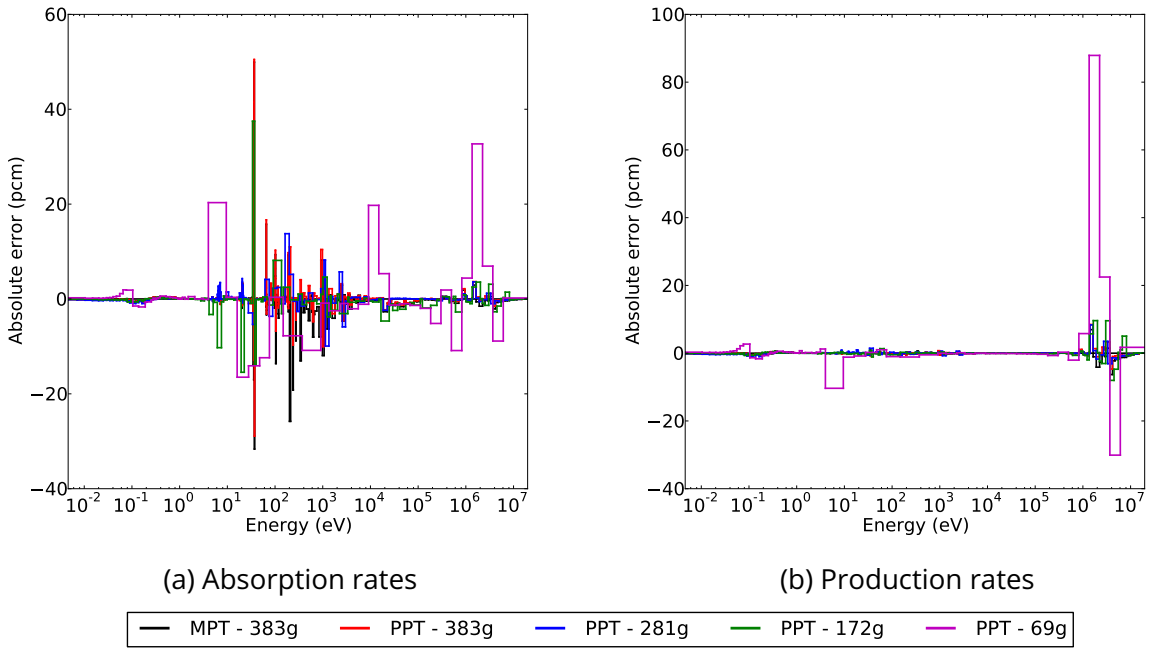

(a) Absorption rates (b) Production rates

Figure 7.1: Error in the mixture absorption and production rates for the "IHM-U8U5-6.5" benchmark

The errors in the absorption rates of the resonant mixture are mainly dominated by the errors on the ^{238}U absorption rates, as the two graphs display the same trends. The production rate of

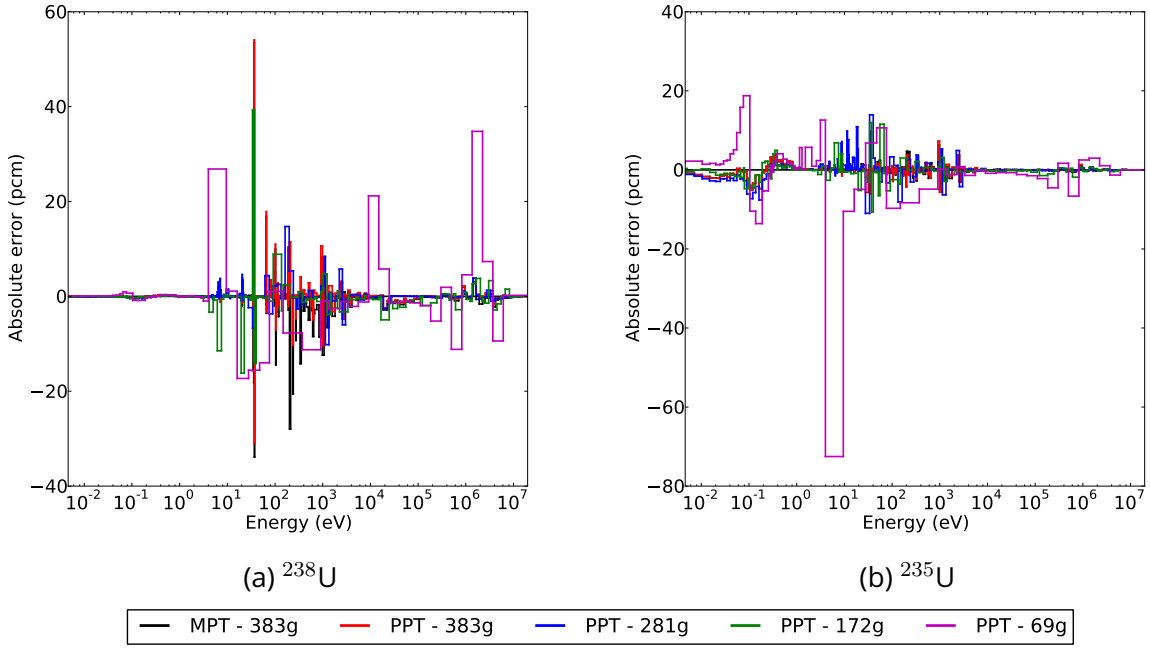

Figure 7.2: Error in the absorption rates per isotope for the "IHM-U8U5-6.5" benchmark

the mixture is very well calculated in the thermal and resonant energy domains. For the 69-group PPT-SG-GR calculation, a significant discrepancy can be noticed in the fast groups. This difference is not due to the self-shielding method itself but to the use of an energy mesh too coarse in this domain. This is also the cause of the non negligible errors observed in the fast and thermal energy domains for ^{238}U and ^{235}U, respectively. The self-shielding model is not applied in these domains; the errors are solely due to the input multigroup nuclear libraries and to the TDT MOC flux solver employed in the lattice calculation. Improvements could therefore be expected by refining the energy mesh at low (below 1 eV) and high energies (above 10 keV), at the cost of an increased number of groups in the flux calculations. This axis of improvement was not pursued in the scope of this thesis work.

In the resonant domain, the 383-group MPT-based SG-GR calculation clearly underestimates the absorption rates of the resonant mixture, hence the positive value of Δk_{eff} observed. For the PPT-based SG-GR calculations, it is difficult to distinguish a particular trend as the error oscillates from one energy group to another. Fine energy meshes display larger errors, which are flattened in coarser meshes, most likely because of compensation effects. The largest error calculated, exceeding 50 pcm, is observed when employing the finest mesh of 383 groups; this explains why the difference on the k_{eff} is found to be negative (-150 pcm) in this case, as the absorption of ^{238}U and of the resonant mixture is largely overestimated. For the 69 group energy mesh, an important error (more than 20 pcm for the ^{238}U and 70 pcm for the ^{235}U) must be pointed out in the group located between 4.0 eV and 9.5 eV. This is the consequence of the use of the deterministic UFG-IHM solver to compute the tabulated cross sections employed for the on-the-fly calculation of the PPTs, which has been shown in Chapter 5 to introduce a large error in this specific group for the ^{238}U - ^{235}U resonant mixture. An improvement of the precision of this ultra fine group solver should therefore improve the precision of

the self-shielding calculation.

This first test case shows that the PPT-based SG-GR calculations have the same accuracy level as the 383-group MPT-based SG-GR calculation. The rates of the mixture in the resonant domain are satisfyingly represented, and the discrepancy measured on the global k_{eff} is of the same order, or less, than the one of the MPT-SG-GR calculation.

7.1.2 . UO_2 pin-cell

The results obtained on the so-called "Cell-UO_2-noClad" and "Cell-UO_2 " benchmarks of Chapter 4 are presented in this subsection.

Table 7.2 recaps the difference on the multiplication factor of the lattice calculation with respect to the Monte Carlo reference value. The difference is measured for both types of probability tables, and in the case of the PPTs, for a number of energy groups ranging from 383 to 69. For both benchmarks, the accuracy of the MPT-based SG-GR method is superior to the one of the PPT-based SG-GR method, even when employing the same energy discretization of 383 groups. The use of the fine MPTs for the subgroup calculation leads to an error of less than 40 pcm on the k_{eff} , which is much less than what has been obtained on the previous IHM benchmark, despite it being simpler. The PPTs introduce large errors of a few hundreds of pcm, even for the finest energy discretization; the error increases even more for coarser meshes, exceeding 500 pcm of difference for a 69 group calculation.

The two calculations carried out on the 383 group energy mesh only differ on the type of probability tables employed in the subgroup self-shielding calculation. The rest of the calculation is strictly identical, as the same input nuclear data libraries have been provided, and the same parameters have been used for the configuration of the TDT solver. This shows that the use of the PPT is solely responsible for the significant increase of the error on the k_{eff} , compared to the use of the MPTs.

It can be remarked that the addition of the cladding leads to an increase of the Δk_{eff} measured for the PPT-SG-GR methods, but to a decrease of the one of the MPT-SG-GR method. This may be due to an error of the opposite sign in the cladding, leading to a compensation with the error of the fuel mixture.

Table 7.2: Difference on the multiplication factor for the pin-cell benchmarks

	Cell-UO_2 -noClad		Cell-UO_2	
	k_{eff}	Δk_{eff} (pcm)	k_{eff}	Δk_{eff} (pcm)
TRIPOLI-4®	1.47085 $\pm$ 3 pcm	-	1.41995 $\pm$ 3 pcm	-
MPT-383g	1.47122	36	1.41998	7
PPT-383g	1.46913	-172	1.41809	-186
PPT-281g	1.46743	-343	1.41544	-451
PPT-172g	1.46741	-344	1.41547	-448
PPT-69g	1.46751	-334	1.41223	-772

Figures 7.3, 7.4 and 7.5 show the errors on the resonant mixture absorption and production rates, as well the ^{238}U absorption rates, respectively, for the "Cell-UO_2-noClad" benchmark.

The use of the PPT leads to an overestimation of the absorption rates of the mixture in the resonant domain. The 69-group calculation renders errors between 10 pcm and 70 pcm in all the groups located between 4.0 eV and 372 eV. The upper part of the resonant domain is treated more accurately for all the energy meshes, with very small errors of a few pcm.

The spatial representation of the errors on the absorption rates in the pin-cell shows that most of the subgroup methods studied in this chapter have an error of the opposite site in the inner rings and the outer rings, leading to a compensation effect. The sign of the error is different according to the type of probability table employed in the self-shielding calculation, explaining the difference of signs observed in Table 7.2.

Figures 7.3 and 7.5 clearly shows the degradation of the precision of the PPT-based SG-GR calculation when decreasing the number of energy groups. The 69-group calculation displays an error larger by a factor almost 6 in the inner rings of the fuel-pin compared with the 383-group calculation.

Figure 7.4 shows that the production rates of the mixture are very accurately calculated with all the SG-GR methods, for both kinds of probability tables and all the energy meshes. Similarly to what has already been remarked in the previous IHM benchmarks, the 69-group PPT-SG-GR calculation displays discrepancies of the production rates in the fast energy domain, that are not caused by the self-shielding procedure. Its discrepancies in the energy group located between 4.0 eV and 9.5 eV are due to the use of the UFG-IHM solver that introduces a significant error on the ^{235}U cross sections in the UO_2 mixture.

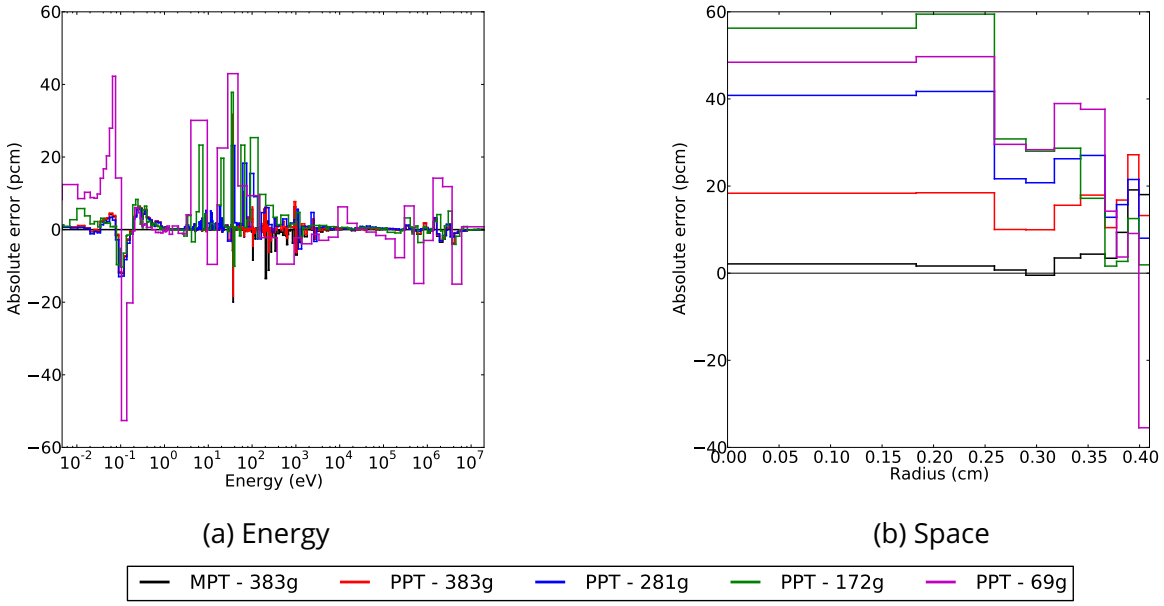

Figure 7.3: Error in the absorption rates of the mixture for the "Cell-UO_2-noClad" benchmark

The results obtained with the "Cell-UO_2" benchmark are very similar to the ones presented for the "Cell-UO_2-noClad" test case. The addition of the cladding exacerbates the errors already remarked when using a PPT based SG-GR method, hence the deteriorated k_{eff} calculated in Table 7.2.

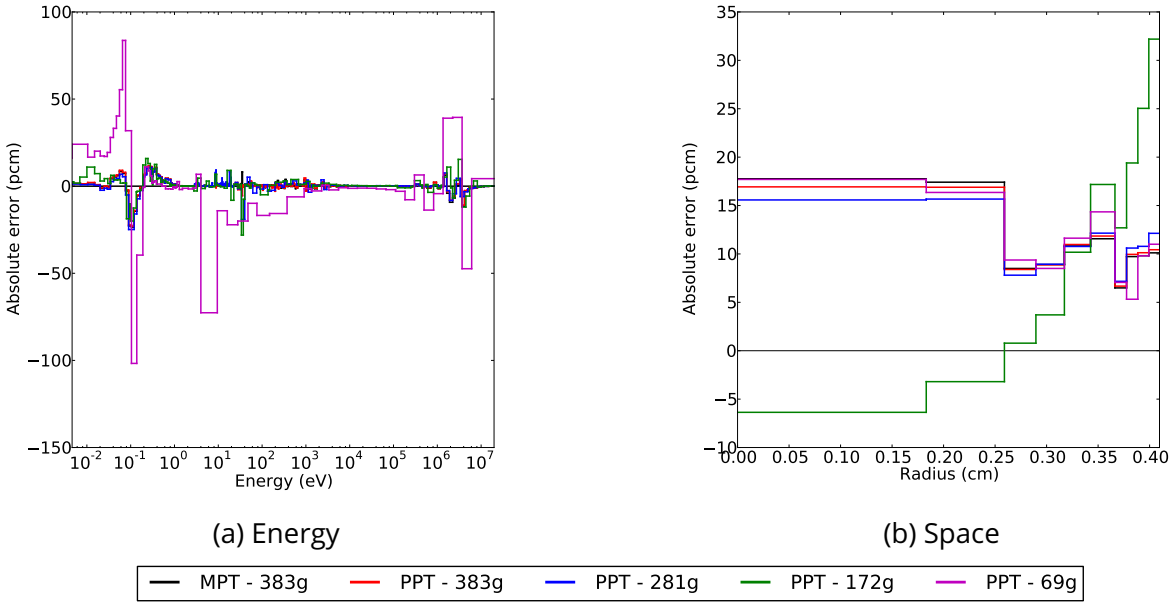

Figure 7.4: Error in the production rates of the mixture for the "Cell-UO_2-noClad" benchmark

The magnitude of the errors observed in these two pin-cell benchmarks shows that the 383-group PPT-based SG-GR calculation accurately represent the rates of the UO_2 mixture, in the resonant domain and in every region of the spatial discretization. The Δk_{eff} obtained is of the order -200 pcm, which is larger than the one of the 383-group MPT-SG-GR calculation, because the latter benefits from a compensation of the errors that has an opposite sign in the inner and outer rings of the pin.

Although the 383-group calculation carried out conjointly with the PPTs renders satisfying results, it should be reminded that the aim of this thesis work was to significantly decrease the number of energy groups of the calculation. The magnitude of the errors observed in these two benchmarks prove that the 69-group PPT-based SG-GR method does not meet the accuracy requirement to be used as a practical self-shielding method.

7.2 . Conclusions

In this chapter, we evaluated the accuracy of the SG-GR self-shielding method of APOLLO3® when coupled to the physical probability tables. Several energy meshes were employed to study the effect of the number of groups on the precision of the calculation. The analysis of the IHM and the pin-cell benchmarks showed that the reaction rates calculated with the 383-group PPT-based SG-GR method can be as accurate as the ones obtained with the 383-group MPT-based SG-GR method in the resonant domain. However, the use of the MPT has been shown to lead to compensation of errors, both in space and energy. The use of the PPTs does not benefit as much from such compensation effect, leading to a degraded k_{eff} . Furthermore, the error increased when decreasing the number of groups.

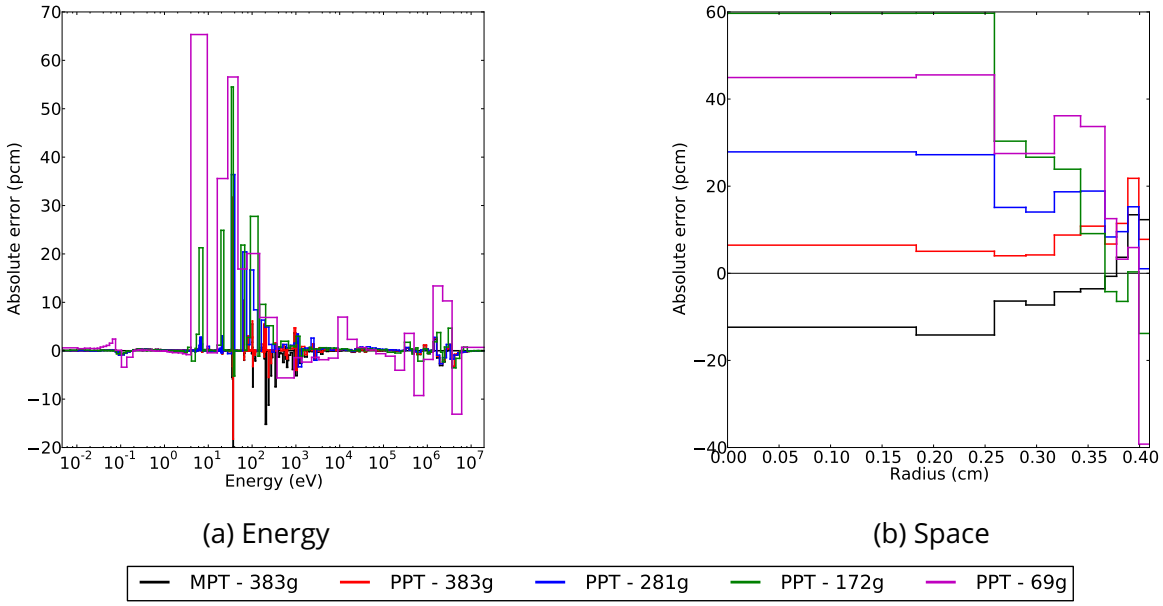

Figure 7.5: Error in the absorption rates of the ^{238}U isotope for the "Cell-UO_2-noClad" benchmark

In this work, the PPTs have been generated using reference cross sections obtained with a slowing-down calculation in an IHM. The calculation of heterogeneous PPTs may lead to better results. However it was suspected that the main source of error in coarse-group calculations was the use of the GR model to approximate the resonant scattering operator in the fine-structure equation. The GR model relies on the assumption that the point-wise resonant scattering source can be approximated by its average in the energy group:

$$r_0\varphi(u) \approx \langle r_0\varphi \rangle^g \quad \text{for } u \in g. \tag{7.1}$$

While this assumption might not introduce too much error on a fine energy structure, it is not valid on a coarse group mesh.

It was also suspected that the use of infinitely-diluted transfer probabilities in the subgroup equation could introduce significant errors in coarse-group calculations.

While it was originally hoped that the use of the PPTs instead of the MPTs in the SG-GR method would be enough to carry out the self-shielding calculations on a coarse energy mesh, it is now clear that an adaptation of the subgroup method itself is required.

In the next chapter, we will present the implementation of the so-called "Intermediate Resonance" model [68] in APOLLO3®, and the subgroup formalism that is derived from it. The performance of this IR-based subgroup method, used conjointly with adapted PPTs, will be evaluated on representative thermal reactor calculations, carried out on the 69-group energy structure.

8 - Development and Evaluation of an "Intermediate Resonance"-based Subgroup Method on a Coarse Energy Mesh

In this chapter, the implementation of the Intermediate Resonance (IR) model [68] in APOLLO3® and its use for the development of an IR-based subgroup method is described. Because this model has never been implemented before in APOLLO3®, nor in its ancestor APOLLO2 [27], the multigroup libraries used as input libraries for the lattice calculations do not contain the required data. Therefore, the first section of this chapter details the calculation of the IR parameters for the coarse 69-group energy structure, for a selection of isotopes. The second section explains the theory of the IR-based subgroup method. Subsequently, this subgroup method is tested out on various numerical benchmarks in the third section. In a fourth section, the computational time of the newly implemented SG-IR method is tested out in assembly calculations. Finally, conclusions of this chapter are provided in the last section.

8.1 . Computation of the "Intermediate Resonance" Parameters

The Intermediate Resonance (IR) approximation, originally proposed by Goldstein and Cohen [68], is a linear combination of the Narrow Resonance (NR) and of the Wide Resonance (WR) model. The multigroup macroscopic scattering operator $R_x\phi$, for an isotope x, is expressed as

$$R_x^{IR}\phi(u) = \lambda_x\Sigma_{p,x} + (1-\lambda_x)\Sigma_{s,x}(u)\phi(u), \tag{8.1}$$

where $\Sigma_{p,x}$ is the macroscopic potential cross section, independent of the energy. The parameter λ_x appearing in this equation is called the Goldstein-Cohen factor or IR factor. Since the legacy self-shielding methods implemented in APOLLO3® do not traditionally rely on the use of the IR model, the λ_x parameters are not included in the nuclear data libraries generated by the GALILEE system [17]. A preliminary work thus had to be done to compute the parameter λ_x on the coarse 69-group energy structure.

8.1.1 . Procedure to determine the IR parameters

The λ parameter of Equation (8.1) takes its value between 0 and 1. The value 0 corresponds to the WR model, where the width of the resonance is considered to be large compared with the maximum lethargy gain of the incident neutron on the target nuclide, while the value 1 corresponds to the opposite situation, known as the NR model. The NR approximation is mostly valid for light moderating isotopes, such as hydrogen. In practice, the IR parameter of hydrogen is always set to 1, in all the energy groups.

The determination of the multigroup IR parameters is a procedure that has been proposed by Alduous [69], under the name of "hydrogen-equivalent" factors. It consists of adjusting the value of λ in order to preserve multigroup absorption cross sections of a reference isotope in an IHM slowing-down calculation. The isotope of reference is often chosen to be ^{238}U, because of its importance in thermal reactor calculations. This is also the choice that has been made in this work.

The procedure employed in this thesis work to compute the multigroup IR parameters is adapted from the WIMSR module of the NJOY nuclear data processing system [70]:

1. The slowing-down equation is solved for a mixture of ^{238}U and purely scattering ^{1}H, in an IHM characterized by its background dilution σ_b and temperature T. σ_b and T are parameters chosen to represent a typical PWR calculation. The density of hydrogen N_1 is calculated with the formula $N_1 = \dfrac{N_0 \sigma_b}{\sigma_{p,H1}}$, where N_0 is the density of ^{238}U and $\sigma_{p,H1} = 20.478$ barns is the potential scattering cross section of ^{1}H. In this procedure, the absorption cross section of ^{1}H is set to 0. The outcome of this first step is the multigroup absorption cross sections of ^{238}U, denoted $\sigma_a^g(\sigma_b, T)$.

2. A slowing-down problem, almost identical to the one of step (1), is solved. The same temperature T is employed, but the background dilution due to hydrogen is this time equal to $\sigma_b + \Delta\sigma_b$, with $\Delta\sigma_b$ also being a small variation of dilution. This leads to the ^{238}U multigroup absorption cross sections $\sigma_a^g(\sigma_b + \Delta\sigma_b, T)$.

3. The third calculation solves the slowing-down equation in an IHM for a mixture of ^{238}U, ^{1}H and isotope x, where x is a purely scattering isotope for which the IR parameter needs to be determined. The temperature of the medium is T and the background dilution is equal to $\sigma_b + \Delta\sigma_b$, where σ_b accounts for the dilution due to hydrogen, and $\Delta\sigma_b$ is due to isotope x. The density of isotope x is calculated as $N_x = \dfrac{N_0 \Delta\sigma_b}{\sigma_{p,x}}$, with $\sigma_{p,x}$ the potential scattering of isotope x. The multigroup absorption cross sections of ^{238}U in this mixture $\sigma_a^{g*}(\sigma_b + \Delta\sigma_b, T)$, where some of the hydrogen has been replaced by the isotope x, are calculated.

4. The multigroup IR parameter for isotope x is retrieved from the following relation:

$$\lambda_x^g = \frac{\sigma_a^{g*}(\sigma_b + \Delta\sigma_b, T) - \sigma_a^g(\sigma_b, T)}{\sigma_a^g(\sigma_b + \Delta\sigma_b, T) - \sigma_a^g(\sigma_b, T)}. \tag{8.2}$$

Steps (1) and (2) of this procedures are only done once, but steps (3) and (4) have to be repeated for every isotope. Reference [71] shows that the choice of the temperature T and of the fraction of background cross section $\Delta\sigma_b$ due to the isotope x does not impact much the calculated λ, but that the choice of the background cross section σ_b may have a significant effect on the values obtained. In this work, we have selected $T = 300$K, $\sigma_b = 50$ barns and $\Delta\sigma_b = 1$ barn.

8.1.2 . Numerical calculation and results of the IR parameters

It was chosen to solve the slowing-down problems of this procedure using Monte Carlo simulations. Because the calculation of the IR parameters is only done once, the computational time is not a constraint. The TRIPOLI-4® code [62] is utilized in its "PROTECTION" mode. Modified nuclear data are employed to simulate isotopes with only their potential scattering cross section [72].

Figure 8.1 illustrates the IR parameters calculated in the resonant domain of the 69-group energy structure for some isotopes, selected for their importance in our calculations. It can be seen that the values of λ are sometimes greater than 1, especially for lighter isotopes such as ^{16}O; in that case, they are set to 1.

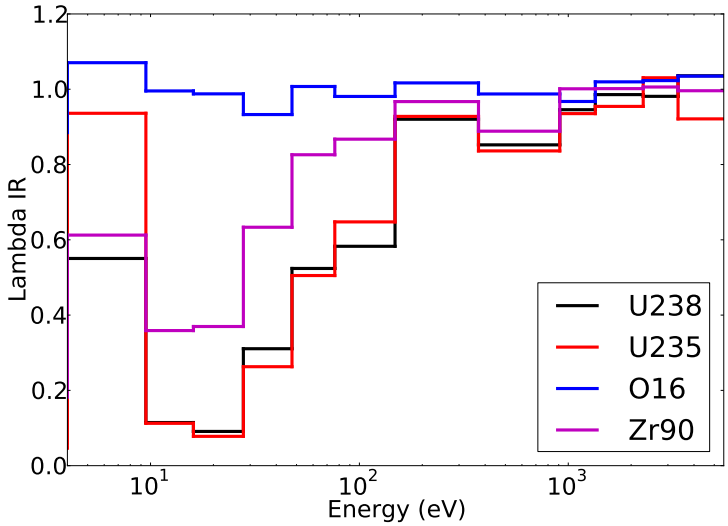

Figure 8.1: Multigroup IR parameter of a few isotopes in the resonant domain of the 69-group energy structure

8.2 . Theory of the "Intermediate Resonance"-based Subgroup Method

This section describes the theory of the subgroup method based on the use of the IR model to approximate the scattering sources of the slowing-down equation. The calculation of the physical probability tables is adapted to also integrate the use of the IR model.

8.2.1 . Adaptation of the physical probability tables calculation procedure

Chapter 6 of this manuscript describes the procedure implemented in APOLLO3® for the on-the-fly calculation of the mixture PPTs. It is based on the fitting of the effective total cross section of the resonant mixture, obtained by an ultra-fine-group slowing-down calculation in an IHM. This procedure is consistent with the use of the GR model.

The calculation of the IR parameters for the implementation of the IR model led to the possibility to generate another kind of PPTs, this time based on the preservation of the resonant cross section of the resonant mixture, as described in the Reference [12]. This is justified by the use of the IR model to approximate the scattering sources in the multigroup slowing-down equation in an IHM of a resonant mixture and purely scattering moderator isotopes, such as hydrogen:

$$\sum_x N_x \sigma_x(u) \phi^{IR}(u) = \sum_x N_x \left[\lambda_x^g \sigma_{p,x} + (1-\lambda_x) \sigma_{s,x}(u) \phi^{IR}(u) \right], \; u \in g, \tag{8.3}$$

where N_x is the density of isotope x, and σ_x^g, $\sigma_{p,x}^g$ and $\sigma_{s,x}^g$ are its microscopic total, potential and scattering cross sections in the group g, respectively. The expression of the IR flux can be obtained from (8.3):

$$\phi^{IR}(u) = \frac{\sum_x N_x \lambda_x^g \sigma_{p,x}}{\sum_x N_x \left[\sigma_{a,x}(u) + \lambda_x^g \sigma_{s,x}(u) \right]}, \; u \in g. \tag{8.4}$$

Reference [12] suggests to consider the resonant mixture as a single isotope, denoted with the index 0. The moderating isotope is supposed to have only potential scattering. The expression of the IR flux becomes:

$$\phi^{IR}(u) = \frac{\sum\limits_{x\in\text{res}} N_{0x}\lambda_{0x}^{g}\sigma_{p,0x} + \sum\limits_{x\in\text{mod}} N_{1x}\lambda_{1x}^{g}\sigma_{p,1x}}{\sum\limits_{x\in\text{res}} N_{0x}\left[\sigma_{a,0x}(u) + \lambda_{0x}^{g}\sigma_{s,0x}(u)\right] + \sum\limits_{x\in\text{mod}} N_{1x}\lambda_{1x}^{g}\sigma_{p,1x}},\ u \in g. \tag{8.5}$$

In order to derive the expression of the background dilution cross section from (8.5), the quantity $\sum\limits_{x\in\text{res}} N_{0x}\lambda_{0x}^{g}\sigma_{p,0x}$ is both added and subtracted from the denominator of the fraction. The final expression of the IR flux reads:

$$\phi^{IR}(u) = \frac{\sigma_b}{\sigma_{res}(u) + \sigma_b},\ u \in g, \tag{8.6}$$

where the resonant cross section is defined as

$$\sigma_{res}(u) = \sum_{x} a_{0x}\left[\sigma_{a,0x}(u) + \lambda_{0x}^{g}(\sigma_{s,0x}(u) - \sigma_{p,0x})\right], \tag{8.7}$$

with $a_{0x} = \dfrac{N_{0x}}{N_0}$ being the fraction of isotope x in the resonant mixture and N_0 the total density of resonant isotopes. The expression of the background dilution is group-dependent

$$\sigma_b = \sum_{x\in\text{mod}} \frac{N_{1x}}{N_0}\lambda_{1x}^{g}\sigma_{p,1x} + \sum_{x\in\text{res}} a_{0x}\lambda_{0x}^{g}\sigma_{p,0x}. \tag{8.8}$$

Equation (8.6) shows that the expression of the flux obtained with the IR model is dependent on the resonant cross section, while the PPT calculation process described in Chapter 6 was made to fit the mixture total cross section; the calculation procedure therefore has to be adapted to fit the resonant cross section instead. The total cross section of the mixture is now treated as a partial cross section. The modified procedure is summarized:

1. The UFG-IHM solver is employed for a list of background dilutions, calculated with the expression of Equation (8.8), to solve the fine-structure equation in an IHM. The effective cross sections of the resonant mixture in an IHM are derived from this calculation.
   The cross sections calculated are the absorption, scattering, total and resonant cross sections.

2. The resonant cross section is approximated using a rational fraction, whose unknown coefficients are computed with the Direct Resolution (DR) method. The coefficients are then employed to determine the weights ω_k^g associated to the base points of the resonant cross section $\sigma_{res,k}^{g}$.

3. The partial cross sections are approximated with a rational fraction, using the DR method, leading to the determination of the base points for the partial cross sections $\sigma_{\rho,x,k}^{g}$. The total cross section of the resonant mixture is treated as a partial cross section in this modified procedure.

Because the IR parameters λ have only been computed in the resonant domain of the 69-group energy structure, the calculation of the IR-based PPTs is restricted to these specific energy groups.

In Chapter 6, it was explained that the number of background dilutions used in the fitting procedure could be larger than the number of unknown parameters to be determined. However it has been remarked that using just the required number of dilutions in some groups led to IR-based PPTs of very low orders, that is to say $K = 1$ or $K = 2$, which is not enough to accurately reconstruct the reference cross sections in the resonant domain. The maximum number of dilutions available is therefore always utilized, leading more often to PPTs of orders 4 or 5. In the current state of the procedure, this maximum number of dilutions is fixed to 13, including the infinite dilution.

8.2.2 . Subgroup equation

In the previous chapter, we tried to employ the PPTs based on the preservation of the mixture total cross section with the APOLLO3® subgroup method (SG-GR). The calculations carried out on coarse energy meshes did not meet the accuracy criteria to be employed as a self-shielding method. In Reference [73], we showed that the use of the IR-based PPTs with the SG-GR method degraded the accuracy even more. We concluded the necessity to have a consistent model in the PPT calculation and the subgroup calculation, hence the implementation in APOLLO3® of a subgroup method based on the use of the IR model to approximate the scattering sources.

In a heterogeneous geometry composed of regions indexed with the letters i and j, the slowing-down equation based on the collision probability formalism reads:

$$\left[\Sigma_{1,i}(u) + \sum_x N_{0x,i}\sigma_{0x,i}(u)\right] V_i\phi_i(u) = \sum_j V_j P_{ij}(u) R_j\phi_j(u), \tag{8.9}$$

where the usual notation has been employed. This equation can be written for a subgroup k belonging to an energy group g with the IR approximation [12]:

$$\left[\Sigma^g_{1,i} + \sum_x N_{0x,i}\sigma^g_{x,k,i}\right] V_i\phi^g_{k,i} = \sum_j V_j P^g_{ij,k} R^{IR}_j \phi^g_{k,j}. \tag{8.10}$$

$R^{IR}_i\phi^g_{k,i}$ is the IR scattering source for a region i. If i is a resonant region then it is the sum of the contributions coming from both the moderator source and the resonant sources:

$$\begin{aligned} R_i\phi^{IR,g}_{k,i} = &\sum_{x\in\text{res}} N_{0x,i}\left[(1-\lambda^g_{0x})\sigma^g_{s,0x,k}\phi^g_{k,i} + \lambda^g_{0x}\sigma^g_{p,0x}\Delta u^g\omega^g_k\right] \\ &+ \sum_{x\in\text{mod}} N_{1x,i}\left[(1-\lambda^g_{1x})\sigma^g_{s,1x,i}\phi^g_{k,i} + \lambda^g_{1x}\sigma^g_{p,1x}\Delta u^g\omega^g_k\right], \end{aligned} \tag{8.11}$$

while for a moderator region, only moderator sources are accounted for:

$$R_i\phi^{IR,g}_{k,i} = \sum_{x\in\text{mod}} N_{1x,i}\left[(1-\lambda^g_{1x})\sigma^g_{s,1x,i}\phi^g_{k,i} + \lambda^g_{1x}\sigma^g_{p,1x}\Delta u^g\omega^g_k\right]. \tag{8.12}$$

Δu^g is the lethargy width of the energy group g, and $\{\omega^g_k, \sigma^g_k, \sigma^g_{\rho,x,k}\}_{k=1,\ldots,K}$ are the parameters of the PPT of order K. In the expressions of the scattering operator, the infinite-dilution multigroup

cross sections are employed for the moderating isotopes, while the PPT parameters are used for the resonant isotopes. When computing the self-shielded cross sections for region i, the same base points are employed for all the regions j, provided that the resonant mixture present in region j contains at least the same resonant isotopes as the ones in region i. This is called the Same Material Approximation (SMA) [19].

The subgroup fixed-source Equation (8.10) is solved with a LU decomposition using the SGETRF and SGETRS routines of the LAPACK library. Once the subgroup fluxes $\phi_{k,i}$ are retrieved in every region i, the resonant self-shielded microscopic cross sections are obtained as a result of the subgroup quantities:

$$\sigma^g_{\rho,0x,i} = \mu^g_i \frac{\sum_{k=1}^{K} \omega^g_k \sigma^g_{\rho,x,k} \phi^g_{k,i}}{\sum_{k=1}^{K} \omega^g_k \phi^g_{k,i}} = \mu^g_i \frac{\tau^g_{\rho,x}}{\phi^g}, \tag{8.13}$$

where μ^g_i is the SPH factor. It is computed through an equivalence procedure enforcing that the solution of the multigroup problem

$$\Sigma^g_i V_i \phi^g_i = \sum_j V_j P^g_{ij} R_j \phi^{IR,g}_j \tag{8.14}$$

yields the same reaction rates as the ones from the subgroup equation (8.10), which are considered to be the reference rates to be preserved. In this work, the μ^g_i multiplication factor is calculated in every region i and resonant group g according to the procedure described in Reference [12]:

1. At the first iteration, set $\mu^{g,(0)}_i$ to 1 in all the regions.

2. At the n^{th} iteration, solve the fixed-source multigroup equation for the multigroup flux, forming a system of uncoupled equations

$$\Sigma^{g,(n)}_i V_i \phi^{g,(n)}_i = \sum_j V_j P^{g,(n)}_{ij} R_j \phi^{IR,g,(n)}_j, \tag{8.15}$$

   where the scattering sources are updated at each iteration

$$\begin{aligned} R_i \phi^{IR,g,(n)}_i = &\sum_{x \in \text{res}} N_{0x,i} \left[(1-\lambda^g_{0x}) \mu^{g,(n-1)}_i \sigma^g_{s,0x,i} \phi^{g,(n)}_i + \lambda^g_{0x} \sigma^g_{p,0x} \Delta u^g \right] \\ &+ \sum_{x \in \text{mod}} N_{1x,i} \left[(1-\lambda^g_{1x}) \mu^{g,(n-1)}_i \sigma^g_{s,1x,i} \phi^{g,(n)}_i + \lambda^g_{1x} \sigma^g_{p,1x} \Delta u^g \right], \end{aligned} \tag{8.16}$$

   if i is a resonant region, otherwise

$$R_i \phi^{IR,g,(n)}_i = \sum_{x \in \text{mod}} N_{1x,i} \left[(1-\lambda^g_{1x}) \mu^{g,(n-1)}_i \sigma^g_{s,1x,i} \phi^{g,(n)}_i + \lambda^g_{1x} \sigma^g_{p,1x} \Delta u^g \right]. \tag{8.17}$$

3. Compute the new SPH factor $\mu^{g,(n)}_i = \dfrac{\phi^{IR,g,(n)}_i}{\phi^{IR,g,(0)}_i}$.

4. Stop if the convergence or the maximum number of iterations is reached. Otherwise, actualize the total macroscopic cross section in the region i with $\Sigma_i^{g,(n+1)} = \mu_i^{g,(n)}\Sigma_{1,i}^g + \sum_{x\in \text{res}} N_{0x,i}\,\mu_i^{g,(n)}\,\sigma_{0x,i}^g$, and go back to step 2.

This SPH correction is also applied to the moderator cross sections, when the standard SPH correction of APOLLO3® described in Chapter 3 was only applied to resonant cross sections.

8.3 . Numerical Evaluation of the IR-based Subgroup Methods

The evaluation of the IR-based subgroup method has been carried out on the numerical benchmarks presented in the dedicated Chapter 4. In this section, we call "SG-IR" the self-shielding method just described, based on the use of the IR-based PPTs and subgroup equation. The Equivalent Dancoff-factor Cell method of APOLLO3®, detailed in Chapter 3, has also been coupled to the SG-IR method, and will be designated by "EDC-IR". In this EDC-IR method, the two-dimensional geometry is transformed into a set of independent one-dimensional cylindrical cells, on each of which the SG-IR method is applied. These two self-shielding methods are employed on the coarse 69-group energy structure. Meanwhile, the APOLLO3® traditional subgroup methods, coupled to the mixture MPTs and GR-based subgroup equation, will be called "SG-GR" and "EDC-GR", and are run on the LWR-383 fine group energy mesh.

The evaluation of the performance of the self-shielding methods is based on the comparison of the multiplication factor and of the multigroup absorption and production rates of the resonant mixtures. For each benchmark, a TRIPOLI-4® calculation is carried out to obtain the reference values. The APOLLO3® and TRIPOLI-4® calculations both employ the CEA V512 library that is based on the JEFF-3.1 nuclear data evaluation [22], and provided by the GALILEE system [17] to ensure the consistency of the data between the two codes. Because the up-scattering treatment is not yet available in the SG-IR and EDC-IR methods, the TRIPOLI-4® reference calculation was carried out using the SVT (Sampling of the Velocity of the Target nucleus) model [74].

In order to simplify the comparisons between the SG-IR, EDC-IR, SG-GR and EDC-GR methods, the results of the fine group SG-GR and EDC-GR calculations have been condensed on the 69-group structure. The analysis of the errors will progress from the most "global" quantity, namely the multiplication factor k_{eff} , to the most "local" ones, such as the reaction rates for a single isotope. The precision obtained on the k_{eff} or on the reaction rates of the resonant mixture measure the quality of the whole calculation, while the detail of the error per isotope enables to identify the sources of discrepancy.

8.3.1 . "IHM-U8U5-6.5" benchmark

In this first numerical test case corresponding to a highly enriched simplified UO_2 fuel mixture in an IHM, only the SG-GR and SG-IR are compared to the reference Monte Carlo calculation, as the EDC method is not applicable in this case.

Table 8.1 gives the difference on the multiplication factor. It can be observed that the accuracy of the SG-IR is similar to the one of the SG-GR, the error being of the order of a hundred pcm.

Figure 8.2 displays the relative error (in percent) and the absolute error (in pcm) on the absorption

Table 8.1: Difference of k_{eff} in the "IHM-U8U5-6.5" benchmark

Method	k_{eff}	Δk_{eff} (pcm)
TRIPOLI-4®	1.26493 ± 2 pcm	-
SG-GR	1.26642	149
SG-IR	1.26607	114

and production rates of the resonant mixture. In most of the resonant domain, the error on the calculated absorption rates is of the same order of magnitude for both the two presented methods, reaching a maximum about 1%. The location of this maximum error is different depending on the self-shielding method employed; it is attained in the energy group between 4 and 9.5 eV, indexed as group 27 in the 69-group energy structure, for the SG-IR, while the SG-GR commits the largest error at higher energies. About -1% on the absorption rate of the resonant mixture contributes to around -75 pcm of error.

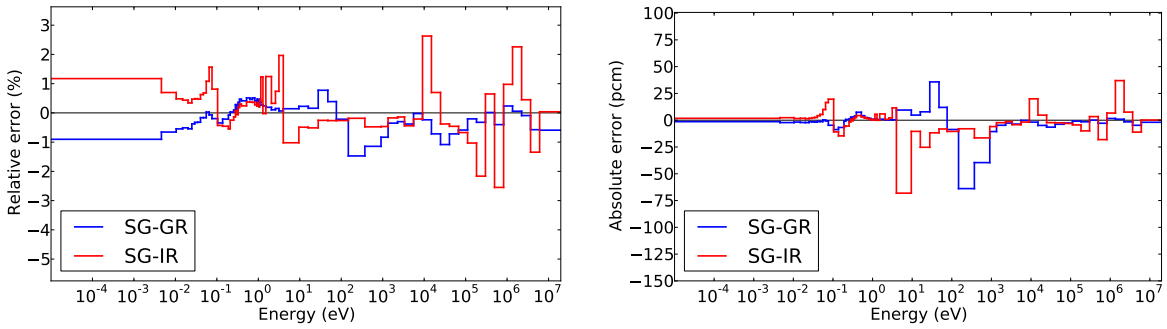

(a) Absorption rates

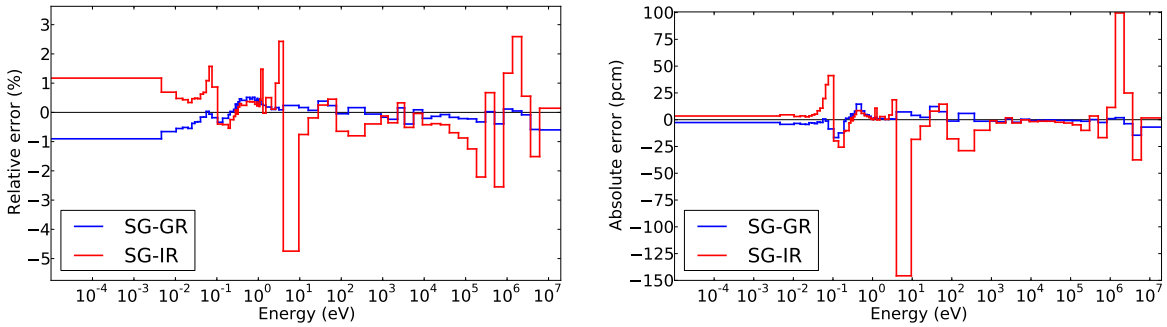

(b) Production rates

Figure 8.2: Error on the absorption and production rates of the resonant mixture in the "IHM-U8U5-6.5" benchmark

The production rates are better calculated with the SG-GR method, with less than 1% of error in all the energy domain. However a very large error exceeding -4%, accounting for almost -150 pcm, is observed with the SG-IR method in energy group 27. This specific energy group is associated to an insufficient resonance interference treatment for the ^{238}U-^{235}U mixture in the solution of the ultra-

fine-group slowing-down calculation using the solver of Chapter 5. The cross sections generated with this UFG-IHM solver are utilized to compute the PPTs of the resonant mixture; it is seen here that the error already observed in Chapter 5 has propagated through the different steps of the calculation and impacts the accuracy of the subgroup calculation.

Large errors around 2% can be also observed in the thermal and fast energy domains for the SG-IR method. They are not due to the self-shielding of heavy isotopes because the self-shielding calculation is not carried out in these groups. They are due to the coarse discretization of the energy domain, leading to imprecise flux calculations. This phenomenon has already been observed in Chapter 7 where the GR-based subgroup method was coupled to the PPTs, and it was decided not to pursue the optimization of the energy structure in this thesis work. The SG-GR method does not present such peaks in the thermal and fast domains because the 383-group energy structure is fine enough to avoid significant errors.

Figure 8.3 shows the detail of the errors, both in percent and pcm, on the absorption rates for each resonant isotope of the mixture, namely ^{238}U and ^{235}U. The SG-IR method leads to a better representation of the absorption rates of ^{238}U in the resonant domain, compared to the SG-GR method. However the opposite observation can be made for the absorption rates of ^{235}U. The focus should be drawn on the large negative peak present in group 27: this underestimation of the absorption rates of ^{235}U leads to an underestimation of the number of fissions occuring at this energy, hence the discrepancy observed in the mixture production rates in this specific energy range.

The errors on the production rates of each one of these resonant isotopes is provided in Figure 8.4. Although the relative error on the ^{238}U production rates can reach a few percents in the resonant domain, in practice this contributes to almost nothing on the global multiplication factor, as they have little importance in the reactor physics. An exception can be noted in the fast groups, where the energy of the incident neutrons is enough to induce the fission of ^{238}U nuclei, the error exceeding 12.5% and contributing for more than 75 pcm. The production rates of ^{235}U however do play an important role in thermal reactor calculations, as is evidenced by the absolute error of almost -75 pcm for an associated error of -3% in group 27. This large negative error is essentially the same one already observed on the absorption rates of ^{235}U, caused by the insufficient mixture treatment in the initial UFG-IHM calculation of the PPT generation.

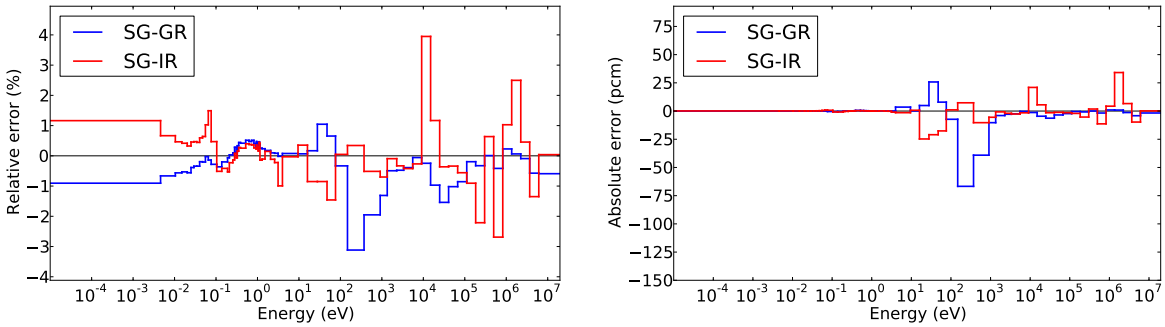

(a) ^{238}U

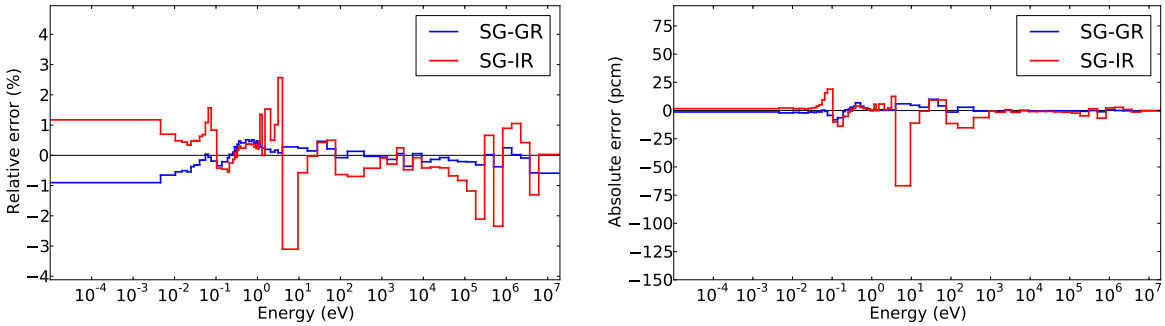

(b) ^{235}U

Figure 8.3: Error on the absorption rates per isotope in the “IHM-U8U5-6.5” benchmark

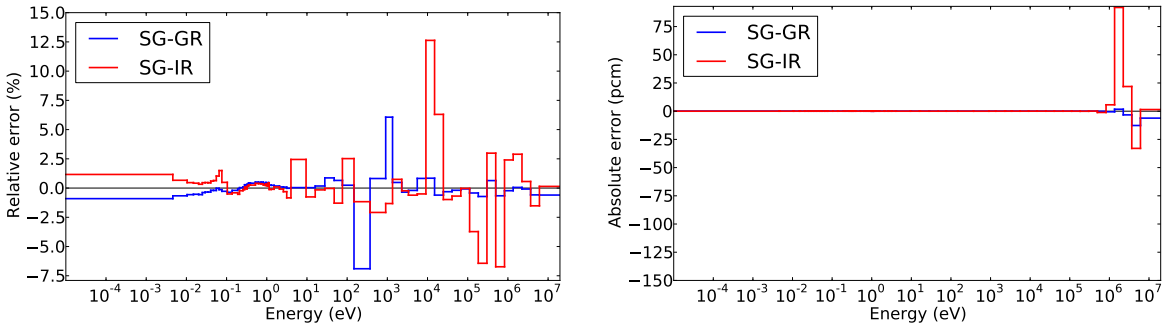

(a) ^{238}U

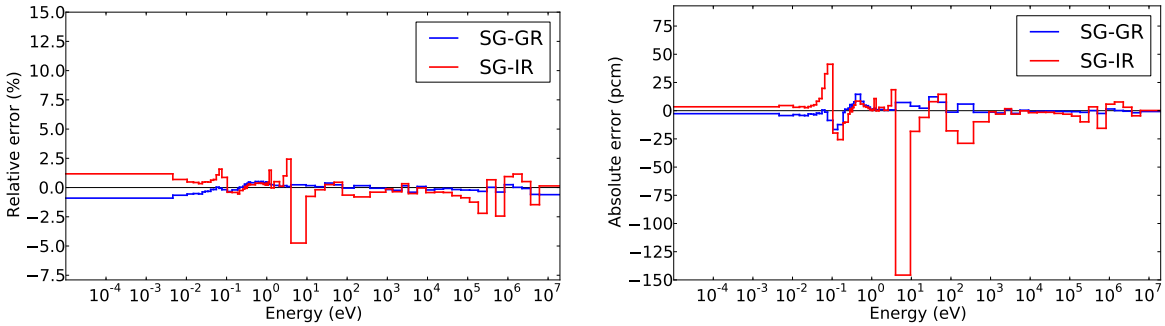

(b) ^{235}U

Figure 8.4: Error on the production rates per isotope in the “IHM-U8U5-6.5” benchmark

This first numerical evaluation of the SG-IR method in an IHM calculation demonstrates that this method can reach the same accuracy level as the SG-GR method, although it is used with a 69-group mesh, as opposed to the fine 383 group energy structure employed by the SG-GR method. Although encouraging, these first results are just preliminary as the IHM benchmark is not representative of a real thermal reactor calculation. The next numerical test will allow to study further the newly implemented IR-based subgroup methods on simple heterogeneous cases.

8.3.2 . PWR fuel-pin cells

The second set of benchmarks are the "Cell-UO_2" and "Cell-UO_2-noClad" numerical tests cases described in Chapter 4. They correspond to simple PWR pin cells with a highly enriched UO_2 fuel, with and without the cladding, respectively.

The difference of k_{eff} compared with the reference TRIPOLI-4® calculation is given in Table 8.2 hereafter. In the simplified cell without cladding, the error on the k_{eff} obtained with the IR-based subgroup methods is two times larger than for the GR-based self-shielding methods, but remain inferior to a hundred pcm. The difference between the methods is aggravated by the addition of the cladding in the "Cell-UO_2" test, where the error of the SG-GR and EDC-GR methods remains less than 10 pcm, while the accuracy of the SG-IR and EDC-IR methods is degraded, exceeding -100 pcm for the SG-IR method and -150 pcm for the EDC-IR method.

The SG-IR method achieves a similar accuracy on the cell test cases than in the previously presented IHM benchmark, of the order of a hundred pcm of difference with respect to the reference value obtained with a Monte Carlo simulation. This seems to indicate that the use of homogeneous PPTs does not induce too much bias in this heterogeneous calculation.

Table 8.2: Difference of k_{eff} in the pin-cells benchmarks

	"Cell-UO_2-noClad"		"Cell-UO_2"	
Method	k_{eff}	Δk_{eff} (pcm)	k_{eff}	Δk_{eff} (pcm)
TRIPOLI-4®	1.47085 $\pm$ 3 pcm	-	1.41995 $\pm$ 3 pcm	-
SG-GR	1.47122	36	1.41998	3
EDC-GR	1.47136	50	1.42014	19
SG-IR	1.46994	-91	1.41845	-150
EDC-IR	1.47032	-54	1.41893	-102

"Cell-UO_2-noClad" benchmark

Figures 8.5 and 8.6 display the energetic and spatial distribution of the relative errors (in %) and absolute errors (in pcm) of the absorption and production rates for the "Cell-UO_2-noClad" benchmark. In this study, there is no error due to the self-shielding of the cladding, so all the discrepancies measured in the self-shielding calculation are solely due to the fuel resonant mixture.

The errors on the absorption and production rates in the resonant domain are of the order of 2% or less, accounting for less than 20 pcm in the most innacurate groups, for all the subgroup methods. Once again the use of the PPTs, generated by fitting the cross sections produced with the UFG-IHM

solver, in the IR-based methods leads to a significant error in the production rates of the mixture in group 27, where around -50 pcm of difference can be evidenced. The most significant errors on the reaction rates of the mixture calculated with the SG-IR and EDC-IR methods are localized outside of the resonant domain, where they are not caused by the self-shielding procedure itself. Overall, the errors observed on the energy spectrum of the reaction rates are the same as the one already noted in the previous IHM benchmark, meaning that the heterogeneity of the pin-cell does not impact very much the results.

When looking at the spatial distribution of the errors in each ring of the fuel pin cell mesh, one can note that the IR-based methods tend to overestimate the absorption rates in the inner rings, while the GR-based methods tend to underestimate them in the same locations. This explains the difference of sign observed in the error on the multiplication factor in Table 8.2.

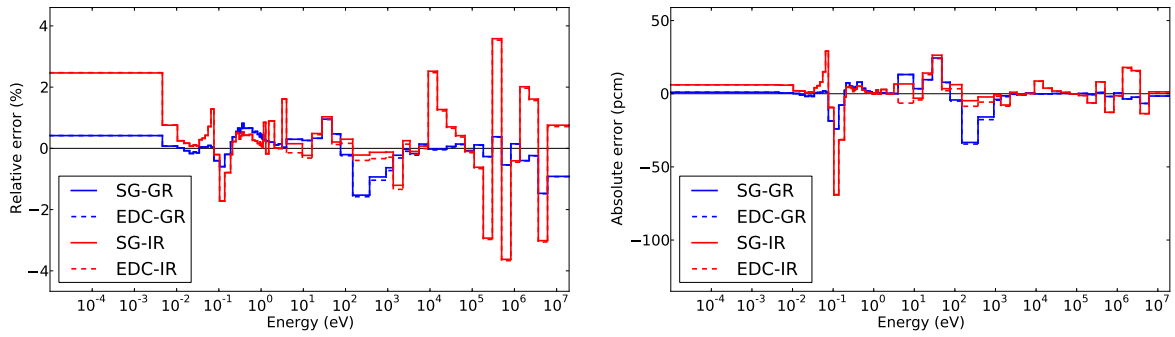

(a) Absorption rates

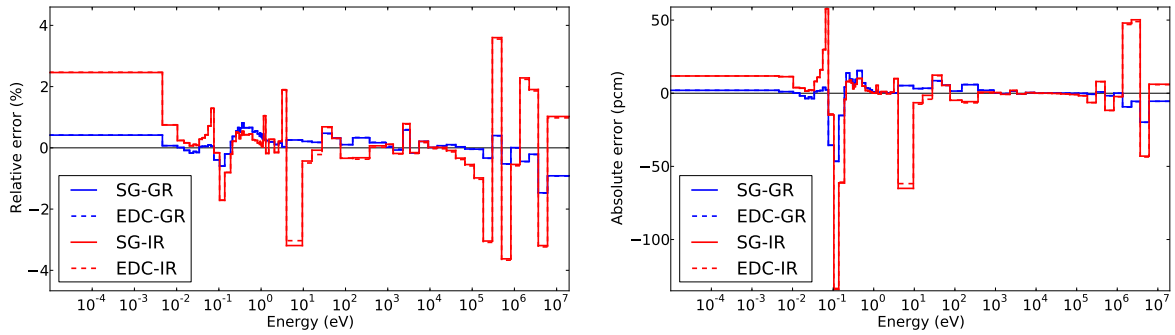

(b) Production rates

Figure 8.5: Error in energy on the absorption and production rates of the resonant mixture in the "Cell-UO_2-noClad" benchmark

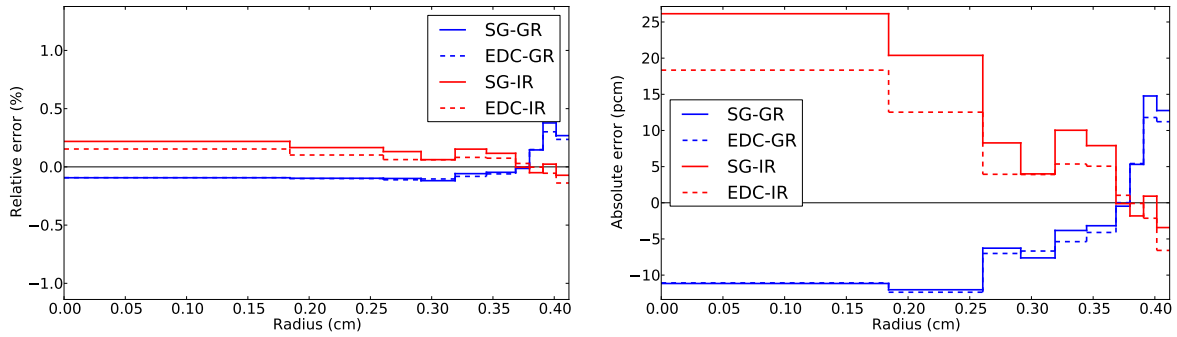

(a) Absorption rates

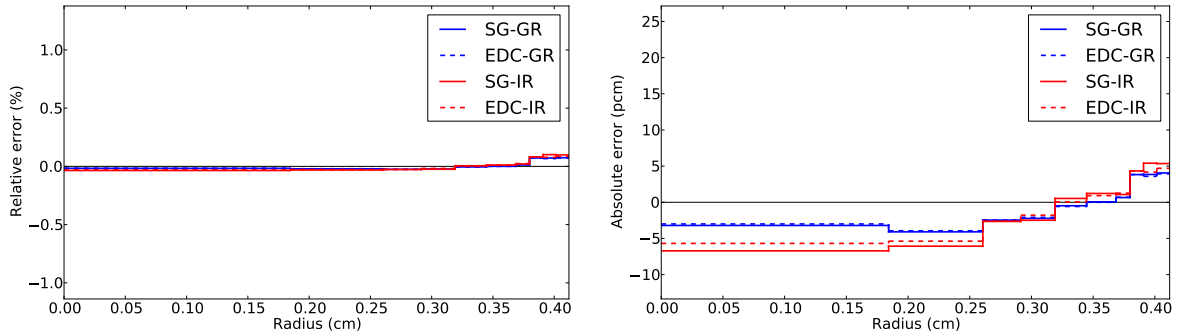

(b) Production rates

Figure 8.6: Error in space on the absorption and production rates of the resonant mixture in the "Cell-UO_2-noClad" benchmark

Figures 8.7 and 8.8 detail the errors on the absorption and production rates for the two isotopes composing the resonant mixture, ^{238}U and ^{235}U. For the sake of compactness, only the absolute errors in pcm are displayed in these two Figures, the idea being to quantify the contribution of each isotope to the global calculation.

As can be expected, the main contributors to the errors on the mixture absorption and production rates are the ^{238}U and ^{235}U, respectively. In group 27, between 4.0 and 9.5 eV, the large negative peak in the absorption rates of ^{235}U is compensated by a large peak of opposite sign in the absorption rates of ^{238}U, leading to an actual small error on the mixture absorption rates in this specific group.

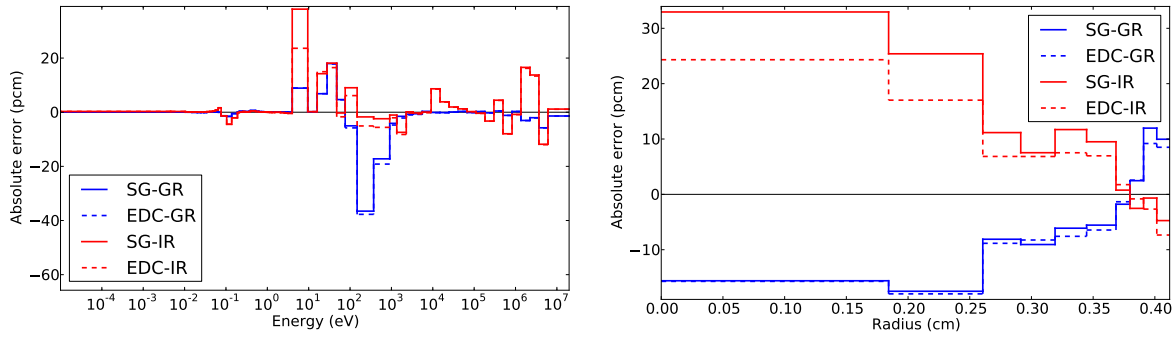

(a) ^{238}U

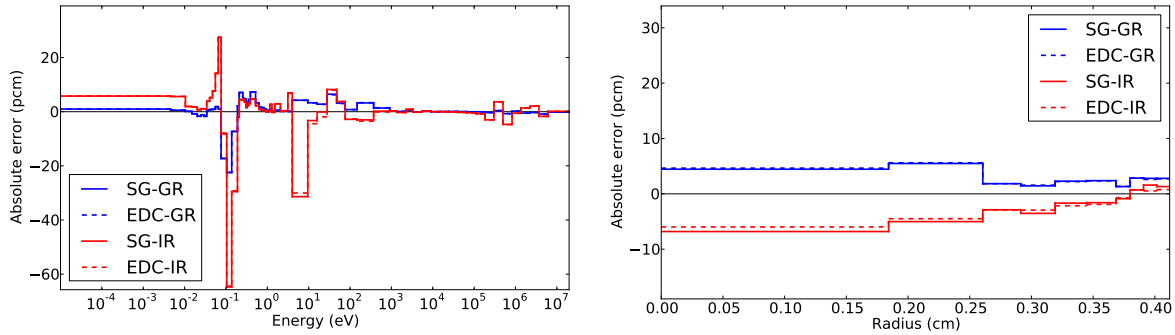

(b) ^{235}U

Figure 8.7: Error on the absorption rates per isotope in the "Cell-UO_2-noClad" benchmark

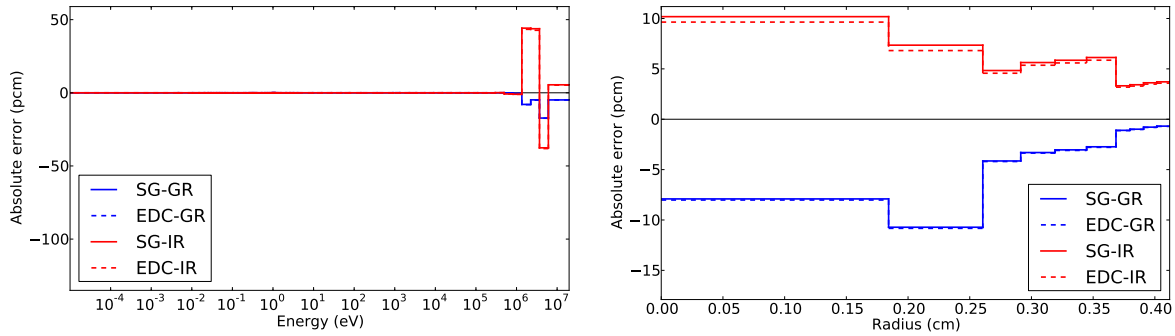

(a) ^{238}U

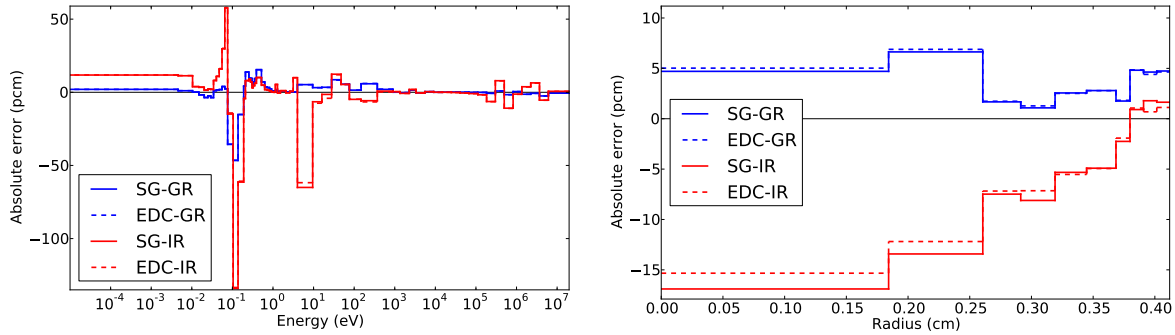

(b) ^{235}U

Figure 8.8: Error on the production rates per isotope in the "Cell-UO_2-noClad" benchmark

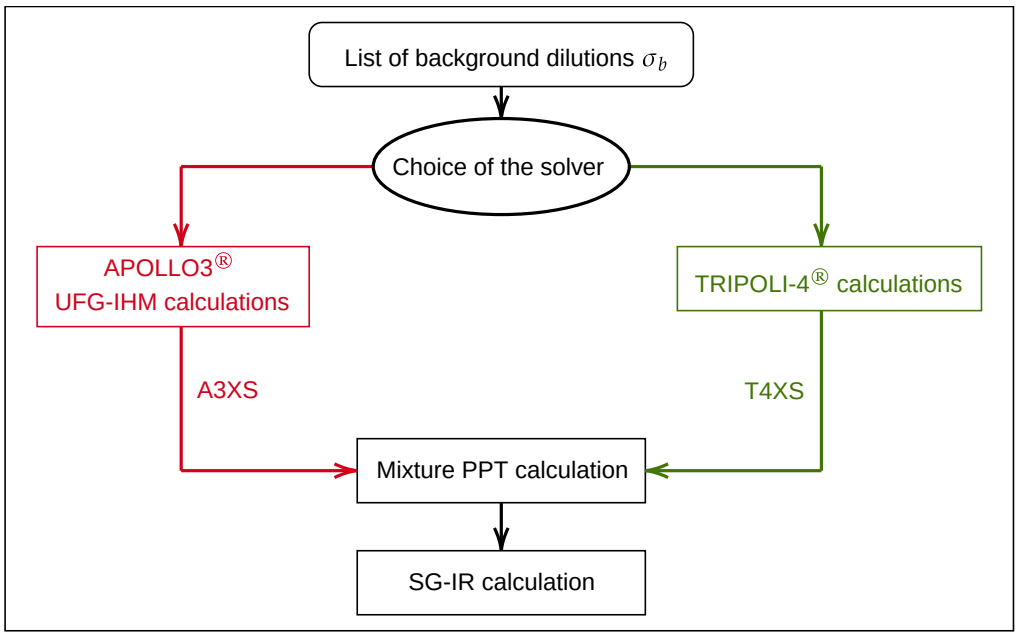

Figure 8.9: Methodology to quantify the errors caused by the use of the cross sections produced with the APOLLO3® UFG-IHM solver on the SG-IR calculation

Estimation of the error propagated through the use of the cross sections produced with the UFG-IHM solver

It has been stated in the previous studies on the IHM and simplified pin-cell benchmarks that a significant error was caused by the use of the UFG-IHM solver of Chapter 5 to produce the cross sections of the resonant mixture in an IHM, which are then employed in the procedure described in Chapter 6 to generate the corresponding mixture PPT. Indeed, the analysis of the cross section obtained with the UFG-IHM solver evidenced that single isotopes were well calculated, but a significant discrepancy has been observed in the case of resonant mixtures. The use of the subsequent mixture PPTs therefore propagates this unsufficient mixture treatment in the final subgroup calculation. In this paragraph, a methodology is proposed to quantify this error. It is applied on the cladless pin-cell test case.

As shown in the diagram of Figure 8.9, the error caused by the use of the cross sections of the UFG-IHM solver is bypassed by producing reference cross sections with Monte Carlo simulations. For each value of background dilution introduced in Chapter 6, a TRIPOLI-4® calculation is carried out to obtain the cross sections of an IHM composed of the ^{238}U-^{235}U mixture, diluted with a purely scattering hydrogen whose scattering cross section is fixed to its potential cross section, and whose density is adjusted to set the dilution. These reference cross sections are denoted T4XS. They are then connected to the PPT generator of Chapter 6 to generate reference PPTs for this specific resonant mixture, which are employed in a SG-IR subgroup calculation. The results are then compared to the standard SG-IR calculation where the PPTs are generated by fitting the cross sections of the UFG-IHM solver of APOLLO3®, denoted A3XS.

The numerical results of Chapter 5 have shown that in the case of the ^{238}U-^{235}U mixture, the

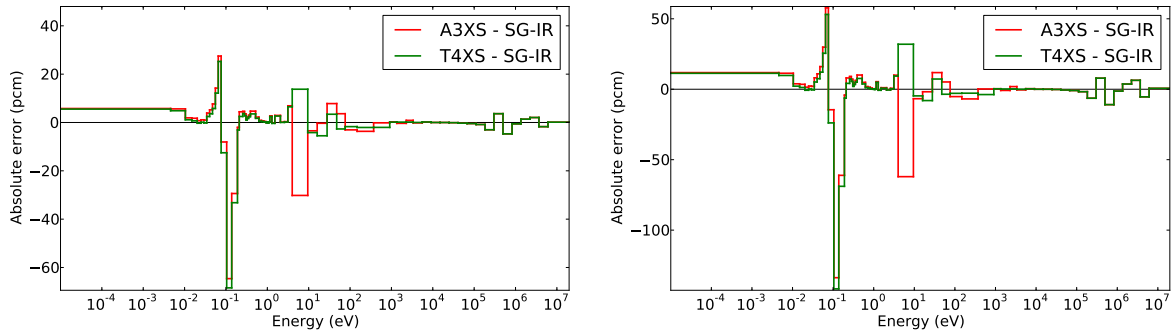

(a) Absorption rates

(b) Production rates

Figure 8.10: Contribution of the errors from the APOLLO3® UFG-IHM solver to the reaction rates of ^{235}U in the "Cell-UO_2-noClad" benchmark

largest error was obtained on the cross sections of the ^{235}U isotope, in the group located between 4 and 9.5 eV, where there is a large resonance of ^{238}U. The ^{235}U absorption cross section obtained with the UFG-IHM solver displayed errors exceeding -15% for the lower values of background dilutions. Figure 8.10 compares the ^{235}U absorption and production rates obtained with a SG-IR calculation, using either the A3XS or T4XS cross sections to generate the PPTs. The use of the reference T4XS instead of the A3XS entirely removes the large negative peak observed in group 27. Even so, this specific energy group is still the source of a significant discrepancy, with more than 25 pcm of error in the production rates of ^{235}U. This test shows that improving the UFG-IHM solver to better take into account the resonance interference effect would indeed improve the accuracy of the calculation, but this potential gain of precision is still limited by factors that are not due to the UFG-IHM solver. The remaining peak, that leads to an overestimation of the absorption and production rates of ^{235}U, can be caused by the definition of the energy mesh, by the use of transfer cross sections at infinite dilution, or by any of the calculation steps occuring after the generation of the mixture cross sections in the IHM for a list of dilutions, namely the PPT calculation and the SG-IR calculation. It has been shown in Chapter 6 that a PPT of order 5 is enough to fit the input cross sections. In group 27 which displays a major resonance, a higher order might be required to accurately represent the subgroup flux. Also, it is very likely that the error in group 27 could be lessened by adjusting the λ parameter of each isotope in this specific group.

"Cell-UO_2" benchmark

The "Cell-UO_2" benchmark is more complex than the "Cell-UO_2-noClad" benchmark because of the presence of the cladding, made of a mixture of natural Zirconium, which also has to be self-shielded. This is a source of additional errors.

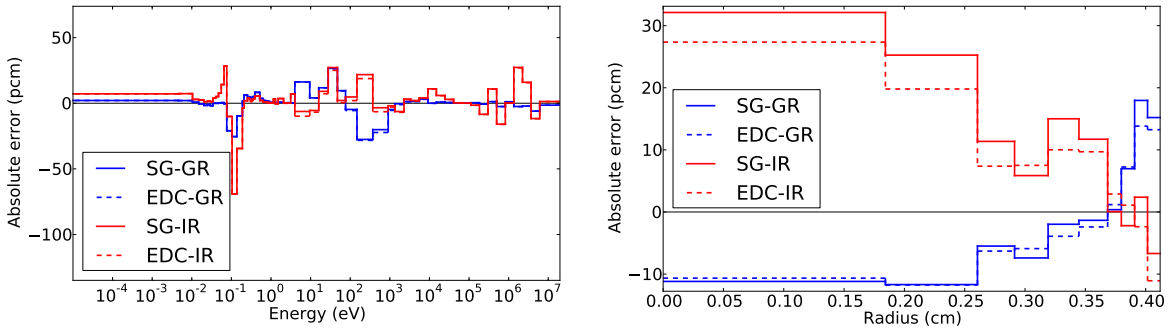

(a) Absorption rates

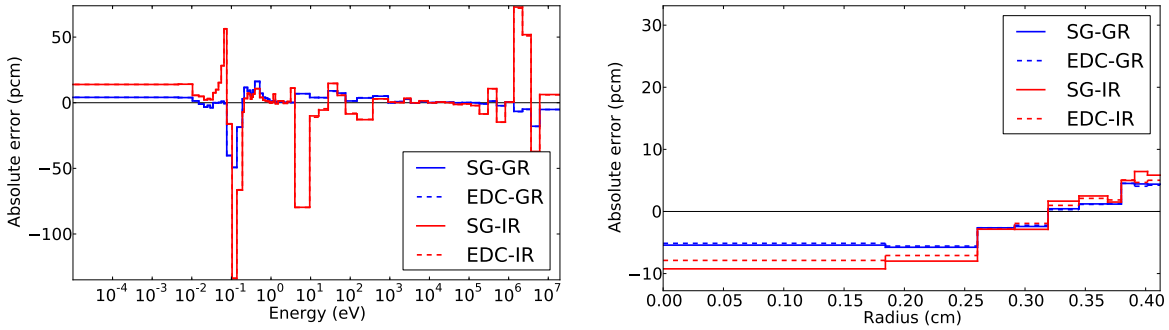

(b) Production rates

Figure 8.11: Error in energy and space on the absorption and production rates of the fuel mixture in the "Cell-UO_2" benchmark

Figure 8.11 shows the error, in pcm, of the absorption and production rates of the fuel mixture in the pin-cell. This is sensibly the same as in the simplified unclad pin-cell, whose results have already been detailed above. Figures 8.12 and 8.13 provide the detail of the reaction rates for the ^{238}U and ^{235}U isotopes inside the fuel mixture.

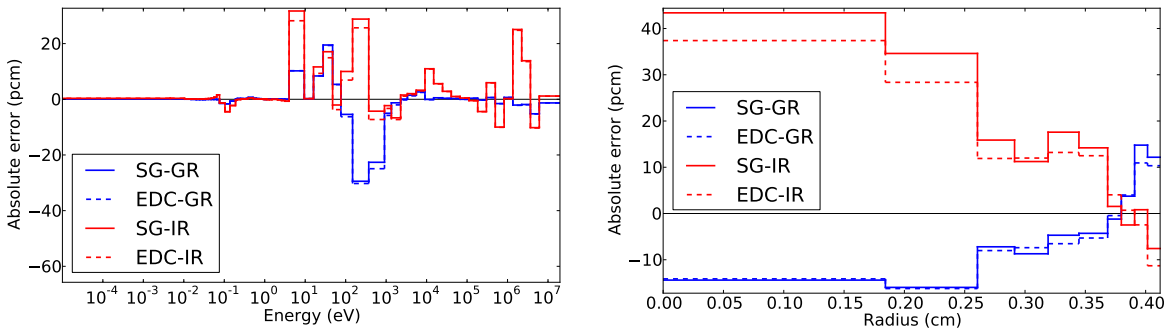

(a) ^{238}U

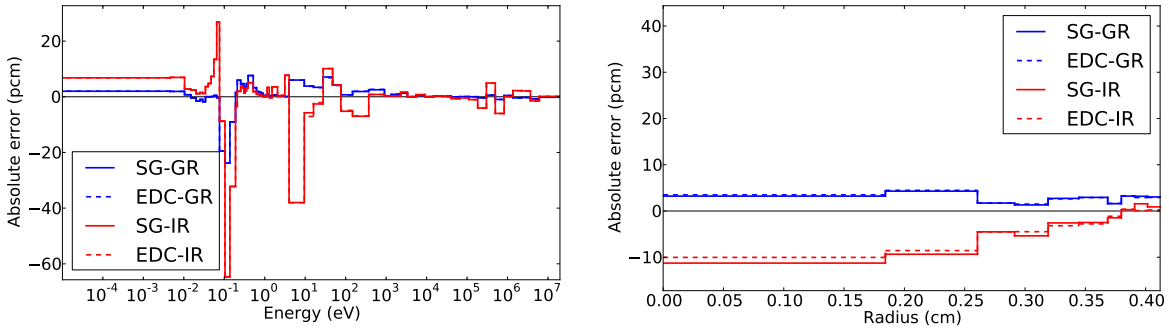

(b) ^{235}U

Figure 8.12: Error on the absorption rates per isotope in the "Cell-UO_2" benchmark

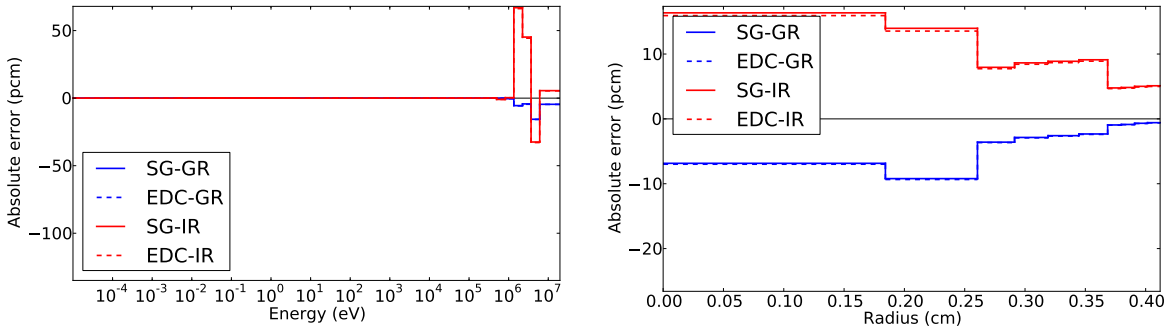

(a) ^{238}U

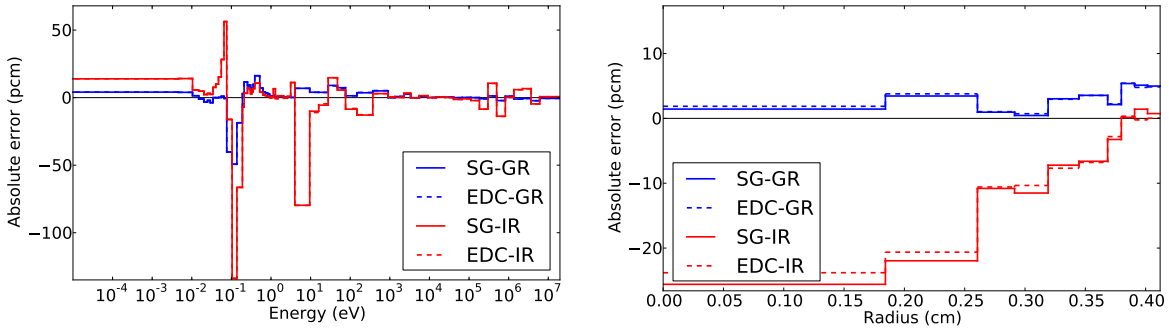

(b) ^{235}U

Figure 8.13: Error on the production rates per isotope in the "Cell-UO_2" benchmark

The two single pin-cell benchmarks presented here establish that the reaction rates of the resonant mixture obtained with the 69-group SG-IR and EDC-IR calculations can be as accurate as the 383-group SG-GR and EDC-GR calculations in the resonant domain. However, the IR-based methods lead to a worse multiplication factor than the GR-based methods, and the study of the pin-cell test cases has enable to quantify the contribution of the use of the cross sections from the UFG-IHM solver of Chapter 5 to the final subgroup calculation. It has highlighted that there are still sources of errors that are left to be identified, in the calculation procedure of the PPT and in the parameters of the IR model. Large errors outside of the resonant domain once again have been noticed but are not due to the self-shielding process, and could be corrected by optimizing the energy mesh.

The evaluation of the SG-IR and EDC-IR methods will now be carried out on larger geometries to estimate their ability to account for the shadowing effect of neighboring fuel pin-cells. The next subsection will introduce the results obtained on a small case of 3×3 cells.

8.3.3 . Motif of 3×3 pin-cells

The benchmarks defined by the motif of 3×3 cells enable to study the effect of the shadowing effect of neighboring rods in the self-shielding calculation. The detailed description of the two benchmarks is given in Chapter 4.

Table 8.3 gives the difference on the k_{eff} obtained with the 383-group GR-based subgroup method calculations and with the 69-group IR-based subgroup method calculations, compared with the reference TRIPOLI-4® value. It can be first remarked that in the case of the "Motif 3×3 Water-hole" benchmark, where the center cell is a guide tube, the error on the k_{eff} is of the same order of magnitude as the one in the single cell calculation. This error is around a few dozens of pcm for the GR-based methods, and a hundred pcm for the IR-based methods. The presence of Gadolinium-UO_2 fuel in the center cell of the second benchmark leads to an increase of the error measured on the k_{eff} of nearly a factor 2. In particular, the accuracy of the SG-IR is clearly degraded by the addition of the Gadolinium isotopes, with a Δk_{eff} of almost -250pcm.

Table 8.3: Difference of k_{eff} in the 3×3 pin-cells benchmarks

	"Motif 3×3 Water-hole"		"Motif 3×3-Gd"	
Method	k_{eff}	Δk_{eff} (pcm)	k_{eff}	Δk_{eff} (pcm)
TRIPOLI-4®	1.46014 $\pm$ 3 pcm	-	1.13558 $\pm$ 3 pcm	-
SG-GR	1.46057	43	1.13630	72
EDC-GR	1.46065	50	1.13630	72
SG-IR	1.45907	-107	1.13310	-248
EDC-IR	1.45923	-92	1.13405	-153

"Motif 3×3 Water-hole" benchmark

Figure 8.14 shows the spatial distribution of the relative error in percent on the absorption rates of the resonant UO_2 mixture. It can be observed that in every cell, the GR-based methods have a very satisfying precision, with less than 0.1% of difference compared with the reference Monte Carlo value.

The error in the upper-right pin-cell is also well under 0.1% for the IR-based methods, but it increases in the pin-cell alongside the guide tube, reaching 0.2%, which is 10 times more than the error of the SG-GR and EDC-GR methods in the same location.

Figure 8.15 displays the relative error on the production rates of the UO_2 mixture. They are accurately calculated by all the self-shielding methods in all the pin-cells, with less than 0.01% of error.

Figure 8.16 details the errors on the absorption rates of the ^{238}U isotope. They are significantly larger than the ones of the resonant mixture, evidencing that there are compensating effects when summing the contribution of every isotope. The highest error observed is obtained with the EDC-IR method, but is still under 1%, showing still a good agreement with the reference value.

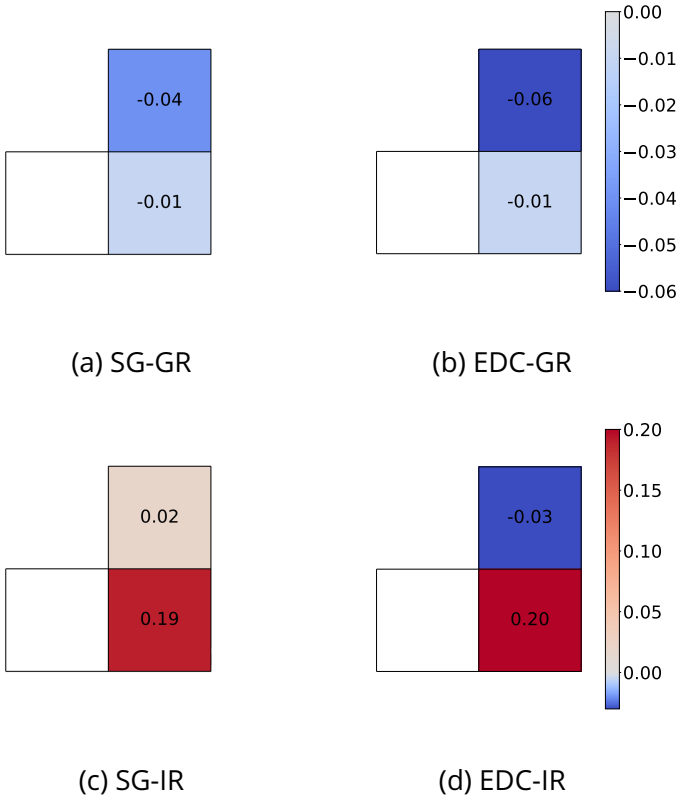

(a) SG-GR (b) EDC-GR

(c) SG-IR (d) EDC-IR

Figure 8.14: Error (in %) on the absorption rates of the UO_2 resonant mixture in the "Motif 3×3 Water-hole" benchmark

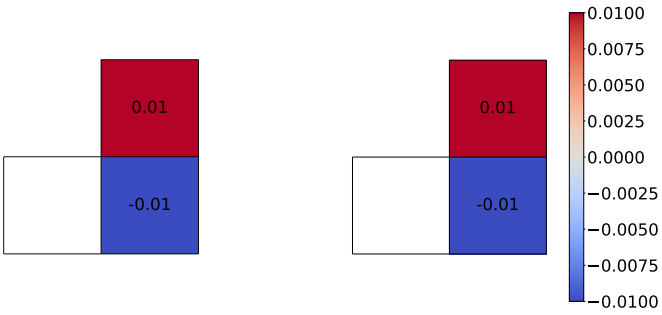

(a) SG-GR (b) EDC-GR

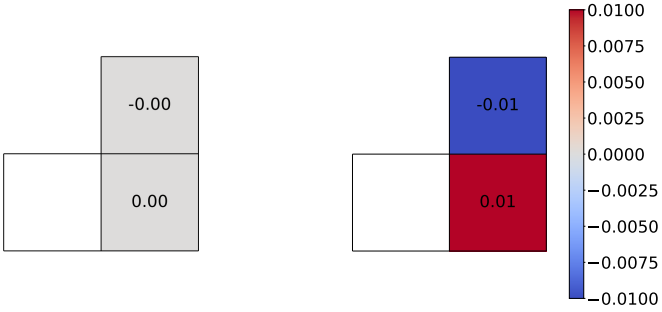

(c) SG-IR (d) EDC-IR

Figure 8.15: Error (in %) on the production rates of the UO_2 resonant mixture in the "Motif 3×3 Water-hole" benchmark

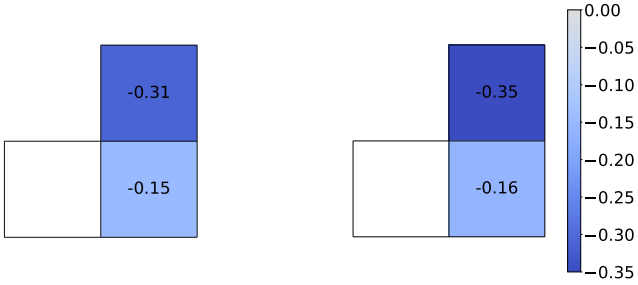

(a) SG-GR (b) EDC-GR

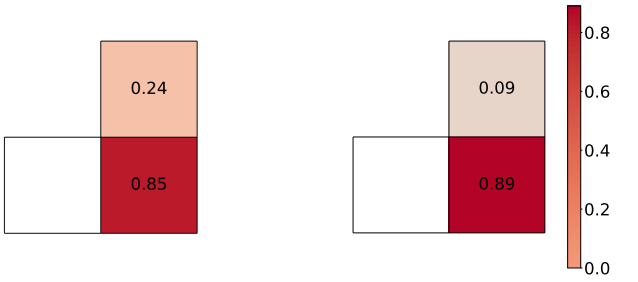

(c) SG-IR (d) EDC-IR

Figure 8.16: Error (in %) on the absorption rates of the ^{238}U absorption rates in the "Motif 3×3 Water-hole" benchmark

Figures 8.14 and 8.16 show that the accuracy of the calculated absorption rates with the SG-IR and EDC-IR methods is very dependent on the position of the pin-cell in the geometry. The error in the cell alongside the tube cell is almost 10 times larger than in the cell placed in diagonal of the tube cell, despite their identical composition.

The analysis of the "Motif 3×3 Water-hole" benchmark shows that while the 383-group GR-based calculations have a better accuracy than the 69-group IR-based calculations, the latter still reach a satisfying precision level, with errors of less than 1% for ^{238}U and less than 0.2% for the UO_2 mixture. The coupling of the subgroup methods with the EDC method does not bring any noticeable difference in this numerical test case.

"Motif 3×3-Gd" benchmark

The errors for the "Motif 3×3-Gd" benchmark are displayed in the Figures 8.17 and 8.18; they correspond to the errors on the absorption and production rates of the UO_2 fuel mixture in the UO_2 pin-cells, and of the Gd-UO_2 fuel mixture in the centrally located Gd-UO_2 pin-cell. Figure 8.19 shows the errors on the ^{238}U absorption rates in every pin-cell.

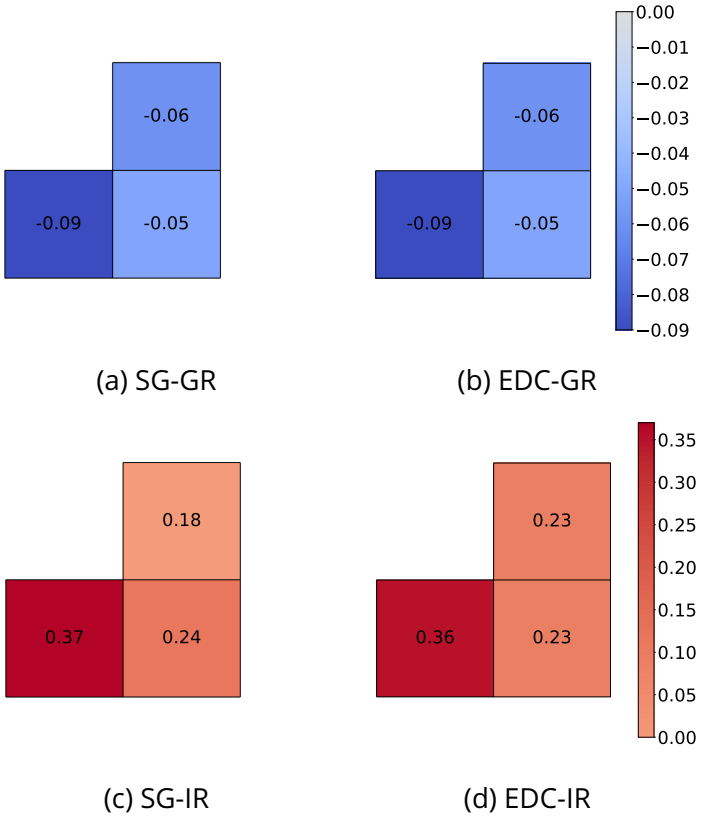

(a) SG-GR (b) EDC-GR

(c) SG-IR (d) EDC-IR

Figure 8.17: Error (in %) on the absorption rates of the Gd-UO_2 and UO_2 resonant mixtures in the "Motif 3×3-Gd" benchmark

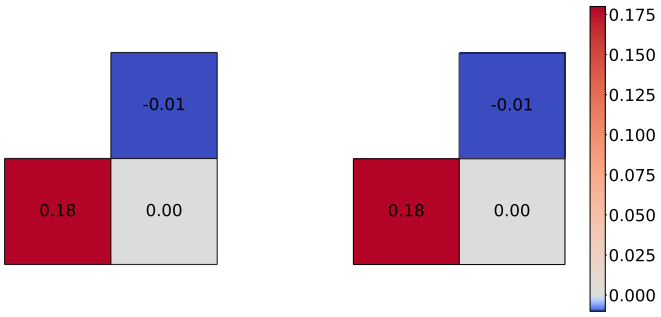

(a) SG-GR (b) EDC-GR

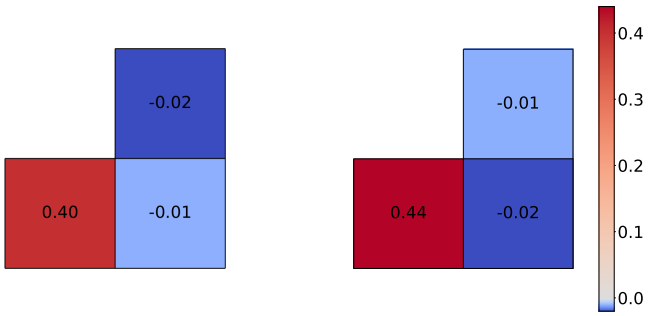

(c) SG-IR (d) EDC-IR

Figure 8.18: Error (in %) on the production rates of the Gd-UO_2 and UO_2 resonant mixtures in the "Motif 3×3-Gd" benchmark

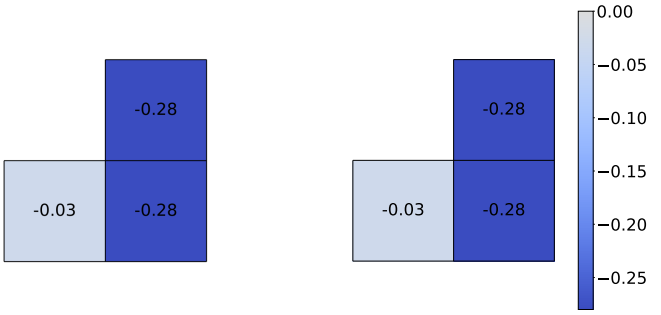

(a) SG-GR (b) EDC-GR

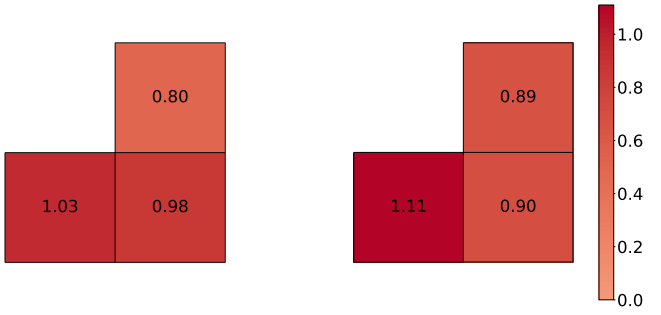

(c) SG-IR (d) EDC-IR

Figure 8.19: Error (in %) on the absorption rates of the ^{238}U isotope in the "Motif 3×3-Gd" benchmark

While the error on the absorption rates of the UO_2 mixture does not increase for the GR-based methods, compared to the previous test case, the addition of the Gd-UO_2 pin-cell does impact the calculation of the UO_2 rates with the 69-group IR-based methods, increasing by a factor almost 10 the overestimation of the absorption in the upper-right cell. Moreover, the absorption of the Gd-UO_2 cell is largely overestimated with the same methods, reaching a relative error of almost 0.4%, when the 383-group GR-based methods have less than 0.1% of error on the absorption rates in the Gd-UO_2 cell. This explains why the difference of k_{eff} is found more negative for the SG-IR and EDC-IR methods. The errors on the ^{238}U absorption rates exceed 1% in the Gd-UO_2 mixture when using the IR-based methods.

Figure 8.20 details the error in each energy group on the absorption rates of the Gd-UO_2 mixture of the central cell. It confirms that the SG-GR and EDC-GR methods yields an accurate representation of the reaction rates for this specific resonant mixture, while large errors are introduced by the use of either the SG-IR or the EDC-IR methods. Two large peaks are noticeable. The first one, accouting for 25% of overestimation (about 100 pcm), is located in the eV range, where reside many isolated resonances of the two isotopes of Uranium, ^{238}U and ^{235}U, and of the two principle Gadolinium absorbers, namely ^{155}Gd and ^{157}Gd. In the current study, no self-shielding is done in that range. The second peak is situated in the range between approximately 10 and 50 eV, and accounts for about -10% of error (-60 pcm).

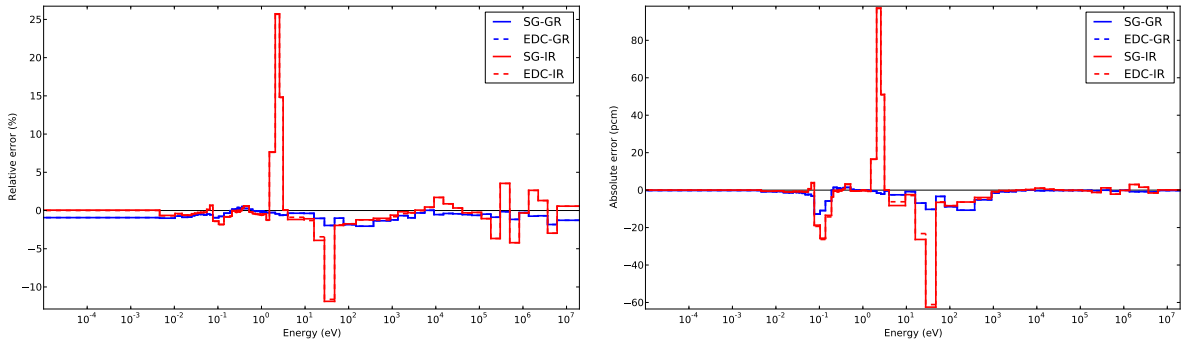

Figure 8.20: Error on the absorption rates of the Gd-UO_2 resonant mixture in the "Motif 3×3-Gd" benchmark

This analysis shows that on this grid of 3×3 cells, the same accuracy as the one obtained on a single pin-cell can be expected, evidencing that the shadowing effect of neighboring cells is well accounted for in the newly implemented subgroup methods. It also prooves that the improvement of the mixture treatment would benefit to the accuracy of the self-shielding calculation, in order to get closer to the reference calculations.

8.3.4 . PWR fuel assembly

Finally, a set of two fuel assemblies has been selected to complete this study. The "UO_2 assembly" and the "Gd-UO_2 assembly" are described in Chapter 4.

The difference of k_{eff} , taking TRIPOLI-4® calculations as references, is given in Table 8.4. The difference in k_{eff} for the two assembly benchmarks is less than 30 pcm for the SG-GR and EDC-GR

methods, and is between -110 and -300 pcm for the SG-IR and EDC-IR methods. In the case of the Gd-UO_2 assembly, the methods based on the Equivalent Dancoff-factor Cell method yield a better multiplication factor than the regular subgroup method. This is because the use of the Same Material Approximation (SMA) in the subgroup method is known to introduce errors in presence of in the geometry of very different mixtures containing common resonant isotopes [19], as it is the case with the UO_2 and Gd-UO_2 mixtures.

Table 8.4: Difference of k_{eff} in the fuel assembly benchmarks

	"UO_2 assembly"		"Gd-UO_2 assembly"	
Method	k_{eff}	Δk_{eff} (pcm)	k_{eff}	Δk_{eff} (pcm)
TRIPOLI-4®	1.45150 $\pm$ 2 pcm	-	1.12990 $\pm$ 2 pcm	-
SG-GR	1.45169	19	1.12961	-29
EDC-GR	1.45178	28	1.12975	-15
SG-IR	1.45024	-126	1.12689	-301
EDC-IR	1.45038	-112	1.12743	-247

Figures 8.21 and 8.22 show the distribution in space of the errors (in %) on the absorption and production rates of the resonant mixtures, in the case of the UO_2 assembly. Figure 8.23 gives the spatial distribution of the errors on the ^{238}U absorption rates. This assembly only contains UO_2 pin-cells and guide tubes.

This numerical test case confirms the trends already remarked before: the SG-GR and EDC-GR methods tend to underestimate the absorption and production rates, while it is the opposite for the SG-IR and EDC-IR methods. The order of magnitude of the errors for the 69-group IR-based calculations is significantly larger than for the 383-group GR-based methods; in particular, the SG-IR and EDC-IR methods present a higher errors on the outer cells and next to the water holes. The EDC-IR yields hardly better results in these locations, although it does significantly diminish by a factor 2 the errors in the cells placed further away from the edge or the assembly or of the guide tubes.

The problem of the inaccuracies noticed in the outer cells of the geometry needs further investigation.

Figures 8.24, 8.25 and 8.26 show the errors for the "Gd-UO_2 assembly" benchmark. Compared to the previous assembly test case, some UO_2 rods have been replaced with Gd-UO_2 pin-cells. All the self-shielding methods compared in this study tend to overestimate the absorption rates in the Gd-UO_2 pin-cells. This effect is not very large in the SG-GR and EDC-GR methods, but for the SG-IR and EDC-IR methods, the relative error can exceed 1.5% in the calculated ^{238}U absorption rates in the Gd-UO_2 cells. This largely contributes to the degradation of the global calculation accuracy, partly explaining that the k_{eff} is almost 3 times less precise than in the UO_2 assembly test case. The errors in the UO_2 cells are also excessive in most locations, reaching values sometimes more than 10 times larger than with the SG-GR and EDC-GR methods. This benchmark highlights that the newly implemented SG-IR method of APOLLO3® needs to be improved for the treatment of the Gd-UO_2 material.

The EDC-IR methods does not improve by much the accuracy of the calculation of the Gd-UO_2

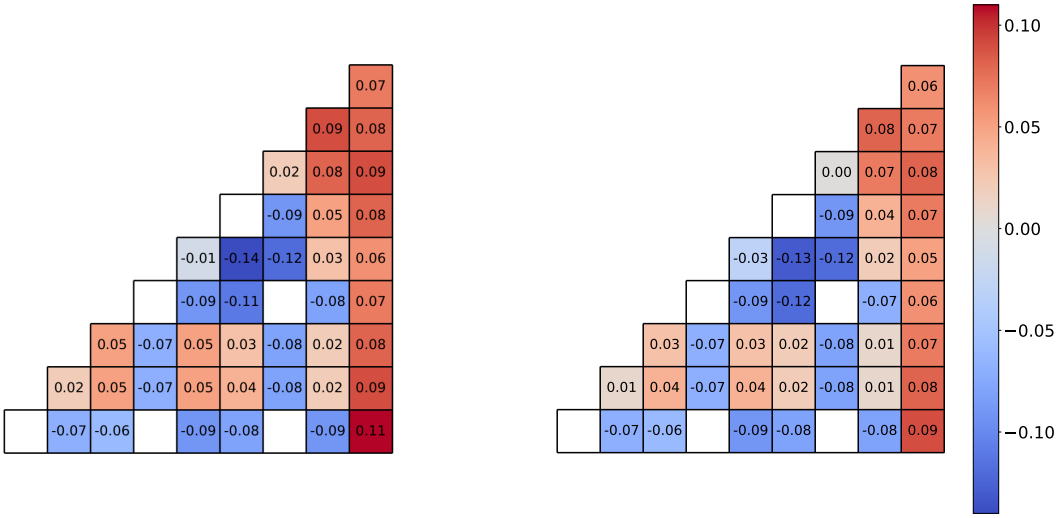

(a) SG-GR

(b) EDC-GR

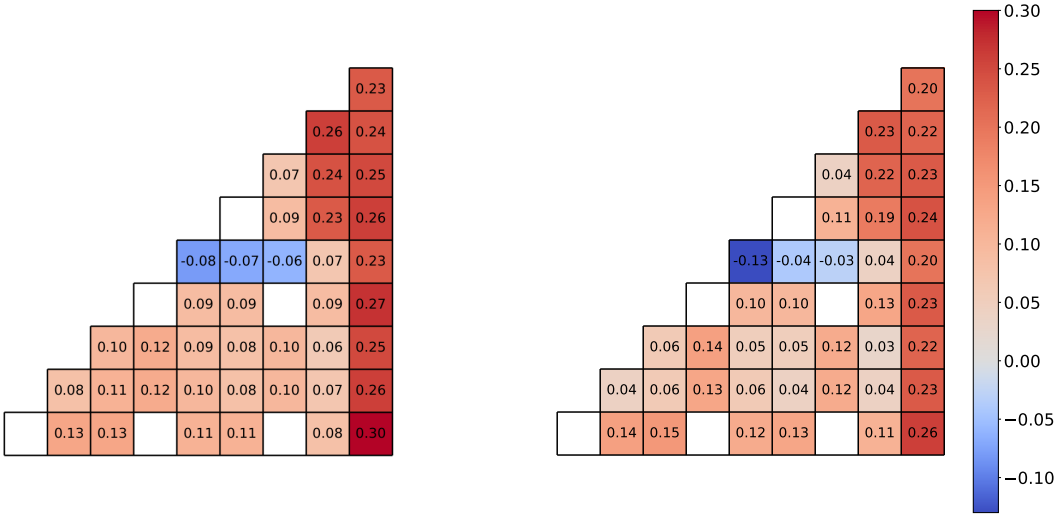

(c) SG-IR

(d) EDC-IR

Figure 8.21: Error (in %) on the absorption rates of the UO_2 resonant mixture in the "UO_2 assembly" benchmark

compared with the SG-IR results, but it does reduce the errors in the neighboring UO_2 rods, leading to a slightly better multiplication factor.

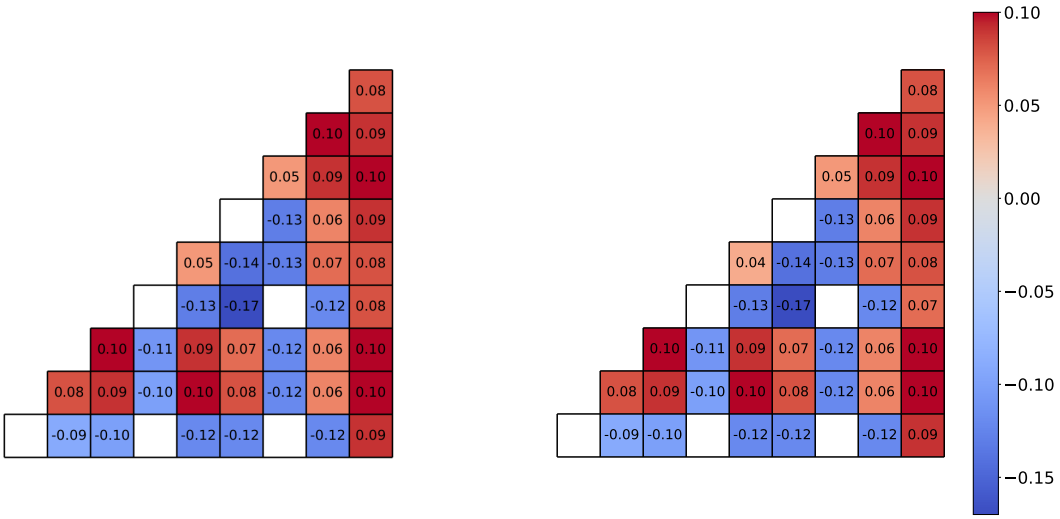

(a) SG-GR

(b) EDC-GR

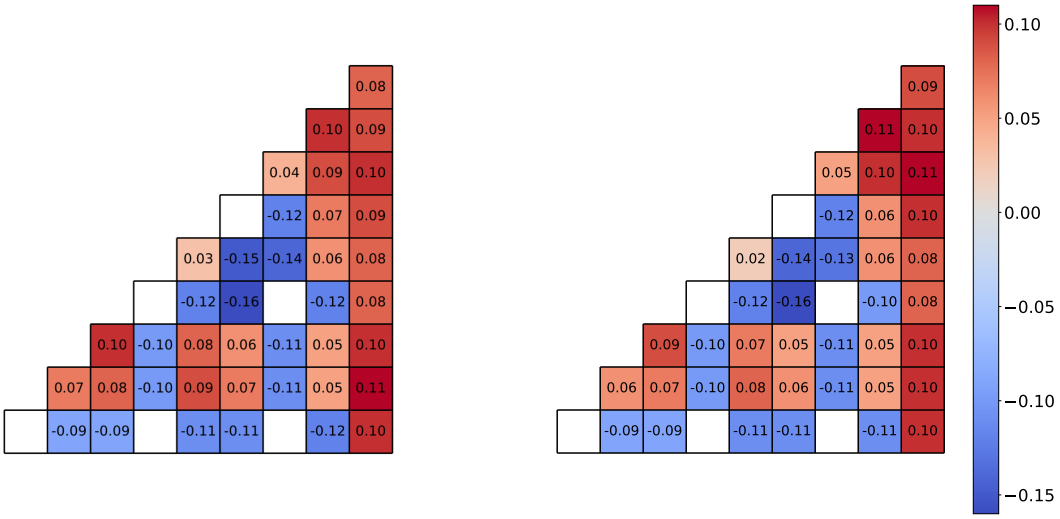

(c) SG-IR

(d) EDC-IR

Figure 8.22: Error (in %) on the production rates of the UO_2 resonant mixtures in the "UO_2 assembly" benchmark

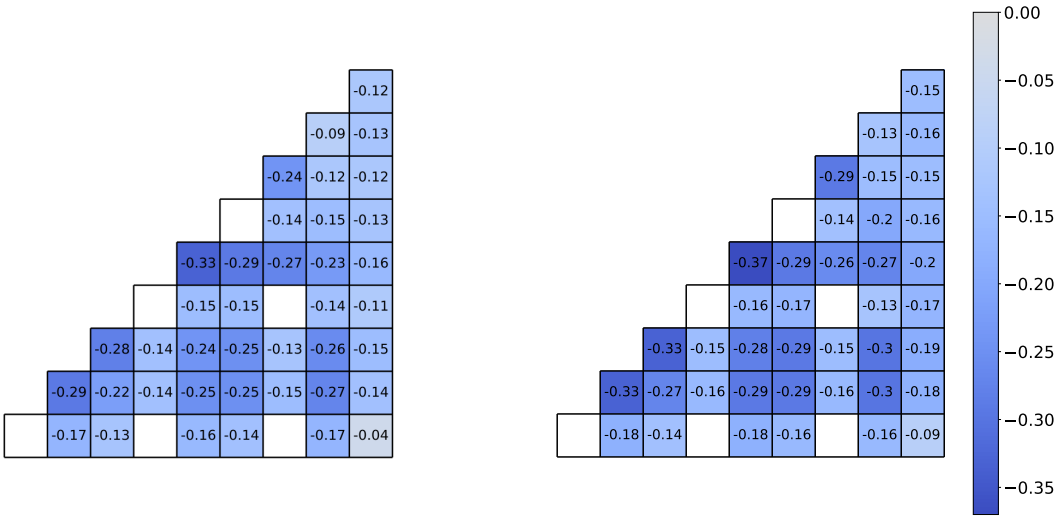

(a) SG-GR

(b) EDC-GR

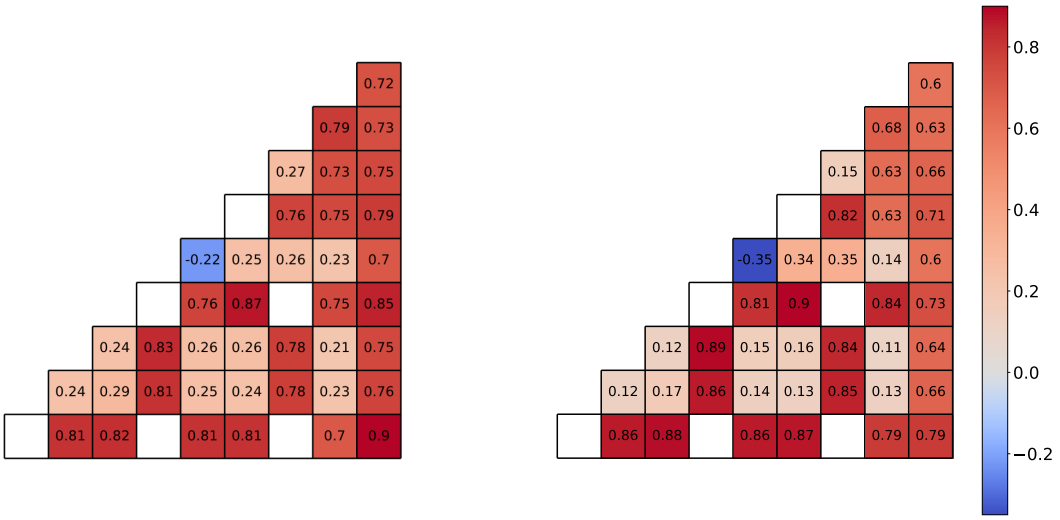

(c) SG-IR

(d) EDC-IR

Figure 8.23: Error (in %) on the absorption rates of the ^{238}U isotope in the "UO_2 assembly" benchmark

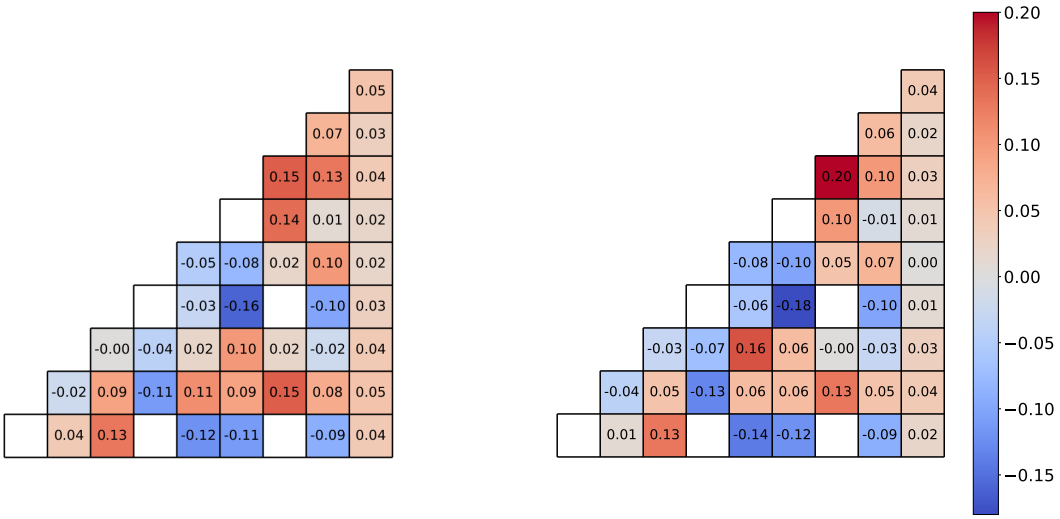

(a) SG-GR

(b) EDC-GR

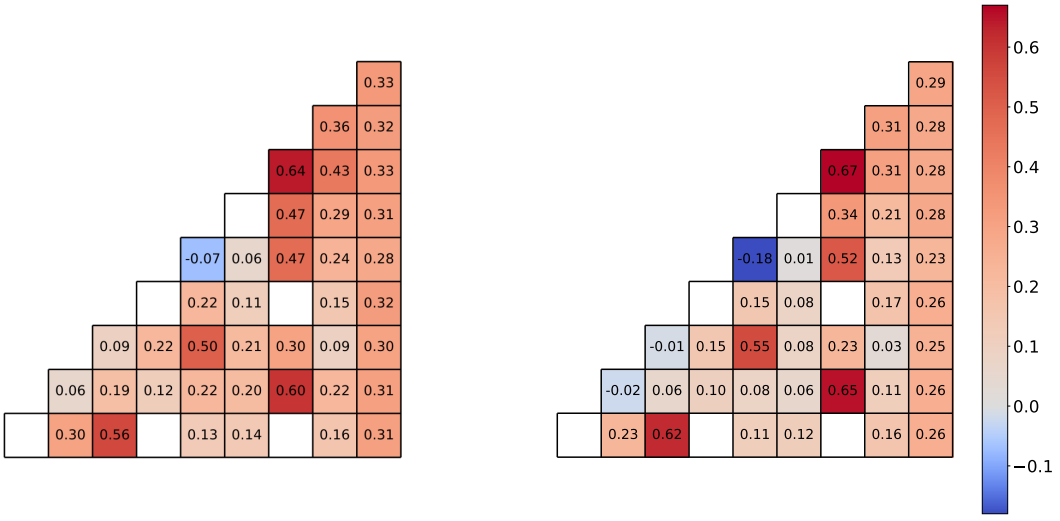

(c) SG-IR

(d) EDC-IR

Figure 8.24: Error (in %) on the absorption rates of the UO_2 and Gd-UO_2 resonant mixture in the "Gd-UO_2 assembly" benchmark

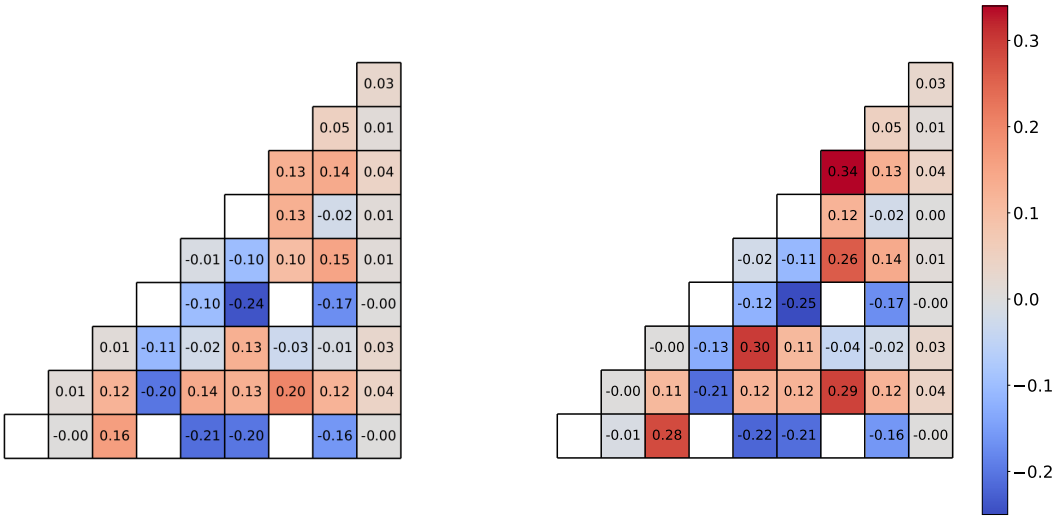

(a) SG-GR

(b) EDC-GR

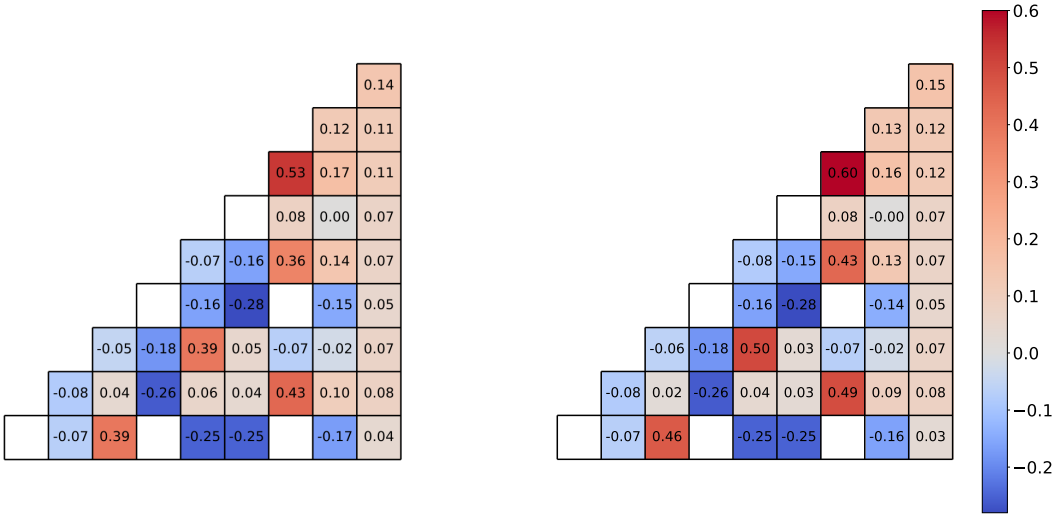

(c) SG-IR

(d) EDC-IR

Figure 8.25: Error (in %) on the production rates of the UO_2 and Gd-UO_2 resonant mixtures in the "Gd-UO_2 assembly" benchmark

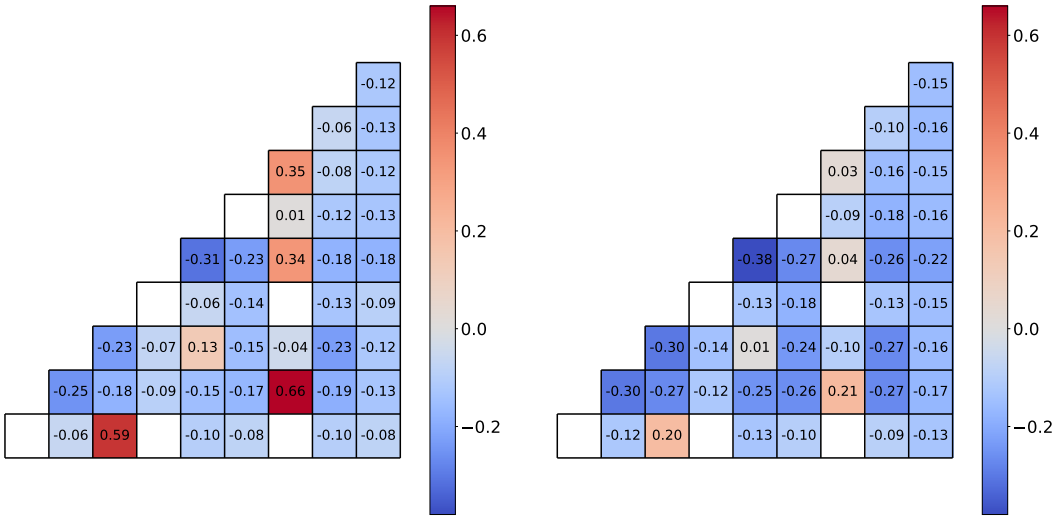

(a) SG-GR

(b) EDC-GR

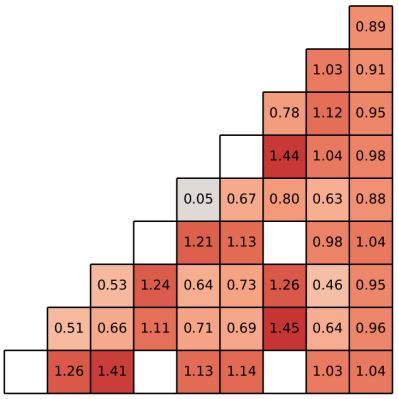

(c) SG-IR

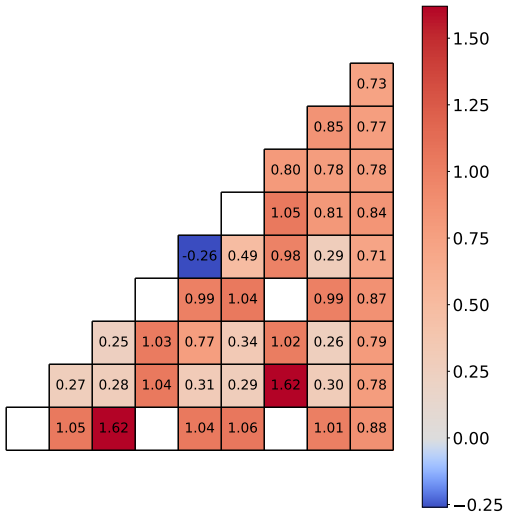

(d) EDC-IR

Figure 8.26: Error (in %) on the absorption rates of the ^{238}U isotope in the "Gd-UO_2 assembly" benchmark

8.4 . Computational Time of the IR-based Subgroup Methods

The two assembly calculations have been selected to quantify the computational time of the SG-IR and EDC-IR methods, because of their significant size. The CPU times of the 383-group SG-GR and EDC-GR calculations, as well as that of the 69-group SG-IR and EDC-IR calculations, are presented in Tables 8.5 and 8.6 for the UO_2 and the Gd-UO_2 assembly benchmarks, respectively.

Table 8.5: Comparison of the computational times on the UO_2 assembly calculation

	CPU (s) [% of the total CPU time]	
	Self-shielding [(a)]	Flux [(b)]
SG-GR	246 [48%]	268 [52%]
EDC-GR	43 [14%]	270 [86%]
SG-IR	10 [15%]	57 [85%]
EDC-IR	6 [10%]	56 [90%]

[(a)] CPU time on one processor
[(b)] CPU time on eight processors

Table 8.6: Comparison of the computational times on the Gd-UO_2 assembly calculation

	CPU (s) [% of the total CPU time]	
	Self-shielding [(a)]	Flux [(b)]
SG-GR	655 [70%]	282 [30%]
EDC-GR	52 [16%]	283 [84%]
SG-IR	27 [32%]	58 [68%]
EDC-IR	11 [16%]	58 [84%]

[(a)] CPU time on one processor
[(b)] CPU time on eight processors

The CPU time required to carry out the Gd-UO_2 assembly calculation is more than twice the time of the UO_2 assembly calculation, because two resonant mixtures have to be self-shielded instead of one.

The use of the EDC methods significantly diminishes the CPU time of the self-shielding calculations by a factor up to 12, even on a single thread, because the one-dimensional collision probability calculation of the cylindrical cells is much faster than the two-dimensional collision probability calculation of the lattice. The use of the EDC method only accelerates the self-shielding calculation, the time spent in the flux calculation is unchanged.

The computational time of the SG-IR method is significantly smaller than the one of the SG-GR method, with both the self-shielding and the flux calculation steps being faster. The CPU time of the flux calculation is almost linearly dependent on the number of energy groups, explaining the difference of a factor 5 observed between the CPU time of the flux calculation of the 383-group SG-GR calculation and the one of the 69-group SG-IR calculation. Also, the self-shielding calculation is only applied to the resonant domain, which is made of 13 groups in the 69-group mesh, and of 309 groups

in the 383-group mesh. This reduction of a factor almost 25 corresponds to the difference measured between the self-shielding calculations of the SG-IR and SG-GR methods.

8.5 . Conclusions

In this chapter, the implementation in the APOLLO3® code of a subgroup method based on the "Intermediate Resonance" model and on the physical probability tables was described. The IR model relies on a parameter, that is not provided in the multigroup libraries supplied by the GALILEE nuclear data processing system; a preliminary step was therefore required to compute in every resonant group of the coarse 69-group energy structure the IR parameter per isotope. It has been determined using Monte Carlo simulations.

The IR parameters are utilized in the implementation of a subgroup method based on the IR model to approximate the scattering sources of the slowing-down equation in a heterogeneous geometry. This subgroup method, called "SG-IR", is employed conjointly with modified physical probability tables that preserve the values of the resonant cross section of the resonant mixture, rather than its total cross section, as it was done in a previous implementation. Because the IR parameters were determined specifically for the coarse 69-group energy structure, the SG-IR method can only run on 69-group calculations. The SG-IR self-shielding method has also been coupled to the Equivalent Dancoff-factor Cell method described in Chapter 3. This is designated by the name of "EDC-IR".

Both the SG-IR and EDC-IR have been evaluated numerically on benchmarks representative of PWR calculations, and compared to the results of a reference calculation run with TRIPOLI-4® and to the outcomes of the APOLLO3® traditional subgroup calculations, based on the "General Resonance" model and on the mixture mathematical probability tables provided by GALILEE. The so-called "SG-GR" and "EDC-GR" self-shielding calculations are carried out on a fine 383-group energy discretization.

The accuracy of the SG-IR and EDC-IR methods have been measured, through the quantification of the errors on the multiplication factor and on the multigroup absorption and production rates. It was observed that in general, the 69-group IR-based self-shielding calculations are less accurate than the 383-group SG-GR and EDC-GR calculations. The reaction rates in the resonant domain have been proven to be physically accurate, but their integration over the space and energy domain do not lead to the same compensation effects observed in the GR-based calculations, hence the larger difference observed on the global multiplication factor, that is in all the cases studied in this chapter of the order of a few hundreds of pcm. The SG-IR and EDC-IR methods tend to overestimate the absorption rates of the resonant mixtures, leading to smaller k_{eff} than expected.

The study of the benchmarks have highlighted different axes of improvements for the IR-based subgroup methods of APOLLO3®.

First, noticeable discrepancies have been noticed in the resonance interference treatment of the UFG-IHM solver described in Chapter 5. This solver is employed to generate the reference cross sections fitted by the physical probability table calculation procedure; the errors on the reference cross sections are therefore transmitted, through the use of the PPTs, to the calculation of the reaction rates. An improvement of the UFG-IHM solver would therefore positively impact the results of the SG-IR method.

The SG-IR method would also benefit from improvements in the calculation procedure of the PPTs. As of today, we are still not able to compute PPTs of order higher than 5. Should this issue be resolved, the use of PPTs of higher orders would certainly improve the accuracy of the self-shielding calculations.

Finally, it has been observed that significant errors on the reaction rates are present outside of the resonant domain. This is not in the scope of the self-shielding calculation, but the refinement of the energy mesh in the thermal and fast domains would improve the precision of the calculation, at the cost of a larger computational time for the flux calculation.

9 - Conclusions and Future Work

9.1 . Conclusions

This manuscript described the approach adopted throughout this thesis work to carry out the self-shielding calculations for thermal reactors with the APOLLO3® code on a reduced number of energy groups.

The first part of this work consisted of implementing in APOLLO3® a module for the on-the-fly calculation of the mixture physical probability tables. An existing fine-structure slowing-down equation solver for an infinite homogeneous medium has been modified to carry out the ultra-fine group slowing-down calculations. This solver produces effective cross sections for a coarse 69-group energy mesh adapted from the energy structure of the WIMS-D library [59]. The validation process of this ultra-fine group solver showed its overall good capability in reproducing reference values, but highlighted significant errors in the treatment of the resonance interference effect in some energy groups.

The effective cross sections provided by the ultra-fine group solver have then been employed to compute physical probability tables taking into account the resonance interference effect, by treating the resonant mixture as a single isotope. Two methods, the Direct Resolution method and the Orthogonal Polynomial method, have been compared in the fitting of the effective cross sections, and have been proven to yield a similar level of accuracy, which is particularly satisfying for probability tables of orders 4 or 5. The OP method was developed for its potential to reduce the ill conditioning that often appears in the solution of minimization problems. Due to the time restriction for the development of the work, one of the two methods, the DR method, has been chosen to be used in the rest of the work. The validation of the OP method remains to be done in future work.

A first assessment of the coupling of the physical probability tables with the APOLLO3® legacy subgroup method has been carried out on simple benchmarks, for different number of energy groups. As can be expected, the accuracy of the calculation decreases with the number of groups. In particular, the 69-group calculations based on the physical probability tables do not meet the accuracy requirements to be employed as a self-shielding method in a standard APOLLO3® calculation.

The "Intermediate Resonance" model is often employed in existing codes to approximate the scattering sources in the slowing-down equation, for a solution on an energy mesh with less than 100 groups. The IR factors have been computed for the resonant groups of the 69-group energy mesh using Monte Carlo simulations, in order to implement in APOLLO3® the IR-based subgroup method using the physical probability tables. The first numerical tests carried out with this newly implemented subgroup method displayed very encouraging results; the errors measured on the multiplication factor are less than 200 pcm on assembly calculations. Speed-up factors of about 25 and 5 were observed in the self-shielding calculation and in the flux calculations, respectively, as a result of the decrease of the number of energy groups from 383 to 69.

The self-shielding method based on the use of the mixture physical probability tables and of the IR model with a 69-group energy mesh has therefore been proven to be a good compromise between accuracy and computational time. It is faster than any other self-shielding method implemented in

APOLLO3® for thermal reactor calculations. Although it is still less accurate than the 383-group mathematical probability table-based SG-GR method, the efforts of development of the SG-IR method will be on-going and further improvements are expected.

9.2 . Perspectives and Future Work

The analysis of the numerical tests carried out throughout this manuscript have highlighted several axes of improvements of the presented work. Furthermore, many approaches have been considered for each part of this thesis work, and some of them have not been tested for the lack of time. They are summarized in this section.

Improvement of the UFG-IHM solver

The APOLLO3® code has been the environment adopted for all the developments of this thesis. It therefore made sense to utilize the already existing functionalities such as the fine-structure equation solver for an infinite homogeneous medium.

Some not too intrusive modifications can be thought of to improve the accuracy of the UFG-IHM solver. The addition of the up-scattering treatment would be straightforward but it has been put on hold until the required nuclear data for the MUSCLET energy mesh are available. Another suggestion is to decouple the UFG-IHM from the online calculation of the mathematical probability tables, as it is known to be a time consuming procedure and it is suspected to not accurately take into account the resonance interference effect. Other quadratures could be derived for a use with the ultra-fine-group energy structure, such as a simple rectangle rule [75]. This could be done using the isotope-wise mathematical probability tables provided for the MUSCLET mesh by the GALILEE system.

Improvement of the physical probability tables

The main limitation observed in the implemented physical probability tables is their inability to reach an order higher than 5. While the preliminary validation study showed that this number seemed to be sufficient to accurately reconstruct the reference cross sections provided by the UFG-IHM solver, we suspect that it is not enough to represent the fluctuations of the neutron flux in a resonant group. While not explored in this work, we are certain that using probability tables of higher order would lead to a better calculation of the reaction rates.

The calculation of the physical probability tables by solving a linear system of equations is not the only existing method [76]. Optimization algorithms minimizing the error on the reconstructed multigroup quantities (cross sections, reaction rates, resonance integral, etc.) have been employed for this purposes in other lattice codes [77] [78] [79]; they oftentimes solve a simplified problem where the subgroup cross sections are fixed in advanced and only the subgroup weights are left to be determined. These kinds of algorithms are interesting because constraints can be added to the procedure to enforce the positivity of the subgroup weights and cross sections. Such algorithm should allow for the calculation of physical probability tables of arbitrarily high orders.

Improvement of the calculation procedure of the IR parameters

The IR factors in this work have been obtained by comparing the effective absorption cross sections of ^{238}U in mixtures of ^{238}U/^{1}H, where some of the hydrogen have been replaced by the isotope of interest. For our preliminary tests, we employed a Monte Carlo code to generate the IR factors for a single value of the temperature and of the background dilution. This procedure could be repeated for several temperatures and dilutions, in order to create a tabulation of the IR factors, that could be read by interpolation in order to approximate the right temperature and dilution conditions.

In groups where the ^{238}U has no significant resonances, another isotope of reference should be considered for the generation of the IR parameter, for example ^{235}U [71]. This idea could be extended to the calculation of mixture IR parameters, where the resonant mixture is treated as a single reference isotope in the slowing-down calculation. This method would not allow for the a priori tabulation of the IR parameters in an external file. They should be computed on-the-fly in every self-shielding calculation, making the use of a Monte Carlo code for the determination of the cross sections of the resonant mixture prohibitively long.

Identification of the errors due to the use of homogeneous PPTs

The definition of the multigroup cross sections induces a dependence on the angular direction $\vec{\Omega}$, that is not accounted for when employing the scalar flux to condense the energy-wise cross sections over the range of the energy groups. The multigroup equivalence procedure, which is achieved through the SPH formalism in the newly implemented SG-IR and EDC-IR subgroup methods, is required not only to preserve the reference reaction rates, but also to correct the angular dependence of the multigroup cross sections. This is only possible if the reference reaction rates themselves account for the angular-dependent effects of the heterogeneous calculation.

In this work, the expression of the multigroup reaction rates $\tau^g_{\rho,x} = \sum_{k=1}^{K} \omega^g_k \sigma^g_{\rho,x,k} \phi^g_{k,i}$ is based on two components:

- The subgroup parameters of the PPTs, namely the subgroup weights ω^g_k and cross sections $\sigma^g_{\rho,x,k}$. The PPTs employed in this work are generated by fitting effective cross sections of an IHM, as described in Chapters 5 and 6. The corresponding subgroup parameters therefore do not incorporate any angular-dependent effect.
- The subgroup flux $\phi^g_{k,i}$, solution of the subgroup Equation (8.10). This transport calculation is achieved in a heterogeneous geometry, leading to a subgroup flux accounting for the angle-dependent effects.

The angular dependence of the reaction rates, and thus of the multigroup cross sections, is therefore accounted for in a mitigated way thanks to the heterogeneous transport calculation. It is possible that a bias is introduced in the calculation because of the use of homogeneous PPTs. In the context of this PhD work, the implementation of heterogeneous PPTs has not been considered because it is not compatible with the objective of generating the PPTs on-the-fly, as it would require too much computational time. However, it seems important to be able to quantify the error introduced by the use of homogeneous PPTs. This could be accomplished with minimalist developments by generating one-dimensional reference cross sections of the resonant mixture with a Monte Carlo simulation for a

list of background dilutions, and then fitting the set of cross sections to obtain heterogeneous PPTs. A similar methodology has been presented in Chapter 8.

The comparison of the results of a SG-IR calculation with, on the one hand, homogeneous PPTs, and on the other hand, heterogeneous PPTs, would enable to measure the error introduced by the homogeneous PPTs.

Appendices

A - Creation of a Coarse 69 Group Energy Mesh

The aim of this thesis is to evaluate the performance of the subgroup methods based on the physical probability tables on a coarse energy mesh of less than 100 groups. In order to be able to condense the cross sections obtained with the ultra-fine-group solver of Chapter 5, the coarse mesh group limits should be extracted from those of the MUSCLET energy mesh [60]. To facilitate the comparison with the 383 group calculations, they should also be a subset of the 383-group limits.

No energy mesh satisfying these criteria was available for the APOLLO3® calculations at the beginning of this thesis.

The WIMS-D library [59] provides a 69 group energy structure, with 13 resonant groups between 4 eV and 9.118 keV, 14 fast groups and 42 thermal groups. This energy structure is also successfully employed in other lattice codes, such as the high fidelity neutronics code NECP-X [21], in which the implemented subgroup method relies on the use of physical probability tables. This inspired us to aim for a 69 group lattice calculation in APOLLO3®. The WIMS 69-group mesh was slightly modified to align its boundaries on the ones of the MUSCLET mesh.

The multigroup library corresponding to this 69-group mesh has been generated using the GALILEE-V0.3.3 nuclear data processing system [17], and its N2A3 module to store them in the correct format to be inputs for the APOLLO3® calculations. Three libraries are created:

1. The "x-section" library provides the infinitely diluted multigroup cross sections for each isotope, for different temperatures ranging from 274K to 2974K.

2. The "autop-1" library contains the 69-group mathematical probability tables per isotope. This library has not been exploited in our PPT calculations.

3. The "autop-2" library contains the description of the 69 group energy mesh and its correspondence with the MUSCLET mesh. It points to a library containing the mathematical probability tables on the MUSCLET mesh.

All the self-shielding methods based on the use of the mathematical probability tables are coupled to the GALILEE code to generate on-the-fly the mixture mathematical probability tables from the fine tables of the MUSCLET mesh.

The boundaries of each of the MESH69 energy groups is shown in Table A.1. The division in the resonant domain, from group 15 to group 27, is superposed to the ^{238}U and ^{235}U total cross sections in Figures A.1a and A.1b, where it is shown that the 69 group structure separates well the first resonances of ^{238}U.

Table A.1: Borns and width (in lethargy) of the 69-group energy mesh

Group	E_{sup} (eV)	E_{inf} (eV)	Δu	Group	E_{sup} (eV)	E_{inf} (eV)	Δu
1	1.974E+07	6.090E+06	1.176	36	1.092E+00	1.079E+00	0.012
2	6.090E+06	3.679E+06	0.504	37	1.079E+00	1.035E+00	0.042
3	3.679E+06	2.240E+06	0.496	38	1.035E+00	1.020E+00	0.014
4	2.240E+06	1.353E+06	0.504	39	1.020E+00	9.961E-01	0.024
5	1.353E+06	8.241E+05	0.496	40	9.961E-01	9.647E-01	0.032
6	8.241E+05	4.979E+05	0.504	41	9.647E-01	9.437E-01	0.022
7	4.979E+05	3.008E+05	0.504	42	9.437E-01	9.195E-01	0.026
8	3.008E+05	1.832E+05	0.496	43	9.195E-01	8.204E-01	0.114
9	1.832E+05	1.115E+05	0.496	44	8.204E-01	7.204E-01	0.130
10	1.115E+05	6.738E+04	0.504	45	7.204E-01	6.251E-01	0.142
11	6.738E+04	4.070E+04	0.504	46	6.251E-01	5.200E-01	0.184
12	4.070E+04	2.479E+04	0.496	47	5.200E-01	3.899E-01	0.288
13	2.479E+04	1.497E+04	0.504	48	3.899E-01	3.528E-01	0.100
14	1.497E+04	9.119E+03	0.496	49	3.528E-01	3.257E-01	0.080
15	9.119E+03	5.553E+03	0.496	50	3.257E-01	3.049E-01	0.066
16	5.553E+03	3.355E+03	0.504	51	3.049E-01	2.803E-01	0.084
17	3.355E+03	2.285E+03	0.384	52	2.803E-01	2.546E-01	0.096
18	2.285E+03	1.348E+03	0.528	53	2.546E-01	2.097E-01	0.194
19	1.348E+03	9.106E+02	0.392	54	2.097E-01	1.898E-01	0.100
20	9.106E+02	3.717E+02	0.896	55	1.898E-01	1.378E-01	0.320
21	3.717E+02	1.481E+02	0.920	56	1.378E-01	1.042E-01	0.280
22	1.481E+02	7.626E+01	0.664	57	1.042E-01	7.639E-02	0.310
23	7.626E+01	4.756E+01	0.472	58	7.639E-02	6.510E-02	0.160
24	4.756E+01	2.783E+01	0.536	59	6.510E-02	5.547E-02	0.160
25	2.783E+01	1.605E+01	0.551	60	5.547E-02	4.727E-02	0.160
26	1.605E+01	9.501E+00	0.524	61	4.727E-02	4.028E-02	0.160
27	9.501E+00	3.999E+00	0.865	62	4.028E-02	3.432E-02	0.160
28	3.999E+00	3.140E+00	0.242	63	3.432E-02	2.925E-02	0.160
29	3.140E+00	2.591E+00	0.192	64	2.925E-02	2.492E-02	0.160
30	2.591E+00	2.071E+00	0.224	65	2.492E-02	2.020E-02	0.210
31	2.071E+00	1.519E+00	0.310	66	2.020E-02	1.497E-02	0.300
32	1.519E+00	1.292E+00	0.162	67	1.497E-02	1.044E-02	0.360
33	1.292E+00	1.148E+00	0.118	68	1.044E-02	4.599E-03	0.820
34	1.148E+00	1.116E+00	0.028	69	4.599E-03	1.001E-05	6.130
35	1.116E+00	1.092E+00	0.022				

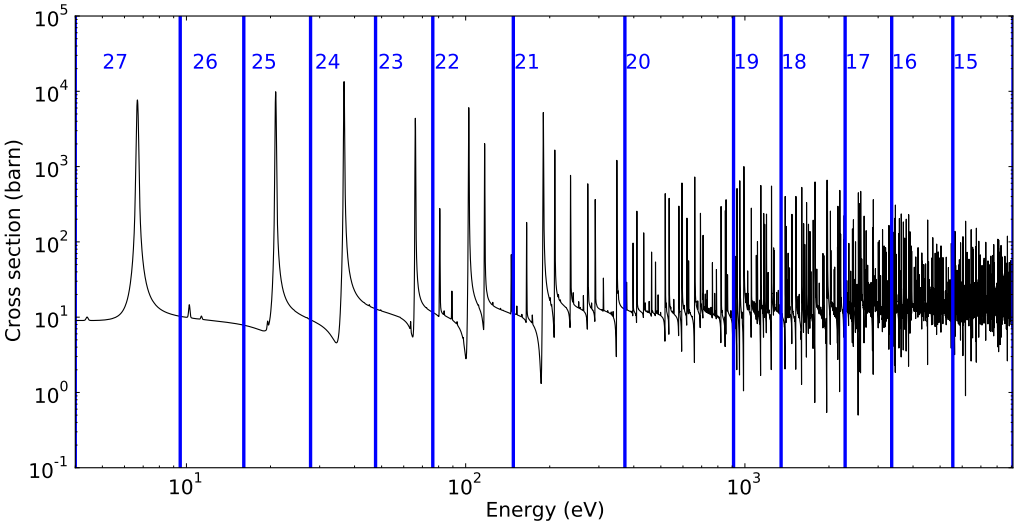

(a) U238 total cross section at 0K

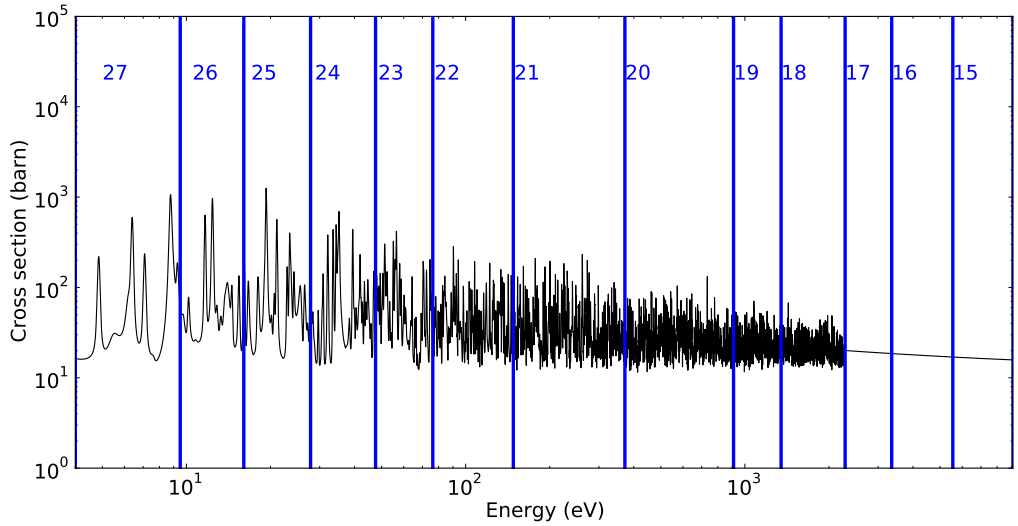

(b) U235 total cross section at 0K

Figure A.1: Division of the 69 group mesh in the resonant domain

B - Résumé en français

La distribution des neutrons au sein d'un réacteur nucléaire est prédite par l'équation de transport des neutrons, aussi appelée équation de Boltzmann pour sa similarité avec la théorie de la cinétique des gaz. La complexité de cette équation provient des fluctuations très rapides en énergie de ses coefficients, appelés sections efficaces macroscopiques.

Les sections efficaces caractérisent la probabilité d'interaction des neutrons avec le milieu qu'ils traversent. Certaines sections efficaces, en particulier celles associées aux noyaux lourds tels que l'uranium, ont un comportement résonant. Entre 1 eV et 100 keV, elles fluctuent de plusieurs ordres de grandeur de manière brusque, comme en témoigne la Figure B.1. La probabilité d'interaction augmentant drastiquement, le flux neutronique subit une dépression au voisinage de ces résonances.

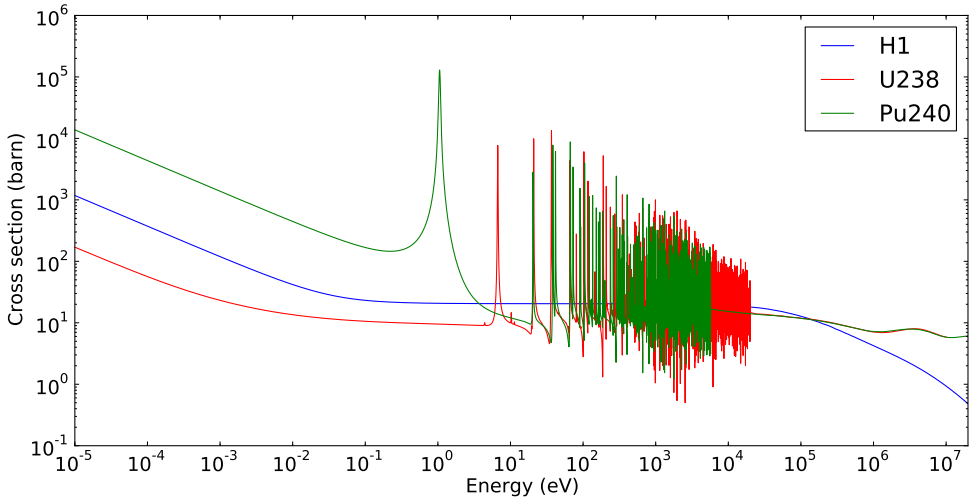

Figure B.1: Sections efficaces à 0K (évaluation nucléaire JEFF 3.1[22])

Les méthodes numériques résolvant l'équation de Boltzmann peuvent être classées en deux catégories.

D'une part, les méthodes Monte-Carlo estiment le comportement moyen du réactor nucléaire à partir d'un nombre conséquent de trajectoires de neutrons, échantillonnées aléatoirement. Ces méthodes ont l'avantage de ne pas introduire d'approximation, les rendant particulièrement fidèles à la réalité. Leur précision est principalement limitée par les incertitudes associées aux évaluations nucléaires. Un nombre important de particules doit être simulé pour diminuer l'incertitude statistique associée à chaque grandeur calculée; les méthodes Monte-Carlo sont donc considérablement coûteuses en temps de calcul, ce qui limite leur champ d'applications.

Les méthodes déterministes consistent à discrétiser l'espace des phases (espace, énergie, temps, direction) pour résoudre l'équation de transport sur chaque pas de discrétisation. Cette discrétisation introduit des approximations et des biais; le choix du raffinement doit donc être un compromis entre précision et temps de calcul. En particulier, le traitement de la variable d'énergie s'effectue à l'aide de

l'approximation multigroupe, qui consiste à diviser le domaine énergétique en groupes dans lesquels les neutrons sont considérés comme mono-cinétiques. Dans l'équation de Boltzmann, les sections efficaces ponctuelles en énergie doivent être remplacées par les sections efficaces multigroupes, calculées comme la moyenne des sections efficaces pondérée par le flux neutronique sur la largeur en énergie d'un groupe. Cependant, le flux neutronique étant au moment de la discrétisation de l'équation de transport encore inconnu, il est nécessaire d'utiliser une fonction de pondération indépendante de l'espace à la place. Cette fonction de pondération est bien sûr représentative du flux dans un réacteur, mais elle ne tient pas compte du comportement résonant des sections efficaces dans certains matériaux. Le calcul d'autoprotection consiste à corriger les sections efficaces multigroupes des isotopes résonants. La précision globale du calcul de transport dépend intrinsèquement de la précision de la méthode d'autoprotection employée.

Ce travail de thèse a été mené au Service d'Étude des Réacteurs et de Mathématiques Appliquées (SERMA) du CEA de Saclay, où le code APOLLO3® [16] est en développement dans le cadre d'un partenariat avec Framatome et EDF. La méthode des sous-groupes d'APOLLO3® [18] repose sur la résolution de l'équation de structure fine [2] sur une discrétisation énergétique fine de 383 groupes. Les grandeurs multigroupes sont calculées grâce aux tables de probabilités mathématiques de mélange générées à la volée par le code de traitement de données nucléaires GALILEE [17]. Cette catégorie de tables de probabilités conserve les premiers moments des sections efficaces ponctuelles, grâce à une procédure similaire à celle utilisée pour calculer une quadrature de Gauss. Les tests numériques effectués avec la méthode des sous-groupes d'APOLLO3® démontrent son excellent niveau de précision, mais soulignent son important coût temporel qui rendent impossible son application à de grandes géométries. L'implémentation de la méthode "Equivalent Dancoff-factor Cell" [19] a conduit à une accélération significative du temps de calcul sur des grandes géométries, mais il est encore fortement limité par l'usage d'un maillage énergétique très fin.

D'autres codes déterministes, tels que HELIOS [8], WIMS [9] [4], DeCART [10], nTRACER [20], MPACT [11], ou encore NECP-X [12] [21], parviennent à mener le calcul d'autoprotection sur seulement quelques dizaines de groupes d'énergie. Leurs méthodes des sous-groupes n'utilisent pas les tables de probabilités mathématiques, mais des tables de probabilités physiques qui conservent une grandeur caractéristique du calcul de réacteur (section efficace effective, taux de réaction, etc.). L'avantage d'une discrétisation énergétique à moins de 100 groupes est évident, car le temps de calcul est linéairement dépendant du nombre de groupes.

L'objectif de cette thèse est donc d'étudier les méthodes des sous-groupes basées sur l'utilisation des tables de probabilités physiques dans le code APOLLO3®, pour le calcul des réacteurs thermiques. Un maillage énergétique à 69 groupes a été adapté à partir du maillage disponible dans la librairie WIMS-D [59], et les bibliothèques de données nucléaires multigroupes non-autoprotégées ont été générées avec le code GALILEE.

Les chapitres 5 et 6 décrivent l'implémentation dans APOLLO3® et la comparaison de plusieurs méthodes pour calculer à la volée les tables de probabilités physiques. Ce calcul incorpore le traitement de mélange grâce à une résolution de l'équation de ralentissement en milieu homogène avec un maillage ultra-fin et avec les tables de probabilités mathématiques de mélange. Deux méthodes de calcul, reposant sur l'utilisation de fractions rationnelles pour représenter des sections efficaces de référence,

ont démontré leur capacité à reproduire très précisemment les sections efficaces fournies par le solveur de ralentissement ultra-fin.

Le chapitre 7 décrit les résultats préliminaires lors du couplage des tables de probabilités physiques avec la méthode des sous-groupes d'APOLLO3®, et l'impact du nombre de groupes d'énergie sur la précision du calcul. Il a été démontré que la méthode des sous-groupes d'APOLLO3®, parce qu'elle fait l'hypothèse que les sources de ralentissement au sein d'un groupe ne sont pas dépendantes de l'énergie, n'est pas adaptée à des calculs sur des maillages énergétiques grossiers.

Le chapitre 8 détaille les différentes étapes de l'implémentation dans APOLLO3® d'une méthode des sous-groupes basée sur l'utilisation du modèle "Intermediate Resonance", optimisée pour un calcul sur notre maillage à 69 groupes, ainsi que les premiers résultats obtenus avec cette méthode. Des erreurs de moins de 200 pcm ont été obtenus sur des calculs de cellules et d'assemblage, représentatif d'un calcul de réacteur thermique. Sur un calcul d'assemblage, l'utilisation de cette nouvelle méthode conduit à une accélération pouvant atteindre un facteur 25 sur le calcul d'autoprotection, par rapport à un calcul traditionnel à 383 groupes.

Des perspectives d'amélioration des travaux de cette thèse sont proposés dans le chapitre 9. Tout d'abord, l'amélioration du solveur de ralentissement utilisé pour générer les sections efficaces en milieu homogène infini pour le calcul des tables de probabilités physiques, et en particulier du traitement de mélange, mènerait à un gain de précision dans la méthode des sous-groupes.

D'autres méthodes de calcul des tables de probabilités physiques, reposant par exemple sur l'utilisation d'algorithmes de minimisation sous contrainte, devraient être étudiées afin de générer des tables d'ordres élevés. Nous pensons que l'utilisation de tables de probabilités d'ordre supérieur à 5 conduirait à une meilleure représentation des flux dans chaque sous-groupe, et donc à un gain de précision.

Le modèle "Intermediate Resonance" implémenté dans APOLLO3® n'a pas encore fait l'objet de beaucoup d'études pour son optimisation. La dépendance en température, en dilution, etc. de ce modèle doit être étudiée pour améliorer le calcul des sources de ralentissement. Dans la génération des paramètres de ce modèle, le ^{238}U a été sélectionné comme isotope de référence à cause de sa prédominance dans les calculs de réacteurs thermiques. Mais dans les groupes où sa section efficace ne présente pas de résonance, un autre isotope, tel que le ^{235}U pour le calcul des mélanges UO_2 , ou un isotope du plutonium pour le calul des combustibles de type MOX, pourrait être choisi.

Enfin, le maillage énergétique à 69 groupes utilisé dans le cadre de cette thèse pourrait lui aussi être optimisé. D'importantes erreurs ont été observées en dehors des groupes résonants ; un raffinement du maillage dans le domaine thermique et dans le domaine rapide devrait mener à une meilleure représentation du flux et des taux de réactions, au prix de davantage de calculs de flux.

Bibliography

[1] A. Hébert. “A review of legacy and advanced self-shielding models for lattice calculations”. In: *Nuclear science and engineering* 155.2 (2007), pp. 310–320.

[2] M. Livolant and F. Jeanpierre. *Autoprotection des résonances dans les réacteurs nucléaires. Application aux isotopes lourds*. Rapport CEA-R-4533. 1974.

[3] M. Coste-Delclaux. “Modélisation du phénomène d’autoprotection dans le code de transport multigroupe APOLLO2”. PhD thesis. 2006. url: http://www.theses.fr/2006CNAM0516.

[4] D.J. Powney and T.D. Newton. “Overview of the wims 9 resonance treatment”. In: *Serco Assurance, Dorchester* (2004).

[5] L. Mao and I. Zmijarevic. “A new Tone’s method in APOLLO3® and its application to fast and thermal reactor calculations”. In: *Nuclear Engineering and Technology* 49.6 (2017), pp. 1269–1286.

[6] Y. Ishiguro and H. Takano. *PEACO: a code for calculation of group constants of resonance energy region in heterogeneous systems*. Tech. rep. Japan Atomic Energy Research Inst., 1971.

[7] N. Sugimura and A. Yamamoto. “Resonance treatment based on ultra-fine-group spectrum calculation in the aegis code”. In: *Journal of Nuclear Science and Technology* 44.7 (2007), pp. 958–966. doi: 10.1080/18811248.2007.9711335.

[8] J. Casal. “HELIOS: geometric capabilities of a new fuel-assembly program”. In: *Proc. Int. Topical Meeting on Advances in Mathematics, Computations and Reactor Physics, Pittsburgh, Pa., USA, April 28-May 2, 1991*. Vol. 2. 1991, pp. 10–2.

[9] M.J. Halsall. “The WIMS subgroup method for resonance absorption”. In: *Transactions of the American Nuclear Society* 72.CONF-950601- (1995).

[10] H.G. Joo et al. “Methods and Performance of a Three-Dimensional Whole-Core Transport Code DeCART”. In: *Proceedings of the PHYSOR 2004: The Physics of Fuel Cycles and Advanced Nuclear Systems - Global Developments* (2004), pp. 22–34.

[11] Y. Liu et al. “Resonance self-shielding methodolology in MPACT”. In: *International Conference on Mathematics and Computational Methods Applied to Nuclear Science and Engineering (M&C 2013)*. American Nuclear Society (ANS), May 2013.

[12] Z. Liu et al. “The pseudo-resonant-nuclide subgroup method based global–local self-shielding calculation scheme”. In: *Journal of Nuclear Science and Technology* 55.2 (2018), pp. 217–228.

[13] P. Ribon and J. Maillard. “Les tables de probabilité: Application au traitement des sections efficaces pour la neutronique”. In: *Report CEA-N, NEACRP-L-294* (1986).

[14] A. Hébert and M. Coste. “Computing Probability Tables for Self-Shielding Calculations in APOLLO2”. In: *Proc. Int. Conf. on Mathematics and Computation, reactor Physics and Environmental Analysis in Nuclear Applications, Madrid, Spain*. 1999.

[15] A. Hébert. *Applied reactor physics*. Presses Polytechnique de Montréal, 3rd edition, 2020.

[16] D. Schneider et al. “APOLLO3: CEA/DEN deterministic multi-purpose code for reactor physics analysis”. In: *Proc. PHYSOR*. 2016, pp. 1–5.

[17] M. Coste-Delclaux. “GALILEE: a nuclear data processing system for transport, depletion and shielding codes”. In: *Proceedings of the Second Workshop on Nuclear Data Evaluation for Reactor Applications*. 2008.

[18] L. Mao, I. Zmijarevic, and K. Routsonis. “Application of the SPH method to account for the angular dependence of multigroup resonant cross sections in thermal reactor calculations”. In: *Annals of Nuclear Energy* 124 (2019), pp. 98–118.

[19] L. Mao, I. Zmijarevic, and R. Sanchez. “A subgroup method based on the equivalent Dancoff-factor cell technique in APOLLO3®for thermal reactor calculations”. In: *Annals of Nuclear Energy* 139 (2020), p. 107212.

[20] Y. S. Jung et al. “Practical numerical reactor employing direct whole core neutron transport and subchannel thermal/hydraulic solvers”. In: *Annals of Nuclear Energy* 62 (2013), pp. 357–374.

[21] J. Chen et al. “A new high-fidelity neutronics code NECP-X”. In: *Annals of Nuclear Energy* 116 (2018), pp. 417–428.

[22] A. Santamarina et al. “The JEFF-3.1. 1 nuclear data library”. In: *JEFF report* 22.10.2 (2009), p. 2.

[23] G.I. Bell and S. Glasstone. *Nuclear reactor theory*. Tech. rep. US Atomic Energy Commission, Washington, DC (United States), 1970.

[24] R. Sanchez and N.J. McCormick. “A review of neutron transport approximations”. In: *Nuclear Science and Engineering* 80.4 (1982), pp. 481–535.

[25] R. Sanchez and A. Chetaine. “A synthetic acceleration for a two-dimensional characteristic method in unstructured meshes”. In: *Nuclear science and engineering* 136.1 (2000), pp. 122–139.

[26] R. Sanchez et al. “APOLLO II: A User-Oriented, Portable, Modular Code for Multigroup Transport Assembly Calculations”. In: *Nuclear Science and Engineering* 100.3 (1988), pp. 352–362. doi: 10.13182/NSE88-3.

[27] R. Sanchez et al. *APOLLO2.5 : Notice théorique*. Tech. rep. SERMA/LENR/RT/99-2719/A. Direction des réacteurs nucléaires (CEA), 2002.

[28] M. Coste-Delclaux and al. *Neutronics*. Éditions du Moniteur, 2015.

[29] H. Golfier et al. “APOLLO3: a common project of CEA, AREVA and EDF for the development of a new deterministic multi-purpose code for core physics analysis”. In: *International Conference on Advances in Mathematics, Computational Methods, and Reactor Physics*. 2009.

[30] N. Hfaiedh and A. Santamarina. “Determination of the optimized SHEM mesh for neutron transport calculations”. In: *International Topical Meeting on Mathematics and Computation, Supercomputing, Reactor Physics and Nuclear and Biological Applications*. 2005.

[31] A. Santamarina and N. Hfaiedh. “The SHEM energy mesh for accurate fuel depletion and BUC calculations”. In: *International Conference on Nuclear Criticality-Safety (ICNC 2007)*. 2007.

[32] A. Hébert. “Refinement of the Santamarina-Hfaiedh energy mesh between 22.5 eV and 11.4 keV”. In: *International Conference on the Physics of Reactors, Interlaken, Switzerland*. 2008.

[33] I. Zmijarevic. “Multidimensional discrete ordinates nodal and characteristics methods for APOLLO2 code”. In: *Proc. of Int. Conf. Mathematics and Computation, Reactor Physics and Environmental Analysis in Nuclear Application, Madrid, Spain*. Vol. 2. 1999, pp. 1587–1597.

[34] I. Zmijarevic. “IDT solution to the 3D transport benchmark over a range in parameter space”. In: *International Conference on the Physics of Reactors ’Nuclear Power: A Sustainable Resource’*. 2008.

[35] E. Masiello, R. Sanchez, and I. Zmijarevic. “New Numerical Solution with the Method of Short Characteristics for 2-D Heterogeneous Cartesian Cells in the APOLLO2 Code: Numerical Analysis and Tests”. In: *Nuclear Science and Engineering* 161 (Mar. 2009), pp. 257–278. doi: 10.13182/NSE161-257.

[36] S. Santandrea and P. Mosca. “Linear surface characteristic scheme for the neutron transport equation in unstructured geometries”. In: *Proceeding of Physor2006* (2006), pp. 10–14.

[37] K. Assogba et al. “Spherical Harmonics and Discontinuous Galerkin Finite Element Methods for the Three-Dimensional Neutron Transport Equation: Application to Core and Lattice Calculation”. In: *Nuclear Science and Engineering* 0.0 (2023), pp. 1–16. doi: 10.1080/00295639.2022.2154546. eprint: https://doi.org/10.1080/00295639.2022.2154546. url: https://doi.org/10.1080/00295639.2022.2154546.

[38] R. Sanchez. “Assembly homogenization techniques for core calculations”. In: *Progress in Nuclear Energy* 51.1 (2009), pp. 14–31.

[39] A. Baudron and J. Lautard. “MINOS: a simplified PN solver for core calculation”. In: *Nuclear Science and Engineering* 155.2 (2007), pp. 250–263.

[40] J.Y. Moller and J.J. Lautard. “Minaret, a deterministic neutron transport solver for nuclear core calculations”. In: *International Conference on Mathematics and Computational Methods Applied to Nuclear Science and Engineering*. 2011.

[41] L. Mao, I. Zmijarevic, and R. Sanchez. “Resonance Self-Shielding Methods for Fast Reactor Calculations—Comparison of a New Tone’s Method with the Subgroup Method in APOLLO3®”. In: *Nuclear Science and Engineering* 188.1 (2017), pp. 15–32.

[42] B. Faure et al. “Neutronic calculation of an axially heterogeneous ASTRID fuel assembly with APOLLO3®: Analysis of biases and foreseen improvements”. In: *Annals of Nuclear Energy* 115 (2018), pp. 88–104.

[43] G. Rimpault. “Physics documentation of ERANOS: the ECCO cell code”. In: *CEA Technical Note RT-SPRC-LEPh-97-001* (1997).

[44] L. Mao and I. Zmijarevic. “The up-scattering treatment in the fine-structure self-shielding method in APOLLO3®”. In: *PHYSOR2014* (2014).

[45] L. Mao, R. Sanchez, and I. Zmijarevic. “Considering the up-scattering in resonance interference treatment in APOLLO3®”. In: *ANS MC2015* (2015).

[46] J. Sublet, P. Ribon, and M. Coste-Delclaux. *CALENDF-2010: user manual*. Tech. rep. Commissariat a l’energie Atomique-CEA (France), 2011.

[47] R. Bulirsch, J. Stoer, and J. Stoer. *Introduction to numerical analysis*. Vol. 3. Springer, 2002.

[48] P. Reuss. *Neutron physics*. EDP sciences, 2012.

[49] M.L. Williams. “Correction of multigroup cross sections for resolved resonance interference in mixed absorbers”. In: *Nuclear Science and Engineering* 83.1 (1983), pp. 37–49.

[50] R. Sanchez and J. Mondot. *A model for calculating multigroup self-shielded cross sections for a mixture of resonance absorbers in heterogeneous media*. Tech. rep. CEA Centre d’Etudes Nucleaires de Saclay, 1984.

[51] Enrico Sartori. “Standard energy group structures of cross section libraries for reactor shielding, reactor cell and fusion neutronics applications: VITAMIN-J, ECCO-33, ECCO-2000 and XMAS”. In: *JEF/DOC-315, Revision* 3 (1990).

[52] J. Rowlands et al. “LWR Pin Cell Benchmark Intercomparisons. An Intercomparison study organized by the JEF Project, with contributions by Britain, France, Germany, The Netherlands, Slovenia and the USA”. In: *JEF Report to be published, OECD/NEA Data Bank* (1999).

[53] A. Hébert. “The Ribon extended self-shielding model”. In: *Nuclear science and engineering* 151.1 (2005), pp. 1–24.

[54] R. Sanchez. “A Transport Multicell Method for Two-Dimensional Lattices of Hexagonal Cells”. In: *Nuclear Science and Engineering* 92.2 (1986), pp. 247–254. doi: 10.13182/NSE86-A18172.

[55] K. Yamaji et al. “Ultra-fine-group resonance treatment using equivalent Dancoff-factor cell model in lattice physics code GALAXY”. In: *Journal of Nuclear Science and Technology* 55.7 (2018), pp. 756–780.

[56] L. Mao et al. “a Subgroup Method Based on the Equivalent Dancoff-Factor Cell Technique Compared with the Fine-Structure Method in APOLLO3®”. In: *EPJ Web of Conferences*. Vol. 247. EDP Sciences. 2021, p. 02017.

[57] R.D. Mosteller. “The Doppler-Defect Benchmark: Overview and Summary of Results”. In: *Form* 836 (May 2007).

[58] A. Yamamoto et al. “Benchmark problem suite for reactor physics study of LWR next generation fuels”. In: *Journal of Nuclear Science and Technology* 39.8 (2002), pp. 900–912.

[59] D.L. Aldama, F. Leszczynski, and A. Trkov. “WIMS-D library update”. In: *Final report of a co-ordinate research project* (2003).

[60] S. Mengelle. *Maillage universel à pas constants en léthargie : MUSCLET*. Tech. rep. CEA Centre d’Etudes Nucleaires de Saclay, 2017.

[61] A. Hébert and M. Coste. “Computing moment-based probability tables for self-shielding calculations in lattice codes”. In: *Nuclear science and engineering* 142.3 (2002), pp. 245–257.

[62] E. Brun et al. “TRIPOLI-4®, CEA, EDF and AREVA reference Monte Carlo code”. In: *Annals of Nuclear Energy* 82 (2015). Joint International Conference on Supercomputing in Nuclear Applications and Monte Carlo 2013, SNA + MC 2013. Pluri- and Trans-disciplinarity, Towards New Modeling and Numerical Simulation Paradigms, pp. 151–160. issn: 0306-4549. doi: https://doi.org/10.1016/j.anucene.2014.07.053. url: https://www.sciencedirect.com/science/article/pii/S0306454914003843.

[63] S. Mengelle. *Private Communication*. 2022.

[64] L. Mao. *Private Communication*. 2020.

[65] A.S. Householder. *Principles of numerical analysis*. McGraw-Hill, 1953.

[66] O. Aberth. “Iteration methods for finding all zeros of a polynomial simultaneously”. In: *Mathematics of computation* 27.122 (1973), pp. 339–344.

[67] R. Larham. “On the Cauchy Bound for the Roots of Polynomials”. In: *MHF Journal* (2010), pp. 2–3.

[68] R. Goldstein and E.R. Cohen. “Theory of resonance absorption of neutrons”. In: *Nuclear Science and Engineering* 13.2 (1962), pp. 132–140.

[69] A.C. Aldous. *Numerical Studies of the Hydrogen Equivalent of some Structural Materials in Their Effect on U-238 Resonance Capture*. Tech. rep. Atomic Energy Establishment, Winfrith (England), 1969.

[70] R. Macfarlane et al. “The NJOY Nuclear Data Processing System, Version 2016”. In: (2017). doi: 10.2172/1338791. url: https://www.osti.gov/biblio/1338791.

[71] Y. Xu, Z. Gao, and T. Downar. “The Calculation of Resonance Parameters for the DeCART MOC Code”. In: *Joint International Topical Meeting on Mathematics and Computations and Supercomputing in Nuclear Applications*. Citeseer, 2007.

[72] C. Jouanne. *Private Communication*. 2022.

[73] E. Rosier et al. “Comparison of two Subgroup Methods based on the Physical Probability Tables”. In: *International Conference on Physics of Reactors 2022 (PHYSOR 2022)*. 2022, pp. 2561–2569.

[74] A. Zoia et al. “Doppler broadening of neutron elastic scattering kernel in TRIPOLI-4®”. In: *Annals of Nuclear Energy* 54 (2013), pp. 218–226.

[75] P.J. Davis and P. Rabinowitz. *Methods Of Numerical Integration 2Nd Edition*. Academic Press, 1984.

[76] A. Hébert. “A Comparison of Three Techniques for Computing Probability Tables”. In: *Int. Conf. on the Physics of Nuclear Science and Technology, Long Island, New York*. 1998.

[77] H. G. Joo, G. Y. Kim, and L. Pogosbekyan. “Subgroup weight generation based on shielded pin-cell cross section conservation”. In: *Annals of Nuclear Energy* 36.7 (2009), pp. 859–868.

[78] S. Peng et al. “Subgroup method with resonance interference factor table”. In: *Annals of Nuclear Energy* 59 (2013), pp. 176–187.

[79] K. S. Kim et al. “Development of the multigroup cross section library for the CASL neutronics simulator MPACT: Method and procedure”. In: *Annals of Nuclear Energy* 133 (2019), pp. 46–58.